Micro-encapsulated poly(vinyl alcohol) nanoparticles for rifampicin delivery to the lungs

Sadouki, Fethi

Awarding institution:
King's College London

Micro-encapsulated poly(vinyl alcohol) nanoparticles for rifampicin delivery to the lungs

Fethi Sadouki

A thesis submitted for the degree of Doctor of Philosophy

King's College London

Pharmaceutical Science Research Division

Abstract

Tuberculosis is a contagious disease caused by *Mycobacterium Tuberculosis* and is recognised as a global public health emergency. New approaches are required to improve the chemotherapy of TB, in particular to target the reservoir of *M. Tuberculosis* that accumulates in alveolar macrophages and lung lesions. The aim of this thesis was to develop polymeric nanoparticle-loaded formulations for the delivery of rifampicin to the lungs. Poly (vinyl alcohol) nanospheres (NS) and nanocapsules (NC) were developed using a modified nanoprecipitation method. Both types of nanocarrier were spherical with a mean diameter of ca. 220 nm (NS) and 150 nm (NC). Rifampicin was successfully encapsulated with efficiencies of 29.3 ± 0.7% and 32.3 ± 0.3%, for NS and NCs, respectively. Methods for enhancing the stability and modifying the release of rifampicin were developed. The uptake of the PVA nanocarriers was studied *in-vitro* using the J774A.1 macrophage-like cell line. After 6 h incubation, the amount of rifampicin imported into macrophages by drug-loaded nanoparticles, containing 1000 µg/ml of drug, was twice (NC) or three times (NS) greater than that attained with rifampicin solution. The drug-loaded PVA nanoparticles were formulated into a powder for pulmonary administration by spray drying into lactose to yield spherical microspheres of ca. 2 µm diameter. The deposition studies of the spray dried powders, carried out using a modified twin stage impinger, showed that the NS-loaded-microspheres had a better deposition profile than the NC-loaded microspheres. This work generated novel PVA nanocarriers, demonstrated that they are effective in targeting rifampicin to macrophages and exemplified their formulation as an inhaled drug delivery system.

To my mother and my father

"In the middle of the difficulty lies the opportunity"

Albert Einstein

Acknowledgements

It is hard to overstate my gratitude to my supervisors: Dr Lea Ann Dailey, Dr. Stuart Jones and Dr. Ben Forbes. Without their excellent academic supervision, guidance and encouragements I could never finish this PhD.

I am grateful to Dr. Helen Collins for providing us with the cell lines and her willingness to help all the time. My special thanks to Steve Ingham his constant assistance and allowing me to use different analytical equipments when I needed. I would also like to thank colleagues at the drug delivery group for making this experience more enjoyable.

I would also like to thank my two best friends Lotfi and Yacine for their support throughout the journey. Special thanks to Lilia, Hadjer, Yousra, Zino, Amir and Nassim for their help and support. I would like to also take this opportunity to thank the Algerian government, for the financial support during my undergraduate and postgraduate studies.

I would like to thank my family. My parents for being my inspiration, for their unconditional love and constant prayers. Fouzia, Houria, Amine, Karima and Sofiane for all the love, support and encouragement.

TABLE OF CONTENTS

Chapter 2

Rifampicin analysis

Chapter 3

Rifampicin-loaded poly (vinyl alcohol) nanocarriers

Chapter 4

Uptake of PVA nanoparticles by the macrophage-like cell line J774A.1

Chapter 5
Inhalable microspheres containing PVA nanocarriers

LIST OF FIGURES

CHAPTER 1

CHAPTER 2

CHAPTER 3

CHAPTER 4

CHAPTER 5

CHAPTER 6

LIST OF TABLES

Abbreviations

BNF	British National Formulary
BCG	Bacillus Calmette-Guerin
COPD	Chronic obstructive pulmonary disease
DOT	Direct Observed therapy
CMI	Cell mediated immunity
CV	Coefficient of variation
HPLC	High Performance Liquid Chromatography
INH	Isoniazid
LOD	Limit of detection
LOQ	Limit of quantification
MDR-TB	Multi-drug resistant tuberculosis
MMAD	Mass median aerodynamic diameter
MS	Microspheres
NS	Nanosphere
NC	Nanocapsule
PLGA	Poly (lactide-co-glycolide)
PVA	Poly (vinyl Alcohol)
PYZ	Pyrazinamide
RSV	3-formylrifamycin SV
Sd	Standard deviation
SEM	Scanning electron microscopy
TB	Tuberculosis
TSI	Twin stage impinge
WHO	World Health Organisation

CHAPTER ONE

Introduction

1.1. Tuberculosis

1.1.1. Background

Tuberculosis (TB), a highly contagious chronic granulomatous bacterial infection, is the second leading cause of death from an infectious disease worldwide after HIV. TB is caused by the inhalation of *Mycobacterium tuberculosis* and was declared as global emergency in 1993. In 2010, there were an estimated 8.8 million people who developed the active disease and 1.5 million people who died from TB (WHO, 2011).

Mycobacterium tuberculosis has a complex cell wall, composed of long-chain fatty acids, glycolipids, peptidoglycan, and proteins, and a slow doubling time (18 – 24 h). It is primarily a respiratory pathogen, and usually transmitted by the cough of a person with active disease (Kumar and Robbins, 2007). Primary TB occurs within the first year or so after exposure, and is the result of an uncontrolled initial infection. The majority (90 %) of infected humans effectively contain, but do not completely eradicate the bacteria, and are defined as having “latent” infection (Kumar and Robbins, 2007; Selwyn *et al*., 1989). This is a clinical term, meaning a person is infected but is asymptomatic and not contagious. It is great concern that TB persists as a latent infection in an estimated one third of the world population (2 billion people), providing a reservoir of potential disease and contagion. Risk of developing active disease varies according time since exposure, age and host immunity. The lifetime risk of infection activation for a latently infected human has been estimated to be 2-23 % (Parish *et al.,* 1998). Schematic representation of the progression of TB is shown in Figure 1.1.

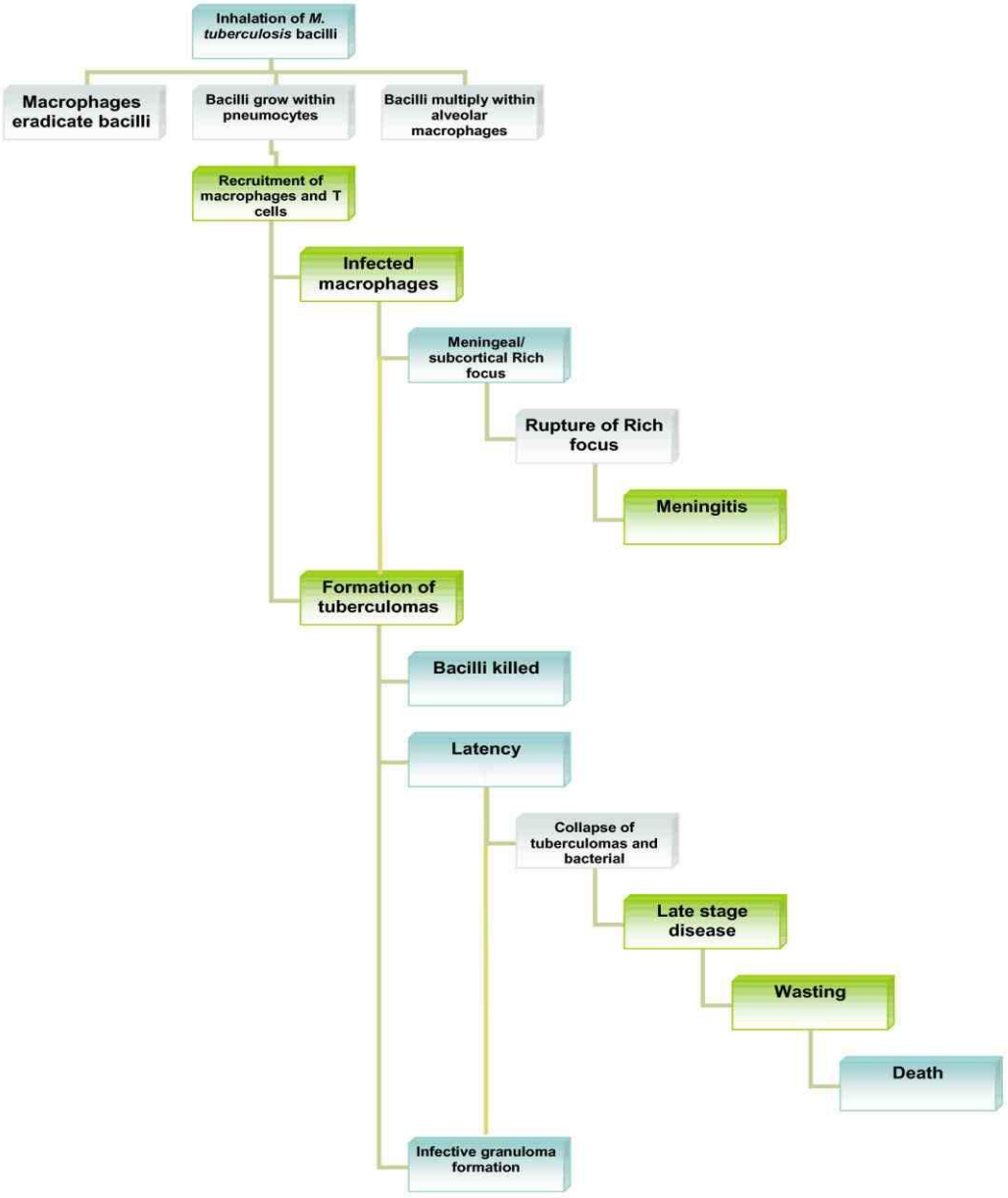

Figure 1.1. Pathogenesis of tuberculosis (adapted from Du Toi *et al*., 2006)

The pathological and inflammatory processes in active TB produce symptoms such as loss of appetite, weakness, fever, weight loss, night sweat, chest pain, respiratory insufficiency, and cough (Bloom and Murray, 1992). The old name for TB was "consumption" as this disease is developed at a leisurely pace and with multiple symptoms which lead to gradual debilitation and physical exhaustion. If untreated, the wasting and weight loss may be very severe, leading to death. Mortality rates of TB range from 50 to 80% in untreated smear-positive individuals to 30% with inconsistent control programmes and drop to lower than 5% when directly observed therapy (DOT) and active TB control programmes are instituted (Singh, 2004, Onyebujoh *et al*., 2006).

TB appears to be under control in developed countries but starkly manifest in places like south eastern Asia and Africa, where 84 % of the estimated new cases in 2010 occurred. This is mostly due to complications of HIV infection and drug resistance (Brennan, 1997). Currently, multidrug-resistant (MDR) TB has a high incidence, in an increasing order. In 2010, there were an estimated 650 000 cases of MDR-TB among the world's 12.0 million prevalent cases of TB (WHO, 2011). It is estimated that 1 billion more people will be infected, 200 million will develop the disease, and 70 million will die in case surveillance and control strategies continue as they are (WHO, 2011).

1.1.2. Primary tuberculosis

Once inhaled, most *M. tuberculosis* organisms will settle in the upper respiratory epithelium, where they are likely to be expelled by the mucociliary escalator (Nardell, 1993). The few bacteria reaching the deep lung are phagocytosed by alveolar

macrophages and either killed or else survive to initiate an infection (Dannenberg, 1993; Schlesinger, 1996). The fate of the bacillus within the infected cell depends on the type and activation state of cell found. It is believed that a bacillus is able to survive within a macrophage if the phenotype of the phagocytic cell interacting with M. tuberculosis displays an anti-inflammatory phenotype also known as “alternative activation state”. These cells have increased expression of pattern recognition receptors such as the mannose and scavenger receptors facilitating cell and bacillus interaction but they also have a reduced oxidative burst and they are unable to eliminate the bacillus (Schlesinger, 1996). Once inside the phagocyte, the mycobacteria modulate the behaviour of its phagosome by preventing its fusion with acidic, hydrolytically-active lysosomes (Rohde *et al*., 2007; Sturgill-Koszycki *et al*., 1994).

Over the next 2 to 3 weeks, surviving organisms multiply, kill their host macrophages and release more bacilli infecting additional host cells. Pulmonary inflammation due to interaction of bacillus with macrophages and other cells results in recruitment of monocytes, neutrophils, and primed T cells and B cells to lungs, culminating in formation of granulomatous lesions (Figure 1.2).

Granuloma formation is the classic pathologic feature of TB, and serves as an effective means for containing pathogens, preventing their continued growth and dissemination. In its early stage, the granuloma has a core of infected macrophages enclosed by foamy macrophages and other mononuclear phagocytes, surrounded by lymphocytes. This tissue response contains the infection and spells the end of the period of rapid replication for the mycobacteria. As the granuloma matures it develops an extensive fibrous capsule that encases the macrophage core and

excludes the majority of lymphocytes from the centre of the structure. Concomitant with this transition is a marked reduction in the number of blood vessels penetrating the granuloma. At this stage there is a noticeable increase in the number of foamy macrophages responsible for the accumulation of caseous debris in the centre of the granuloma, which portends progression to active disease. Although *M. tuberculosis* bacilli are unable to multiply within this caseous tissue, due to its acidic pH, low availability of oxygen, and the presence of toxic fatty acids, some organisms may remain dormant there for decades.

The strength of the host's cell mediated immunity (CMI) determines whether an infection is arrested here or progresses to the next stages. With good CMI, the infection may be arrested permanently at this point. The granulomas subsequently heal, leaving small fibrous and calcified lesions. However, if CMI is insufficient, macrophages containing ingested but viable *M. tuberculosis* organisms may escape from the granuloma via the intrapulmonary lymphatic channels. This results in the rapid spread of the infection to the regional hilar lymph nodes. As disease progresses further, the semisolid caseous, necrotic centre of the granuloma liquefies and cavitates spilling thousands of infectious virulent bacilli into the airways. This damage to the lungs triggers development of a productive cough facilitating generation of the infectious aerosol and completion of the bacterium's life cycle resulting in relatively large areas of necrotic debris, each surrounded by a layer of epithelioid histiocytes and multinucleated giant cells. At this stage, effective antibiotic therapy is required for patient survival survive.

1.1.3. Post-primary tuberculosis

There are two routes to a repeat episode of TB (post-primary pulmonary TB): either by reactivation of a dormant primary lesion or by inhalation of additional *M. tuberculosis* organisms. In post-primary TB, infection proceeds in spite of existing immunity.

M. tuberculosis bacilli can persist for decades in a dormant state inside a granuloma, particularly in the apical regions of the lung. Reactivation of these latent organisms can also lead to post-primary disease, even in persons who successfully fought their initial battle against TB. The mechanisms which govern dormancy and reactivation, within either the organism or the host, are not yet understood. The host typically mounts an inflammatory response to reactivation TB, with the lesion appearing circumscribed and necrotic. Reactivation TB that progresses to the cavitary stage favors the propagation of virulent and drug resistant strains, as the increased oxygen concentration allows multiplication of the organisms producing large numbers that are thought to be necessary for the evolution of drug resistance mutants (Nardell, 1993).

In recurrent exposure to *M. tuberculosis*, a hypersensitivity reaction is the characteristic response, accompanied by tissue necrosis and caseation. Lymphocytes and other cells converge upon the site and form a wall of fibrous tissue in an attempt to seal off the necrotic site (Spencer, 1985). Some lymphatic spread may occur, but in this case, the hilar lymph nodes are not implicated. Most often, caseated granulomas heal over time, shrinking as they become fibrotic and then calcified. However, if healing is impaired, the growing lesions may erode adjacent bronchi, resulting in the formation of cavities in which *M. tuberculosis* organisms

multiply freely, leading to huge numbers of bacilli (Nardell, 1993). An open cavitated lesion can leak infectious material directly into the bronchus, resulting in the continuous discharge of bacilli into the sputum (Spencer, 1985). Leaked *M. tuberculosis* bacilli can also be inhaled into other portions of the host's lungs, resulting in tuberculous bronchopneumonia. If the growing granulomatous lesion erodes the wall of a vein, organisms can spread in the circulating blood, resulting in miliary disease (Hopewell, 1994).

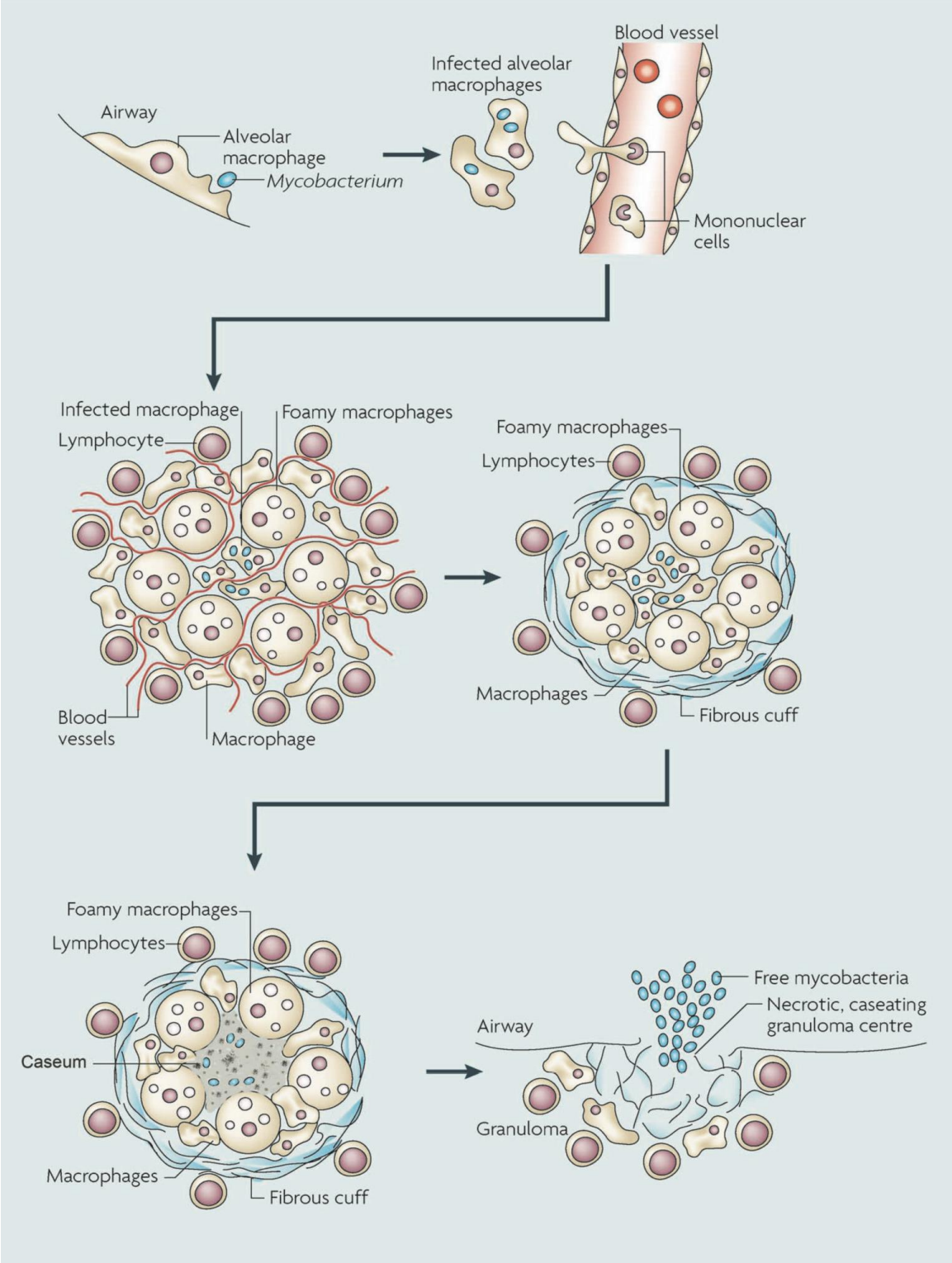

Figure1.2. Histological progression of the human tuberculosis granuloma (adapted from Russel *et al*., 2009).

1.1.4. Drug treatment of TB

Since the control measures for TB such as Bacillus Calmette-Guerin (BCG) vaccination and chemoprophylaxis appear to be unsatisfactory, treatment with anti-tubercular (anti-TB) drugs is the only option available. The principal objective of chemotherapy in TB patients is the eradication of the whole bacillary load (Petrini and Hoffner, 1999). Modern therapy relies on a combination of potent bactericidal agents, such as isoniazid, rifampicin, pyrazinamide and ethambutol in a treatment with six month duration. In some instances, there can be an initial resistance of the bacillus to isoniazid, making it necessary to add streptomycin to the treatment. In the case of MDR-TB, in which the virulent bacilli is resistant to at least rifampicin and isoniazid (Telenti and Iseman, 2000), the treatment period is extended, and frequently relies on the use of more side effect-associated second-line drugs.

First-line drugs are mainly bactericidal, and combine a high degree of efficacy with a relative low toxicity to the patient during treatment; these include isoniazid, rifampicin, streptomycin, ethambutol, and pyrazinamide. Second-line drugs are mainly bacteriostatic, have a lower efficacy and are usually more toxic; these include para-aminosalicylic acid, ethionamide, and cycloserine among others (Cohn *et al*. 1997). Effective TB chemotherapy must include early bactericidal action against rapidly growing organisms and subsequent sterilization of dormant populations of bacilli.

The first-line drugs exhibit early bactericidal activity against actively metabolizing bacilli and the bacteriostatic second-line drugs are reserved for treatment in the advert of resistance. Among all first-line anti-TB agents, isoniazid has the greatest bactericidal activity against microorganisms growing actively in cavities, followed by

rifampicin, streptomycin. However, isoniazid frequently causes fever, and is one of the drugs with the highest degree of toxicity (Morehead, 2000). Although TB is a serious illness, it can be cured in most new cases as long as, once diagnosed, appropriate chemotherapy is employed.

The treatment currently recommended by the WHO consists of the combined administration of isoniazid, rifampicin, pyrazinamide and streptomycin (or ethambutol) during the first 2 months, followed by the combination of isoniazid and rifampicin for at least 4 additional months (Table 1.1). This revolutionary treatment aims initially at a bacteriostatic action, inhibiting the synthesis of cell wall, nucleic acids and mycobacterial proteins (Figure 1.3), and, thereby, leading to a rapid elimination of most part of the infecting bacilli. The therapy also aims at a subsequent bactericidal action to consolidate the treatment through the elimination of all remaining bacilli.

	Initial phase	**Continuous phase**
Duration	Two months	Four months
Antibiotics (Dose)	• Rifampicin (450-600 mg) • Isoniazid (300 mg) • Ethambutol (15 mg/kg) • Pyrazinamide (1.5-2 g)	• Rifampicin (450-600 mg) • Isoniazid (300 mg)
Frequency	Daily	Daily

Table 1.1. Anti-tuberculosis drug regime (British National Formularly, 2011).

WHO invested in universal treatment adherence programs, through a process currently known as the directly observed treatment short-course (DOTS), where health care workers counsel patients, perform progress surveillance, and make sure that each medication dose is correctly taken (NSB Editorial Comment, 2000). DOTS strategy prevents the occurrence of new infections and, more importantly, makes MDR/XDR-TB generation impractible. However, TB continues to be a leading killer of humans worldwide (WHO, 2011). The long treatment period and the associated side effects of the administered drugs lead to patient non-compliance, infection recurrence, increased mortality rates and development of drug-resistance.

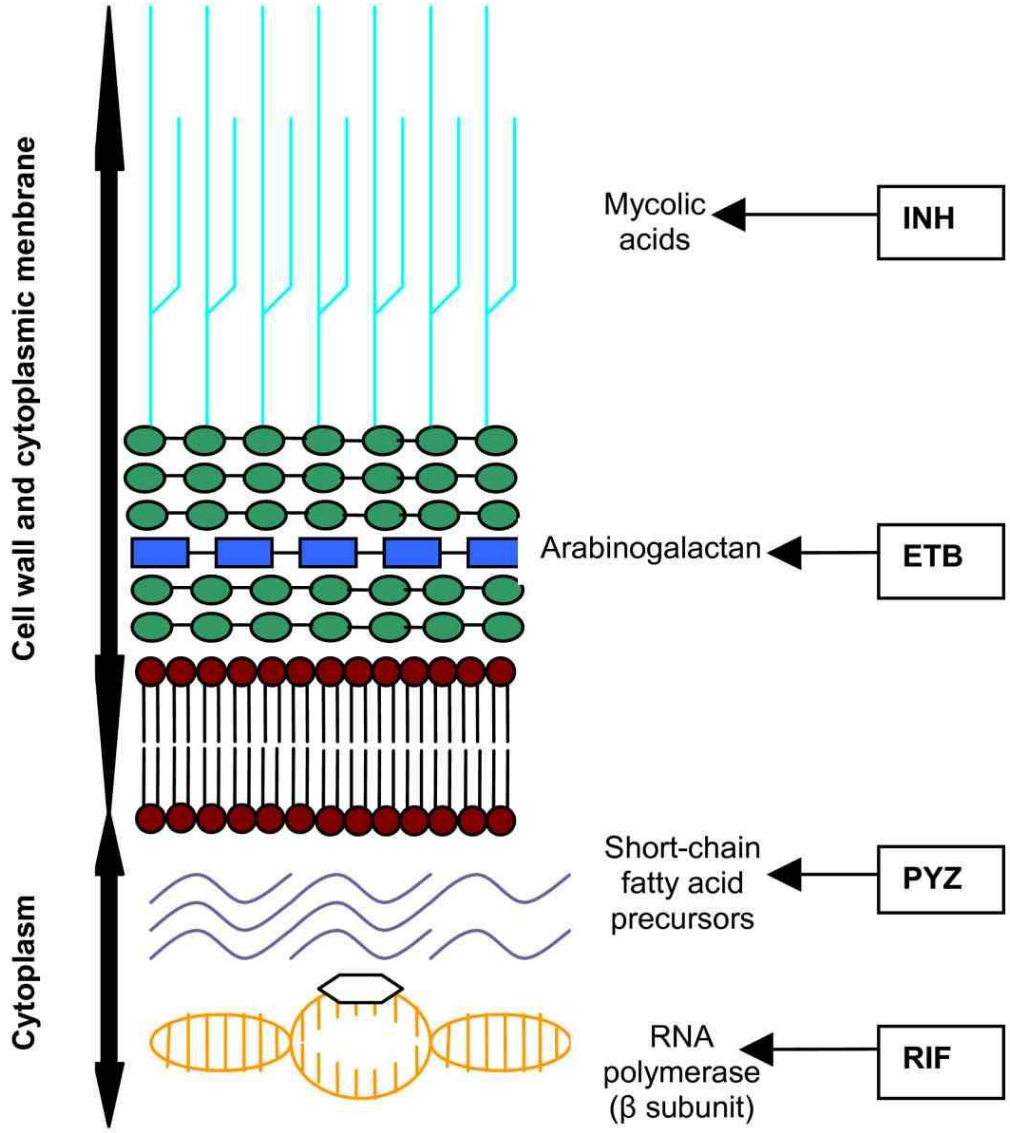

Figure 1.3. Sites of action of the principal anti-TB drugs (adapted from Du Toi *et al*., 2006)

1.2. Pulmonary drug delivery

Local delivery of drugs to the lower respiratory tract by aerosol inhalation is highly desirable in patients with pulmonary diseases like asthma (Georgitis, 1999), chronic obstructive pulmonary disease (COPD) or cystic fibrosis (Touw *et al*., 1995). This route of administration is characterised by the rapid response which is achieved by the delivery of the drug in close proximity to its intended site of action. In addition, the inhaled route allows the local administration of smaller doses compared to delivery by the oral route, thereby reducing the potential incidence of adverse systemic effects and reducing drug costs (Guo *et al. 2005*).

1.2.1. Structure and physiology of the airways

The human respiratory system can be divided in two functional regions: the conducting airways and the respiratory region (Figure 1.4). The conducting airways, which are composed of the nasal cavity and associated sinuses, the pharynx, larynx, trachea, bronchi, and bronchioles, filter and condition the inspired air. From trachea to the periphery of the airway tree, the airways repeatedly branching dichotomously into two daughter branches with smaller diameters and shorter length than the parent branch (Weibel, 1991). For each new generation of airways, the number of branches is doubled and the cross sectional area is exponentially increased. The conducting region of the airways generally constitutes generation 0 (trachea) to 16 (terminal bronchioles). The respiratory region, where gas exchange takes place, generally constitutes generation 17-23 and is composed of respiratory bronchioles, the alveolar ducts, and the alveolar sacs. The number of times the bronchial tree

branches before the gas exchange area is reached can vary from as few as 6 to as many as 28-30 (Plopper, 1996).

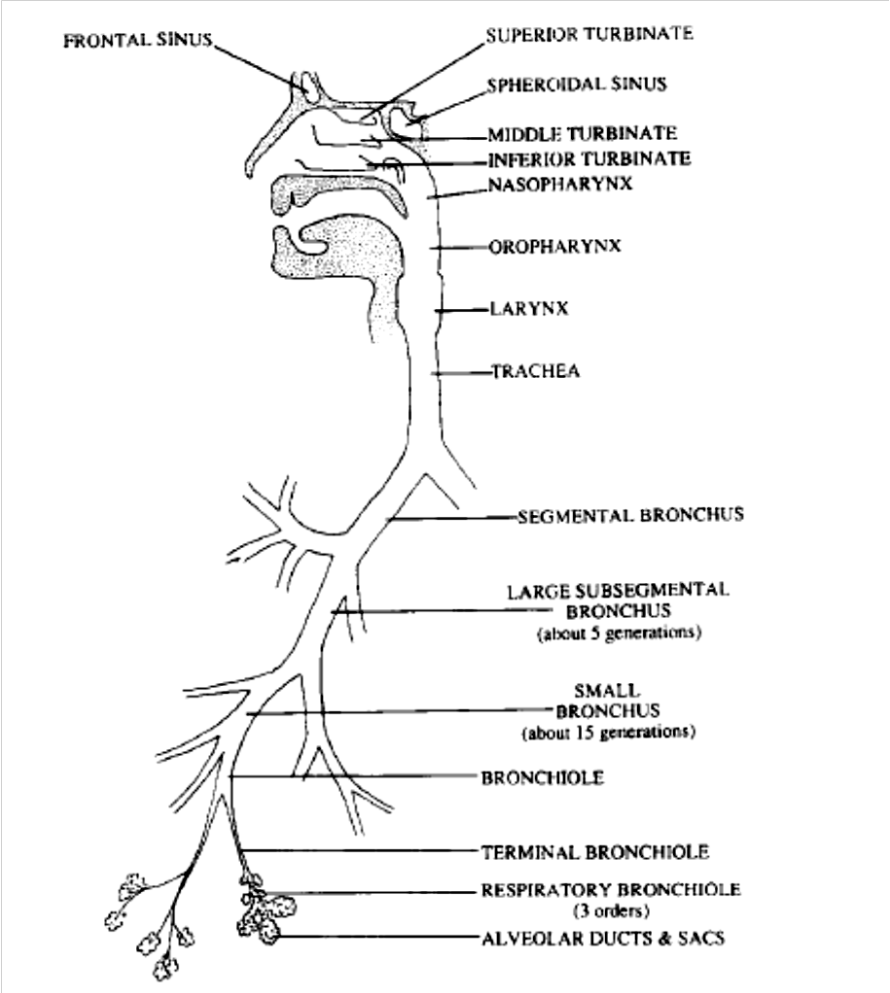

Figure 1.4. The human respiratory tract (Lansley, 1993)

The human airway epithelium consists of a pseudostratified layer composed of at least six distinct epithelial cell types: ciliated cells, mucous goblet cells, Clara cells, serous cells, basal cells, and granulated cells. Cellular composition of the epithelium varies substantially at different levels of the lung between the trachea and the terminal bronchioles. The human airway epithelial surface principally comprises

ciliated cells, which are the most abundant cell at all levels of the airways. In the higher airways, the ciliated cells are interspersed by secretory cells, mainly mucus-secreting goblet cells. At lower levels the ciliated cells are interspersed mainly by Clara cells (Forbes, 2000). Diagrammatic representations of the typical epithelium in the higher airways, at the bronchiolar level, and in the alveolar region are illustrated in Fig.1.5.

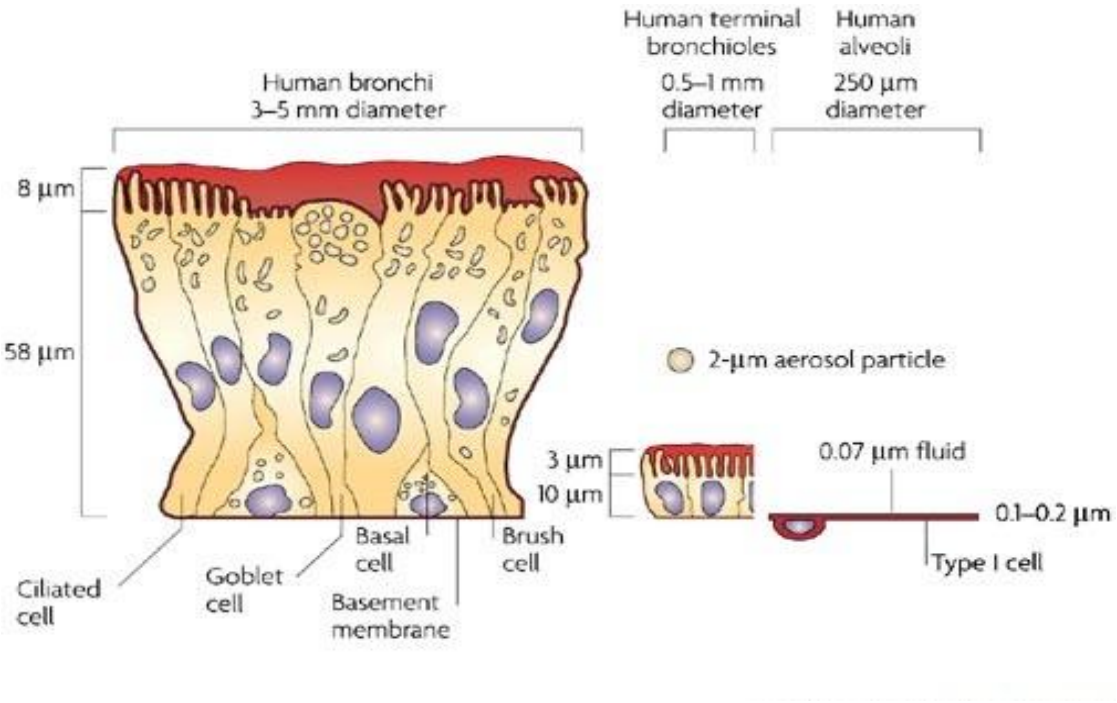

Figure 1.5. Comparison of the lung epithelium at different sites within the lungs (adapted from Patton and Byron, 2007).

1.2.2. Particle deposition in the airways

During inhalation, drug particles are transported into the airways within inspired air. A proportion of the particles travelling through the respiratory system will be trapped after coming into contact with the wet airspace surfaces, a phenomenon which is called deposition (Schultz *et al*., 2000). Particle deposition is complex and depends

on particle properties (e.g. size, shape, density, and charge), respiratory tract morphology, and the breathing pattern (e.g. airflow rate and tidal volume) (Heyder *et al*., 2002). These parameters determine not only the quantity of particles that are deposited but also in what region of the respiratory tract the particles are deposited. As the cross-sectional area of the airways increases, the airflow rate rapidly decreases, and consequently the residence time of the particles in the lung increases from the large conducting airways towards the lung periphery (Schulz *et al*., 2000).

The most important mechanisms of particle deposition in the respiratory tract are inertial impaction, sedimentation, and diffusion. Inertial impaction occurs predominantly in the extrathoracic airways and in the tracheobronchial tree, where the airflow velocity is high and rapid change in airflow direction occurs (Schulz *et al*., 2000). The mass median aerodynamic diameter (MMAD) is considered to be the most important physical parameter influencing particle deposition in the lungs (Schulz *et al*., 2000). Generally, particles with a diameter larger than 10 μm are most likely deposited in the extrathoracic region, whereas 2- to 10 μm particles are deposited in the tracheobronchial tree by inertial impaction (Schulz *et al*., 2000). A long residence time of the inspired air favours particle deposition by sedimentation and diffusion (Heyder *et al*., 2002). Sedimentation is of greatest importance in the small airways and alveoli and is most pronounced for particles with a diameter of 0.5-2 μm (Schulz *et al*., 2000). Sub-micron particles (<0.5 μm in diameter) are deposited mainly by diffusional transport in the small airways and lung parenchyma where there is a maximal residence time of the inspired air (Heyder *et al*., 2002). The

relationship between particle size and total respiratory tract deposition has been demonstrated to be similar among species (Schlesinger, 1996).

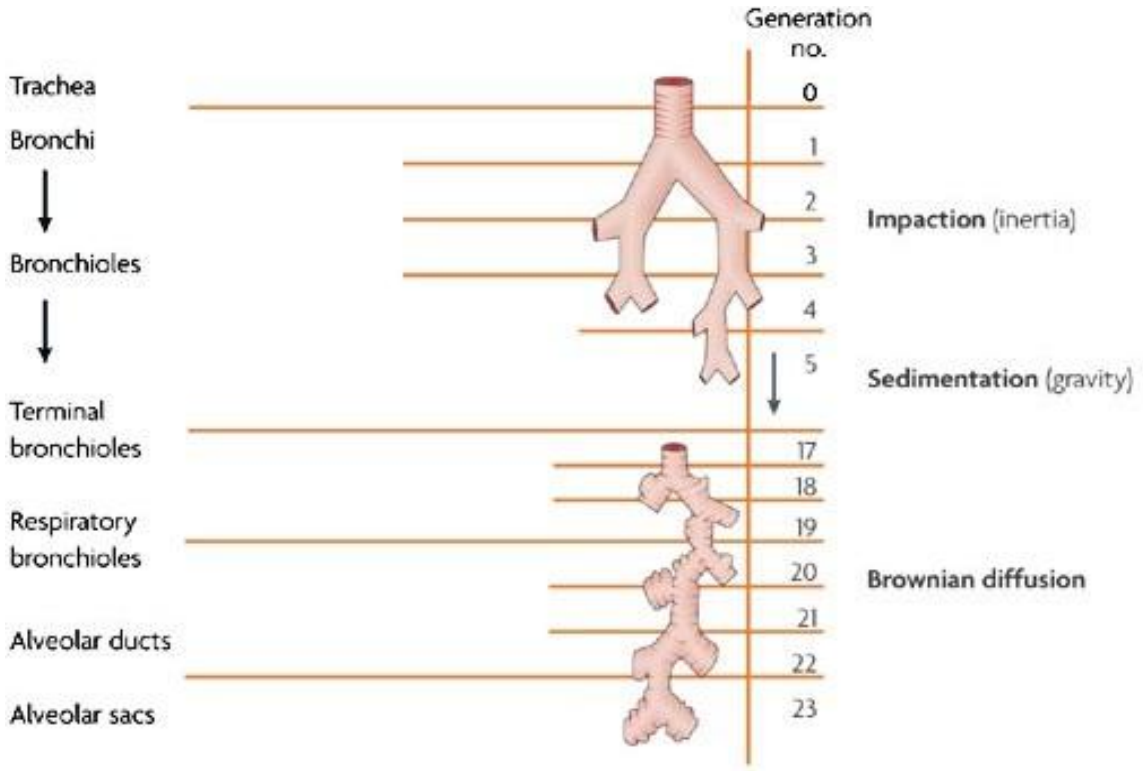

Figure 1.6. The deposition of inhaled particles in the lungs (adapted from Patton & Byron, 2007).

1.2.3. The fate of particles in the airway

1.2.3.1. The mucociliary clearance

The mucociliary clearance is one of the most important mechanical host defense in the lung. By the coordinated movements of cilia, mucus is swept out of the nasal cavity and lungs, respectively, towards the pharynx where it is swallowed. In the nose, clearance rates of 3-25 mm/min have been shown in normal subjects (Mygind *et al.,* 1998). There is an inverse relationship between mucus velocity and airway generation, which relates to the lower percentage of ciliated cells, shorter cilia, lower ciliary beat frequency, and lower number of secretory cells in the peripheral airways. The thickness of the mucus layer varies along the conducting being about 8 μm in the trachea and about 2 μm in the bronchioles (Mercer *et al.,* 1992). The mucus layer is continuous in the larger human bronchial airways, but consists of discontinuous rafts in the smaller bronchi and bronchioles (Mercer *et al.,* 1992). The surface liquids of the ciliated airways are composed of two phases: an aqueous periciliary phase of epithelial lining fluid close to the cell surface in which the cilia beat, plus a gel phase of mucus on top of the aqueous phase. A phospholipid layer between the phases lowers the surface tension between them (Samet *et al.,* 1994). Mucus is secreted primarily from the serous cells of submucosal glands and from goblet cells, and is composed of water (95%), glycoproteins (mucins) (2%), proteins (1%), inorganic salts (1%), and lipids (1%) (Samet *et al.,* 1994). Regulation of the water content is of importance to maintain the optimal viscoelastic properties of the mucus.

1.2.3.2. Alveolar clearance

Alveolar macrophages are found on the alveolar surface. These phagocytic cells play important roles in the defense against inhaled bacteria and particles that reach the alveoli. Particles deposited in the lung parenchyma of rabbits and rats have been demonstrated to be phagocytized by alveolar macrophages within a few hours. The macrophages are cleared from the alveoli to the bronchioles by the lining fluid, and then from the airways by the mucociliary escalator (Jeffery, 1995).

1.2.3.3. Enzymatic activity

The lung presents lower enzymatic activity when compared to other mucosal surfaces, such as those found in the gastro-intestinal tract (Evora *et al.,* 1998). However, some enzymes have already been identified including; protease inhibitors and isozymes of the cytochrome P450 family (Patton and Platz, 1992), which are most concentrated in clara cells, Type 2 cells and to a lesser extent in alveolar macrophages. Lysozyme is a 14.5 kDa cationic enzyme which is synthesized and released by the human surface epithelial cells, as well as pulmonary alveolar macrophages (Duszyk, 2001). Other enzymes include esterases, peptidases, UDP-glucuronosyl transferases and sulphotransferases (Lombry *et al,.* 2004).

1.3. Nanoparticle drug delivery systems

1.3.1. Definition

Nanoparticles are defined simply as solid, colloidal particles that vary in size from 10 to 1000 nm (Sanjeeb *et al*., 2003). A therapeutic agent may be dissolved, entrapped, adsorbed, attached or encapsulated into the nanoparticle matrix. Depending on their structure, nanoparticles can be further classified as either nanospheres (NS) or nanocapsules (NC) (Figure 1.7). Nanospheres are matrix systems in which the therapeutic agent is physically and uniformly dispersed, whereas nanocapsules are vesicular systems in which the drug is confined to a cavity surrounded by a polymer membrane (Sanjeeb *et al*., 2003). Nanoparticles can be made from biocompatible and biodegradable materials such as solid lipids or polymers which may be natural (e.g. gelatin) or synthetic (e.g. poly (lactide)) (Soppimath *et al*., 2001). Liposomes, nanovesicular structures produced from natural phospholipids, are the most widely investigated delivery system for phagocyte-targeted therapies (Kelly *et al*., 2010). However, it is beyond the scope of this review to describe these nanoparticulate systems and highlight their advantages and method of manufacture.

High carrier capacity, high stability and the feasibility of incorporating both hydrophobic and hydrophilic drugs are among the important technological advantages of nanoparticles as drug carriers. In addition, it has been claimed that the clearance of drug-loaded nanoparticles from the lung can be minimized to enhance drug retention at topical sites (Schurch *et al*., 1990). Such properties make nanoparticles a very attractive delivery vehicle for the treatment of pulmonary TB.

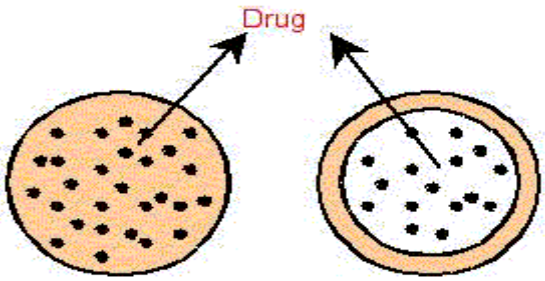

(a) **(b)**

Figure 1.7. Schematic representation of the two classes of nanoparticles: (a) nanospheres (matrix systems in which the therapeutic agent is physically and uniformly dispersed), (b) nanocapsules (vesicular systems in which the drug is confined to a cavity surrounded by a unique polymer membrane) (Adapted from Sanjeeb *et al*., 2003).

1.3.2. Manufacture of polymeric nanoparticles

1.3.2.1. Emulsification-solvent evaporation

The emulsification-solvent evaporation method was the first method used to prepare biodegradable and injectable lattices by Gurny *et al*. (1981). Briefly, this method is carried out by dissolving the drug and polymer are in a volatile, water immiscible organic solvent such as dicholoromethane, chloroform or ethyl acetate. The emulsion is prepared by adding water and a surfactant to the polymer solution. The nanosized polymeric droplets are induced using high energy homogenization or sonicator. The organic phase evaporation is achieved using a rotary evaporator or by continuous stirring and the nanoparticles are collected by centrifugation or lyophilisation (Cheng *et al*., 1998).

1.3.2.2. Solvent displacement and interfacial deposition method

One of the easiest and reproducible techniques for preparing nanoparticles is the solvent displacement (also called nanoprecipitation) method developed by Fessi *et al.* (1989) which has been widely used to prepare nanoparticles. The method is based on the precipitation of preformed polymer following displacement of a semi-polar solvent miscible with water in the presence or absence of surfactant. The basic principle of this technique is similar to spontaneous emulsification of the organic phase containing drug and polymer into the external aqueous phase. In brief, both the polymer and drug are dissolved in a water miscible organic solvent (polymer solvent phase) of intermediate polarity (e.g. acetone and ethanol). The resulting organic phase is injected into a stirred aqueous phase (non-solvent phase) containing a surfactant as stabilizer. The nanoparticles are formed instantaneously during the rapid diffusion of the organic phase into the aqueous phase. Parameters affecting the physicochemical properties of the prepared nanoparticles include: miscibility of the organic solvent with the nonsolvent; nature of the polymer solvent interactions and concentration of the polymer in the organic phase.

1.3.2.3. Emulsification–solvent diffusion

The emulsification solvent diffusion or emulsification-solvent displacement method is the most widely used method for preparing nanoparticles due to several advantages. These include high drug entrapment efficiency for poorly water soluble drugs, narrow particle size distribution, high batch-to-batch reproducibility, no requirement for homogenization, simplicity, ease of scale up and rapid organic solvent extraction (Moinard-Chécot *et al*., 2006). The drug and polymer are dissolved in a partially

water soluble solvent. The organic phase is saturated with water to ensure the initial thermodynamic equilibrium. It is then diluted with an extensive amount of pure water to facilitate diffusion of the organic solvent from the organic phase droplets leading to the precipitation of the polymer. The aqueous phase may contain surfactants while the organic phase sometimes contains an emulsifier. Finally, the solvent is eliminated by evaporation or filtration, depending upon the boiling point. Several parameters can affect the size of the nanoparticles such as miscibility of the water with the organic solvent, stirring rate, concentration of the surfactant(s) and concentration of the polymer is the organic phase.

1.3.2.4. Salting out method

The salting-out procedure can be considered as a modification of the emulsification/solvent diffusion method (Galindo-Rodriguez *et al*., 2004). The separation of a water miscible solvent from aqueous solution is achieved via a salting-out effect. Briefly, a water miscible organic solvent, usually acetone, containing polymer and drug is added drop wise to an aqueous phase saturated with an electrolyte or non-electrolyte (such as magnesium chloride, calcium chloride or sucrose) with a colloidal stabilizer (such as polyvinyl pyrrolidone) under agitation to form an o/w emulsion. A sufficient volume of water is added to enhance the diffusion of acetone to the water phase and NSs are thus obtained. The technique offers advantages such as the avoidance of chlorinated solvents and surfactants, minimization of stress, useful for heat-sensitive substances, high encapsulation efficiency and easy scaling up. The method is not popular because of the extensive

washing steps required to achieve purity of the nanoparticles and the possibility of incompatibility between drugs and salts.

1.3.2.5. Polymerization method

In the polymerization method, monomers are polymerized to form nanoparticles in aqueous solution. The polymerization method can be classified into emulsion and interfacial polymerization. The emulsion polymerization method is the fastest and most scalable method of producing nanoparticles. It can be classified into two categories; continuous organic phase or continuous aqueous phase methodology depending on the use of the continuous phase. In general, the monomer is dissolved into an organic or aqueous continuous phase. Additional monomer molecules are then emulsified into the emulsion droplets and stabilized by surfactant. The polymerization is started by chemical initiation, pH shift or by irradiation of gamma, ultraviolet or visible rays. In the continuous phase, chain growth starts when the initiated monomer ions or monomer radicals collide with each other to form aggregates which are stabilized by polymeric emulsifier particles.

1.3.3. Anti-TB drugs encapsulation into nanoparticles

The encapsulation of anti-TB drugs in nanocarriers has a number of advantages. These include improved stability of these drugs against degradation, minimized toxicity, improved bioavailability by reducing fluctuations in therapeutic ranges, controlled release and reduced dosing frequency, which may resolve the problem of non-adherence to prescribed therapy and improve patient compliance (Gelperina *et al*., 2005).

Several studies reported the efficacy of anti-TB drug-loaded nanoparticles administered orally, subcutaneously or intravenously. Pandey *et al.,* (2003) administered poly (DL-lactide-co-glycolide) (PLG) nanoparticles encapsulated with three front-line anti-tubercular drugs subcutaneously to mice. They showed that therapy with drug-loaded PLG nanoparticles resulted in undetectable bacterial counts in the lungs and spleen of infected mice. The particle preparation showed a better chemotherapeutic efficacy compared with a daily drug treatment. A similar study was performed by Johnson *et al*. (2005) in which treatment using nanoparticle encapsulated and non-encapsulated drugs significantly reduced the bacterial count and lung histopathology. However, the nanoparticle formulation was administered every 10 days and may lead to better patient compliance compared to nonencapsulated formulations. In another study Pandey et *al.* evaluated the efficiency of oral encapsulated ethambutol in combination with PLG nanoparticles loaded with rifampicin, isoniazid and pyrazinamide in a murine tuberculosis model. The study concluded that the combination of 4-drugs in a nanoprticluate formulation had the potential to shorten the duration of TB chemotherapy besides reducing the dosing frequency.

These studies showed that that the delivery of anti-TB drugs incorporated in nanoparticles is a promising alternative to conventional oral drug delivery to achieve better patient compliance. The obtained results in the TB management using nanoparticles might be due to different effects. It is possible that the constant drug plasma levels are more effective than fluctuating drug plasma levels after oral administration of free drugs, or even that a small nanoparticle accumulation in the lungs might produce an effective increase in local drug concentration. Combined with

a controlled release of the therapeutic agent, this undetectable local drug targeting might be the key advantage considered by nanoparticle formulation.

1.4. Pulmonary delivery of nanoparticles

1.4.1. Local delivery of anti-TB drugs

The lung is the primary, if not the sole, portal of entry for mycobacteria that cause TB. In addition, more than 80 % of TB cases present exclusive pulmonary infection. High chemotherapeutic doses are required, but only a small fraction of the total dose reaches the lungs after oral administration. Even this small fraction is cleared in few hours explaining the need to administer anti-TB on a daily basis. Clearly, the local delivery of these drugs via inhalation offers a number of advantages over the systemic route. Exposing the mycobacteria in the lung to high drug concentrations maximises the chances of complete eradication of the virulent bacilli.

Moreover, the lung mucosa represents a large surface from which drugs may be systemically absorbed into the bloodstream (Mathias *et al.,* 2010). During the process of systemic absorption from the lungs, drugs introduced into this organ provide early and high concentrations within it. This is advantageous if, as in pulmonary TB, the lungs are the target site of drug delivery. In addition, lung macrophages are efficient at fulfilling their role of phagocytosing material entering the lungs. It has long been established that particulate (Moller *et al*., 2001; Evora *et al.,* 1998) or vesicular (Myers *et al.,* 1993; Shephard *et al.,* 1981) drug delivery systems introduced into the deep lung are likely to be taken up up by alveolar macrophages (AM) (Sibille *et al.,* 1990). Finally in addition to accumulating drug at

the site of infection, it has been argued that uptake of drug delivery systems by infected macrophages effects rescue of the macrophage from 'alternative activation,' (Kahnert *et al.,* 2006) enabling the elaboration of innate bactericidal responses (Sharma *et al.,* 2007).

1.4.2. Method of delivering nanoparticles to the lungs

1.4.2.1. Delivery of nanoparticle suspensions via nebulisation

One method for the delivery of nanoparticles is nebulization of a nanoparticle suspension using a nebulizer. Yamamoto *et al*. (2005) prepared surface modified PLGA NSs with chitosan to improve the pulmonary delivery of calcitonin by mucoadhesion after deposition in the lungs. They administered nanoparticles into the trachea of guinea pigs using a nebulizer and showed that chitosan modified PLGA NSs-loaded with elcatonin, reduced blood calcium levels by 80% of the initial calcium concentration. The treatment also prolonged the pharmacological action for up to 24 h, which when compared to unmodified NSs was significantly longer. They attributed these results to the retention of NSs by adhesion to the bronchial mucus and lung tissue combined with a sustained drug release at the adherence site. In another study, McConville *et al.* (2006) formulated itraconazole nanoparticles using either evaporative precipitation into an aqueous solution (EPAS) or spray freezing into liquid (SFL) technologies. They demonstrated that nanoparticles of itraconazole, a poorly water-soluble drug, can be dispersed into aqueous liquid and nebulized effectively to the lungs using a murine model which resulted in high drug concentrations in the lungs. They showed that local delivery of itraconazole

nanoparticles is a promising alternative to oral or intravenous administration, thus potentially decreasing the incidence of side effects associated with a high drug serum concentration (McConville *et al*., 2006).

With regard to TB, Pandey *et al.* (2003) studied different routes for administration of treatment. They compared different routes of administration with aerosol delivery of anti-tubercular drugs (rifampin, isoniazide and pyrazinamide) using loaded to PLG nanoparticles in guinea pigs. The animals were treated with either a free drug orally or intravenously administered, nebulized drug-loaded PLG nanoparticles and nebulized empty PLG nanoparticles at the same dose. They sprayed the nanoparticle suspensions using a saline solution and a compressor powered-nebulizing system with an exposure time of 3-4 min/ animal. The results showed that plasma Tmax and AUC were much higher for the nebulized PLG nanoparticles compared to oral or intravenous administration. In their study, they showed that five doses every ten days of nebulized drug-loaded nanoparticles had the same effect as 46 daily oral doses. No colony-forming unit (cfu) count was detected in previously infected guinea pigs. They repeated the study but instead of PLG nanoparticles they used solid lipid nanoparticles incorporating three major anti-TB drugs, rifampicin, isoniazid and pyrazinamide. They showed that after a single nebulization to guinea pigs, drugs levels were maintained in plasma for 5 days and in the organs (lungs, liver and spleen) for 7 days, whereas the free drugs were cleared by 1–2 days. Also their study showed that mean residence time and bioavailability improved using nebulized nanoparticles. They showed that tubercle bacilli could not be detected in the lungs/spleen of infected guinea pigs after 7 doses of treatment every 7 days whereas 46 daily doses of orally administered drugs were required to obtain the

same therapeutic benefit. Therefore nebulization of nanoparticles containing anti-tubercular drugs improves the bioavailability and reduces the dosing frequency for better management of pulmonary TB. Taking the results of the oral nanoparticle administration into account (discussed in Section 1.2.3) both results confirm that an improved drug delivery of the anti-TB drugs can be linked to the use of a nanoparticle based delivery system.

However in spite of their initial promising results, the potential of these systems is limited by the nanoparticle instability in aqueous medium. Indeed, during storage aqueous suspensions of these colloidal particles present some disadvantages such as polymer hydrolysis leading to drug leakage and physicochemical instability due to the particle agglomeration and sedimentation. Therefore, the application of an effective technique or principle capable of prolonging the shelf life of these particles is of a considerable benefit (Pandey *et al., 2003)*.

1.4.2.2. Delivery of nanoparticles using dry powder carriers

Pulmonary delivery of nanoparticles via different dry powder formulations has gained more attention in recent years. Since nanoparticles are in a size range which is not suitable for deep lung delivery, the major challenge for pulmonary delivery of nanoparticles is to find a proper carrier system. Several researchers have prepared carrier systems for nanoparticles to improve the delivery of nanoparticles to the alveolar area. Kawashima *et al*. used ultrafine hydrophilic particles, hydroxypropylmethyl cellulose phthalate (HPMCP) nanospheres, to improve the aerosolization properties of a dry powder inhalation of a hydrophobic drug, pranlukast hydrate. In their study they prepared a drug containing HPMCP

nanospheres and then mixed the surface modified drug powder dispersion with lactose and then spray- or freeze-dried the suspension to obtain a dry powder. This powder was mixed with larger lactose particles for better dispersion when used in an inhaler. They performed an in vitro inhalation test using a twin impinger and showed that the inhalation properties of the surface modified powder dramatically improved. They showed that the emission of the powder increased two fold and that the dry powder delivery to the deep lung might increase 3 fold compared to the original unmodified powder. They attributed this improvement to the increased surface roughness and hydrophilicity of the surface-modified particles, which resulted in an increased dispersibility in air. Tsapis *et al.* (2002) developed large porous carriers of nanoparticles for pulmonary drug delivery. They used a spray drying technique to produce large porous particles (LPP) which have extremely thin walled structures. They added two different surfactants, 1, 2-dipalmitoyl-sn-glycero-3-phosphocholine (DPPC) and 1,2-dimyristoyl-sn-glycero-3-phophoethanolamine (DMPE), and lactose to the nanoparticles suspension and spray dried the mixture. The particles were made from nanoparticles which attached to each other via lactose and the surfactants when spray dried. They showed that the spray dried powder has suitable characteristics for pulmonary delivery and can be re-dissolved in a mixture of ethanol/water (Tsapis *et al*., 2002)

The concept of administering nanoparticles incorporated into a carrier matrix for lung delivery was first introduced by Shama *et al*. (2005) for the preparation of the carrier powder containing nanoparticles (gelatin or iso-butyl cyanoacrylate), they dissolved lactose as a carrier powder in a nanoparticle suspension and spray dried it. They showed that the particle size of the nanoparticles before and after spray drying might

change significantly due to the heat involved in the spray drying process. This study proved the possibility of delivering and releasing nanoparticles in the lungs for applications such as treatment of lung cancer, cystic fibrosis or asthma (Azarmi *et al., 2008*).

Grenha *et al*. (2005) incorporated insulin loaded chitosan nanoparticles in microspheres using aerosol excipients like lactose and mannitol by means of a spray drying technique for pulmonary delivery as a dry powder. They showed that the microencapsulation process does not affect the insulin release from nanoparticles. They propose this method for systemic delivery of macromolecules through the pulmonary route of administration to promote peptide absorption (Grenha *et al.,* 2005).

1.4.3. *In vitro* measurement of particles aerodynamic diameter for aerosol systems

Inertial impaction is the standard method to measure the particle or droplet aerodynamic size from pharmaceutical aerosol delivery systems (Barry *et al*.,1999). It describes the phenomenon of the deposition of aerosol particles on the walls of an airway conduct. The impaction tends to occur where the airway direction changes. The big particles have high momentum (inertia) and are more likely to travel in the initial direction of airflow, while those with low momentum adjust to the new direction of flow and pass around the obstruction. Inertial impaction employs Stokes' law to determine the aerodynamic diameter of particles being evaluated. This has the advantage of incorporating shape and density effects into a single term (Hickey, 2008).

1.5. Aim and scope of the thesis

The failure of anti-tubercular chemotherapy is mainly due to poor patient compliance, which is attributed to the requirement for multidrug administration daily for at least six months. The high frequency of pulmonary TB demands the development of novel drug delivery approaches that enhance the bioavailability of drugs in the lungs. In recent years, one of the best ways to achieve higher sustained drug levels in the lungs has been the development of particulate-based formulations that are directly delivered to the lungs via the inhaled route. Nanoparticles represent a class of drug delivery vehicles which can serve as promising vehicles for ferrying large doses of the drug to the target site with interception of minimal side effects. As a drug delivery carrier they offer several advantages, such as ease of purification and sterilization, possibility of drug targeting, and a sustained release action. However, a possible obstacle to using nanocarriers for pulmonary delivery is that their MMAD is too small for extensive particle deposition in the lungs.

The overall aim of this thesis was to develop novel PVA nanoparticles for the pulmonary delivery of rifampicin for the treatment of *Mycobacterium* Tuberculosis. The limitations of delivering nanoparticles to the lungs will be solved by incorporating the developed rifampicin-loaded PVA nanoparticles in an inert carrier to produce particles in the micrometer size of a suitable size for deposition in the alveolar regions of the lungs. The formulation was designed such that after deposition in the lung, the carrier matrix will dissolve readily releasing the nanoparticles, which will deliver the therapeutic payload in a controlled manner. It was hypothesized that uptake of the nanocarriers by AMs will result in rifampicin delivery directly to the infected reservoir.

The specific objectives of this thesis were as follows:

1. To develop and characterise novel rifampicin-loaded PVA nanocarriers.
2. To evaluate the biocompability and interaction of the nanocarriers with macrophage-like cells.
3. To encapsulate the nanocarriers into microspheres and characterise the dry powder formulation for pulmonary delivery.

Chapter TWO

Rifampicin analysis

2.1. Introduction

Rifampicin, the key component in the combination treatment of TB and leprosy recommended by the World Health Organization (WHO, 2003; Venkatesan, 1989), was used in this thesis as a clinically relevant model drug to investigate nanomedicines. High Performance Liquid Chromatography (HPLC) was employed throughout the thesis for the analysis of this drug and monitoring of its degradation. In this Chapter, the method development for this technique is outlined. It was anticipated that the HPLC method would be applied in a number of important subsequent experiments to address the main aims of the thesis. Drug stability in different matrices and drug solubility at different pHs were also investigated to underpin key analytical procedures such as drug loading and release studies which are crucial when delivering medicines using colloids.

Rifampicin (Figure 2.1) is a complex semi-synthetic macrocyclic antibiotic derived from *streptomyes mediterranei*. It is a member of the rifamycin class of antibiotics used for treatment of TB, staphylococcal endocarditis, osteomyelitis and chemoprophylaxis of meningitis caused by Haemophilus influenza (Mandell *et al.,* 1985). Depending on its indication, the dose varies from 10 mg/kg daily to 15 to 30 mg/kg divided into three doses for other uses (British National Formulary, 2011).

Rifampicin is amphoteric with a pKa_1 of 1.7 (4-hydroxyl group) and a pKa_2 of 7.9 (3-piperazine nitrogen) (Oppolzer and Prelog., 1973; Pelizza *et al*., 1977). It is a hydrophobic drug (Log P 3.179) with low solubility and high permeability and hence it

is classified as a class II drug in the Biopharmaceutical Classification System (BCS) (Kasim *et al*., 2004). Rifampicin chemical stability and its pH dependent solubility are two major factors contributing to its low bioavailability and poor therapeutic outcomes (Agrawal *et al*., 2002).

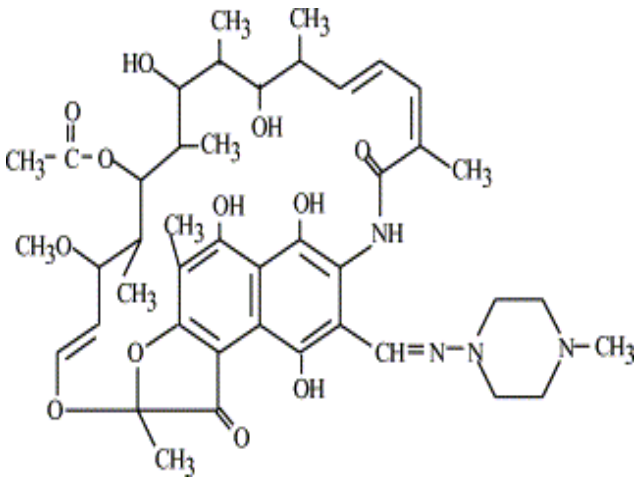

- Molecular formula: $C_{43}H_{58}N_4O_{12}$
- MW: 822.96
- Melting point: 183-188 ^{o}C
- Log P: 3.179
- pKa: 1.7, 7.9

Figure 2.1. Chemical structure and summary of the physico-chemical characteristics of rifampicin

Rifampicin exists in aqueous solutions as a zwiterrion with an iso-electric point of 4.8 (Maggi *et al*., 1966; Fourie *et al*., 1999; Howes *et al*., 2007). At basic pH values a zwitterionic agent behaves primarily as an acid whereas at low pH values it behaves as a base. A number of studies have reported the solubility of RFP at 37^{0}C in buffered media of different pHs (Table 2.1) (Mariappan and Singh, 2003; Agrawal and Panchagnula, 2005). However, these studies did not appear to consider the influence of chemical degradation. Rifampicin is known to form a number of degradants in the solution state (Bain *et al*., 1998; Gharbo *et al.,* 1989; Seydel, 1970; Nahata *et al*., 1994). Two major decomposition products exist: 3-formylrifamycin SV

(RSV) and rifampicin quinone (RQU) formed by hydrolysis and oxidation respectively (Seydel, 1970). RSV, which results from the hydrolysis of the 4-methylaminopiperazine moiety in acidic medium, is insoluble and has poor absorption (Maggi *et al*., 1966). It shows high antimicrobial activity *in vitro* (Maggi *et al*., 1965) but it is inactive *in vivo* (USP DI, 1996). RQU, which is formed in alkaline medium in the presence of oxygen, is purple and inactive, due to the fact that the free hydroxyl groups on C1 and C8 are essential for binding the drug to bacteria (Foye *et al*., 1995). A third decomposition product 25-desacetylrifampicin (DAR) is formed in alkaline medium in the absence of oxygen. The two agents 25-desacetyl-21-acetylrifampicin (25-21) and 25-desacetyl-23-acetylrifampicin (25-23), formed sequentially from DAR, both have negligible antimicrobial activity (Gallo and Radaelli, 1968). HPLC has been used to analyse the stability of RFP (Bain *et al*., 1998; Nahata *et al*., 1994).

Reference	pH	Medium	Solubility (mg/ml)
Mariappan and	1.0	HCl, NaCl, H_2O	127.21
Singh, 2005	1.5	HCl, citric acid, NaOH, NaCl, H_2O	42.68
	2.0	HCl, citric acid, NaOH, NaCl, H_2O	19.21
	2.5	HCl, citric acid, NaOH, NaCl, H_2O	3.19
	5.5	NaCl, Na2HPO_4,H2O	0.64
	7.0	NaCl, Na_2HPO_4,H_2O	0.85
Agrawal and	1.4	HCl solution	125.54
Panchagnula,	2.0	HCl solution	11.40
2004	2.3	HCl solution	11.40
	3.0	Sodium citrate/citric acid buffer	1.15
	3.5	Sodium citrate/citric acid buffer	0.75
	4.0	Sodium citrate/citric acid buffer	0.99
	4.5	Sodium citrate/citric acid buffer	1.25
	5.2	Phosphate buffer	1.53
	6.0	Phosphate buffer	1.65
	6.8	Phosphate buffer	2.54
	7.4	Phosphate buffer	3.35
	8.0	Phosphate buffer	5.44

Table 2.1. Literature Data for the Solubility of Rifampicin at 37^{o}C

The aim of the Chapter was to establish HPLC techniques for rifampicin quantification, solubility testing and chemical degradation assessment. It was anticipitated that these methods would be applied to address the main aims of the thesis. The specific objectives of this Chapter were:

- To develop and prove 'fit for purpose' an HPLC method for the quantification of rifampicin.
- Determine the solubility of rifampicin in aqueous solutions of different pHs.
- Establish the effect of a number of experimental conditions on rifampicin recovery.
- To develop and prove 'fit for purpose' an HPLC method for the co-analysis of rifampicin and RSV

2.2. Materials

Rifampicin (95% pure) was purchased from Sigma-Aldrich (UK) and 3-formylrifamycin SV was from the British Pharmacopoeia Commission Laboratory (UK). L-Ascorbic acid, sodium citrate dehydrate, citric acid and butylhydroxytoluene were obtained from Sigma-Aldrich (UK). Phosphate Buffered Saline tablets were from Oxoid Ltd (UK). Acetonitrile (HPLC grade) and methanol were purchased from Rathburn Chemicals Ltd (UK) and VWR International Ltd (UK).

2.3. Methods

2.3.1. HPLC analysis of rifampicin

HPLC quantification of rifampicin was performed using a 600 HPLC pump (Waters, UK) with a 717 auto-sampler (Waters, UK) and a 2487 dual λ absorbance detector (Waters, UK). The column used was a reversed-phase C18 (250 x 4.6 mm). UV-photodiode array detection was performed at 254 nm. The mobile phase consisted of acetonitrile: citrate buffer (35:65 % v/v) at a flow rate of 1 ml/min. Final pH of the mobile phase was adjusted to 6.2 by diluted hydrochloric acid. Column temperature was set to 28°C and a 10 µl sample injection volume was employed throughout.

Calibration standards were produced using a 1 mg/ml rifampicin stock solution in acetonitrile (containing 0.02% w/v butylhydroxytoluene (BHT) to avoid drug oxidation). Six serial dilution of the rifampicin stock generated calibration standards in the range of 1-0.01 mg/ml. Calibration plots were constructed for rifampicin in standard solutions by plotting the concentration of compound versus peak area response. The linearity of the calibration plots were evaluated using least square regression analysis. Three calibration curves were run on a single day to determine the intra-day sample variance; this data was combined with two additional calibration curves on two further days to determine the inter-day sample variance.

Precision and accuracy were calculated according to equations 2.1 and 2.2:

$$precision = \left(\frac{sd}{Mean} \right) \times 100 \qquad (2.1)$$

$$Accuracy = \left(\frac{A}{T}\right) \times 100 \quad (2.2)$$

where sd is the standard of deviation; Mean is the mean peak area; T is the theoretical concentration of analyte and A is the actual concentration of analyte. Limits of detection (LOD) and quantification (LOQ) were calculated according to equations 2.3 and 2.4:

$$LOD = Y_B + 3s_B \quad (2.3)$$

$$LOQ = Y_B + 10s_B \quad (2.4)$$

where S_B is the standard error of the y estimate and Y_B is the intercept from the regression equation. Peak symmetry (A_s) was calculated according to equation 2.5:

$$As = \frac{W_{0.05}}{2d} \quad (2.5)$$

where $W_{0.05}$ is the width of the peak at one-twentieth of the peak height and *d* the distance between the perpendicular dropped from the peak maximum and the leading edge of the peak at one-twentieth of the peak height. Theoretical plate number (N) was calculated according to equation 2.6:

$$N = 5.54\left(\frac{t}{W_{h/2}}\right)^2 \quad (2.6)$$

where $W_{h/2}$ is the width of the peak at half the peak height and *t* the retention time of the peak.

2.3.2. Determination of rifampicin aqueous solubility

A series of rifampicin saturated aqueous solutions at different pHs (pH 2.5-7.4, citric acid-phosphate buffer, 0.5 M) were prepared by adding an excess of drug to a 15 ml scintillation glass vials containing 10 ml buffer. The suspensions were agitated for 24 hours and hydrochloric acid was used to adjust any pH drift when appropriate. The samples were filtered using 0.2 µm cellulose acetate syringe filter (Fisher scientific, Leicestershire, UK), diluted using mobile phase and analysed by HPLC. All samples were stored under light protected conditions at ambient temperature (23 ± 2^{o}C) during the solubility study (*n = 3*).

The percentage of rifampicin ionisation values for rifampicin's two functional groups (4-hydroxy group and 3-piperazine nitrogen group) at each test pH were calculated using Eq. (2.7 and 2.8). A pKa of 1.7 was used for the 4-hydroxy group and 7.9 for the 3-piperazine nitrogen group:

$$Ionisation\ \%\ (3-piperazine\ nitrogen) = \frac{10^{pka-pH}}{1+10^{pka-pH}} \quad (2.7)$$

$$Ionisation\ \%\ (4-Hydroxy\ group) = \frac{10^{pH-pKa}}{1+10^{pH-pKa}} \quad (2.8)$$

where Ionisation% was the percentage of a functional group ionisation in an aqueous solutions at different pHs and the pKa was the dissociation constant.

2.3.3. Chemical stability of rifampicin

The chemical stability of rifampicin was determined in the absence and presence of an anti-oxidant in aqueous solutions. Either 0.02 or 0.2 % w/v of ascorbic acid were added to a 1 mg/ml solution of rifampicin in PBS buffer (pH 7.4). The solutions were constantly stirred and at pre-determined time point (0, 6, 24, 48 and 72 h), samples were withdrawn from the solutions, diluted using mobile phase and analysed by HPLC. All samples were stored under light protected conditions at ambient temperature (23 ± 2^{o}C) during the stability study (*n = 3*). The effect of rifampicin concentration and temperature on drug stability was also investigated by using two drug concentrations of rifampicin (1 mg/ml and 0.01 mg/ml) containing 0.02 % w/v ascorbic acid at two different temperatures, ambient temperature (23 ± 2^{o}C) and 37^{o}C.

The hydrolysis of rifampicin was also investigated in PBS buffer (pH 7.4). For the co-analysis of rifampicin and RSV, a second HPLC method was developed. Analysis was performed using a 600 HPLC pump (Waters, UK) with a 717 auto-sampler (Waters, UK) and a 2487 dual λ absorbance detector (Waters, UK). The column used was a reversed-phase C18 (250 x 4.6 mm). UV-photodiode array detection was performed at 240 nm. The mobile phase consisted of acetonitrile: PBS buffer (36:64 % v/v) at a flow rate of 1.4 ml/min. Final pH of the mobile phase was adjusted to 7.5 by diluted hydrochloric acid. Column temperature was set to 28°C and 10 µl of samples was injected to the HPLC system. Calibration standards were produced by making up a stock solution in acetonitrile containing 1 mg/ml rifampicin and 1 mg/ml RSV (0.02% w/v butylhydroxytoluene (BHT) to avoid drug

oxidation). Six serial dilutions were used to produce calibration standards in the range of 1-0.01 mg/ml. Calibration plots were constructed for rifampicin and RSV in standard solutions by plotting the concentrations of the compounds versus peak area response. The linearity was evaluated by linear regression analysis, which was calculated by the least square regression method. Three calibration curves were run on a single day to determine the intra-day variance; this data was combined with two additional calibration curves on two further days to determine the inter-day variance. Precision and accuracy were calculated according to equations 2.1 and 2.2. Limits of detection (LOD) and quantification (LOQ) were calculated according to equations 2.3 and 2.4.

2.3.4. Data analysis and statistics

All data was expressed as mean ± standard deviation (S.D.) Statistical analysis was performed in SPSS, version 16.0, using either student *t*-test or an analysis of variance (ANOVA) with the chosen level of significance at $p \leq 0.05$.

2.4. Results

2.4.1. HPLC analysis of rifampicin

A single peak was eluted in the HPLC chromatogram (Figure 2.2) with a retention time of 6.66 ± 0.3 min (*n*=210). The peak shape had a high degree of symmetry (A_s ranged from 0.88 to 1 (*n*=10)) and column efficiency remained constant throughout the study, N=650 ± 27 (*n*=10, two from each of the five calibration runs). The calibration curve displayed excellent linearity over the concentration range of 1-0.01 mg/ml, with correlation coefficient of >0.999 for the peak area calculations (Figure 2.3).

The calculated LOD value was 5.4 µg/ml while the LOQ was 18 µg/ml using peak area. The results obtained for assay precision and accuracy are presented in Table 2.1. The data illustrates that precision of the peak area measurements was very similar at all concentrations. The method has an average of 1.4 ± 0.9% for intra-day precision, 1.9 ± 0.8% for inter-day precision and a 99.5 ± 1.9 % mean accuracy (Table 2.2).

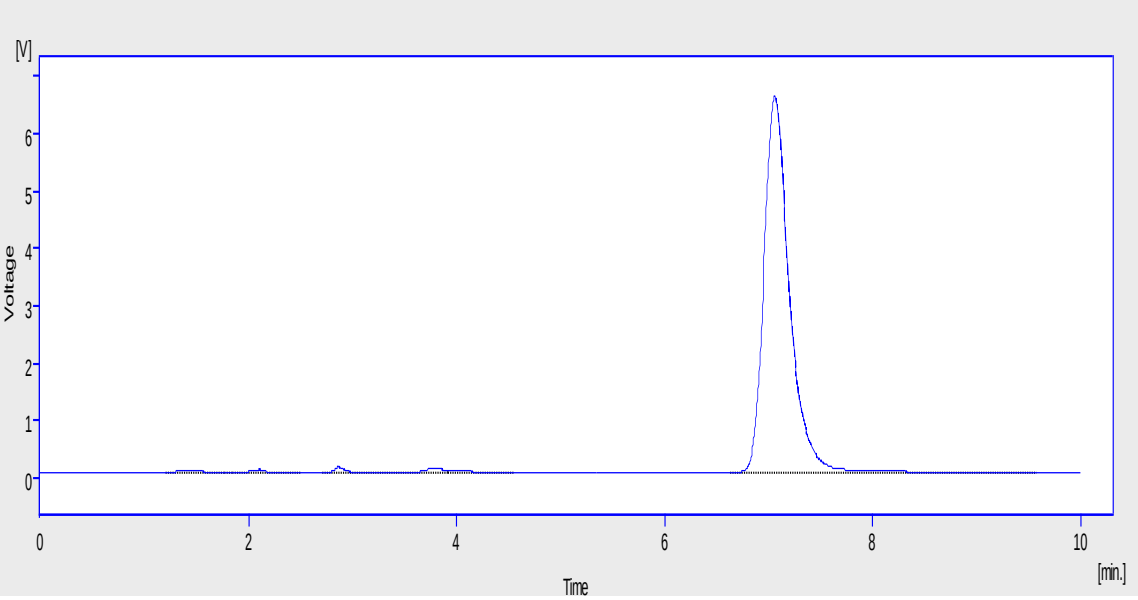

Figure 2.2. Typical high performance liquid chromatography chromatogram of a rifampicin standard (rifampicin 1 mg/ml in acetonitrile with 0.02% w/v butylhydroxy butolene) detected at 254 nm.

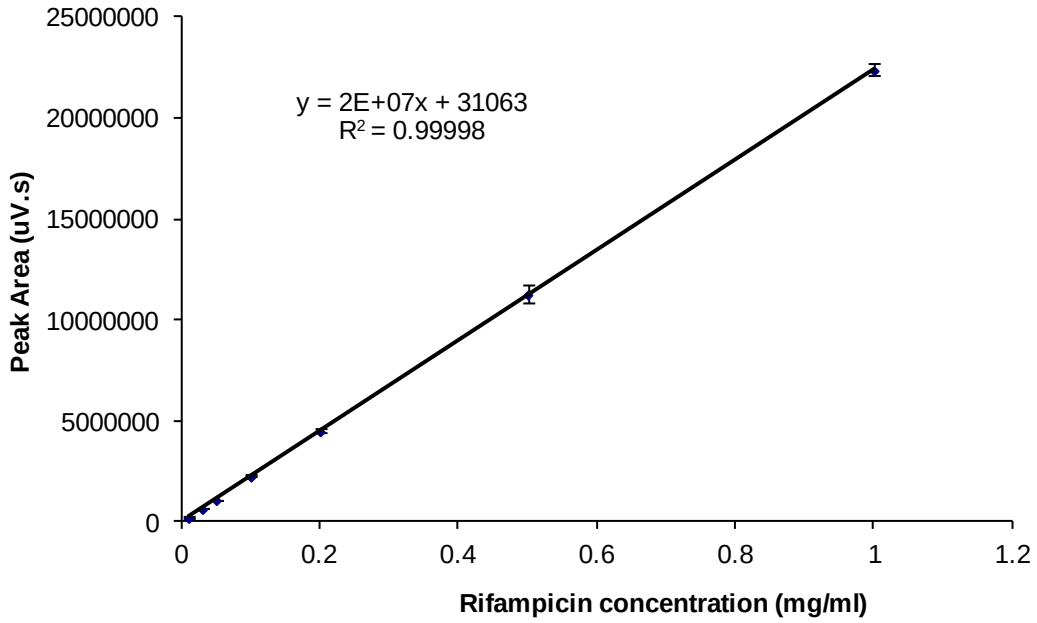

Figure 2.3. Calibration curve for the HPLC assay for rifampicin. Data represent mean ± sd, *n*=5 calibration curves (each each calibration curve having 6 analyses at each concentration).

Calibration standards (mg/ml)	Intra-day		Inter-day	
	Precision (% RSD)	Accuracy (% recovery)	Precision (% RSD)	Accuracy (% recovery)
1	0.77	99.6	1.69	100.1
0.5	2.72	101.8	2.13	99.1
0.2	0.70	98.1	2.60	102.0
0.1	2.54	100.9	2.72	101.5
0.05	0.62	97.7	1.14	97.8
0.03	0.79	97.9	0.85	96.8

Table 2.2. Inter- and intra-day variation in the HPL assay for rifampicin based on peak area (intra-day: 3 x calibration curves on day 1, inter-day: 3 x calibration curves on days 1, 2 and 3 respectively, *n=6* at each concentration).

2.4.2. Aqueous solubility of rifampicin

In the pH range of 2.5- 4.5, the aqueous solubility of rifampicin decreased as the pH of the aqueous vehicle in which it was dissolved increased (Table 2.3). In contrast, in the pH range of 4.5-7.4, the drug aqueous solubility increased as the pH increased (Figure 2.4). The lowest rifampicin aqueous solubility (0.75 mg/ml) was obtained at pH 4.5, where both functional groups are fully ionised.

PH	Grp	1	2	3	4	5	6	7	8	9	10	11	12
% ionisation	-OH	17	67	95	100	100	100	100	100	100	100	100	100
	-NH	100	100	100	100	100	99	89	44	7	1	0	0

Table 2.3. The inonisation percentages of the two functional groups at different pHs

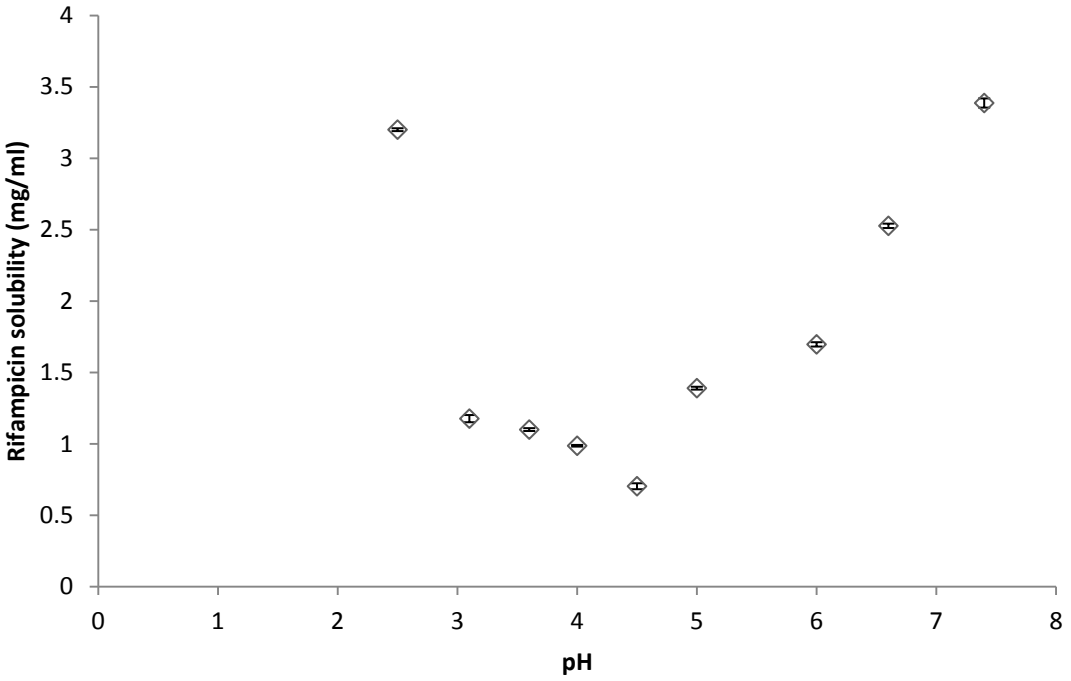

Figure 2.4. The aqueous solubity of Rifampicin at different pHs *(n=3)*

2.4.3. Chemical stability of rifampicin

In the absence of the anti-oxidant, rifampicin (1 mg/ml) recovery at PBS buffer pH 7.4 decreased by approximately 24% over 72 hr (Table 2.4). The addition of ascorbic acid (0.02% w/v) significantly increased rifampicin recovery ($p < 0.05$) Further increase of the anti-oxidant concentration to 0.2 % w/v had no significant effect on the drug recovery.

Rifampicin degradation at pH 7.4 was concentration dependant (table 2.5). At higher concentration (1 mg/ml) in the presence of an anti-oxidant (0.02 % w/v), rifampicin recovery was 88.3 ± 2.14 %. At lower concentration (0.01 mg/ml), rifampicin

degradation rate was significantly higher, 66 ± 2.1 %. The temperature also seems to have a significant effect on the rate of rifampicin degradation (Table 2.5).

Time (h)	Rifampicin recovery (%)		
	0 % w/v	**0.02 % w/v**	**0.2 % w/v**
0	99.2 ± 0.82	99.9 ± 0.95	99.8 ± 0.64
6	92.3 ± 1.36	96.7 ± 1.05	97.7 ± 1.35
24	86.0 ± 1.12	94.3 ± 1.42	93.3 ± 1.55
48	82.6 ± 1.89	91.6 ± 1.92	92.6 ± 1.83
72	76.3 ± 1.20	88.3 ± 2.14	89.3 ± 1.94

Table 2.4. Percentage recoveries of rifampicin (1 mg/ml) at ambient temperatures over 72 h in the presence of different amounts of ascorbic acid, (*n=3*).

Time (hrs)	Rifampicin recovery (%)			
	25°C		**37°C**	
	1 mg/ml	**0.01 mg/ml**	**1 mg/ml**	**0.01 mg/ml**
0	99.9 ± 0.95	96.9 ± 2.4	101.9 ± 4.4	97.3 ± 1.8
6	96.7 ± 1.05	93.5 ± 0.1	99.6 ± 4.6	92.6 ± 1.8
24	94.3 ± 1.42	86.5 ± 1.9	96.7 ± 4.2	68.7 ± 1.2
48	91.6 ± 1.92	72.5 ± 0.5	92.9 ± 4.4	59.1 ± 4.5
72	88.3 ± 2.14	66.0 ± 2.1	89.7 ± 4.6	54.6 ± 8.0

Table 2.5. Percentage recoveries of rifampicin at 25°C and 37°C over 72 hr, *n=3* at each concentration)

For the co-analysis of rifampicin and RSV two peaks were eluted in the HPLC chromatogram with retention times of 5.81 ± 0.4 min (*n*=210) for rifampicin and 9.66 ± 1.5 min (*n*=210) for RSV. The peaks shapes had a good degree of symmetry (A_s ranged from 0.81 to 1 (*n*=20)) and column efficiency remained constant throughout the study, N=545 ± 36 (*n*=20, Four from each of the five calibration runs). The calibration curves were linear over the concentration range of 1-0.03 mg/ml, with correlation coefficients of >0.999 for the peak area calculations for both rifampicin and RSV (Figure 2.5). The calculated LOD values were 2.8 µg/ml and 1.2 µg/ml, for rifampicin and RSV, respectively. The LOQ values were 10.2 µg/ml and 8.4 µg/ml, for rifampicin and RSV, respectively. The precision and accuracy were very similar at all concentrations (tables 2.6 and 2.7).

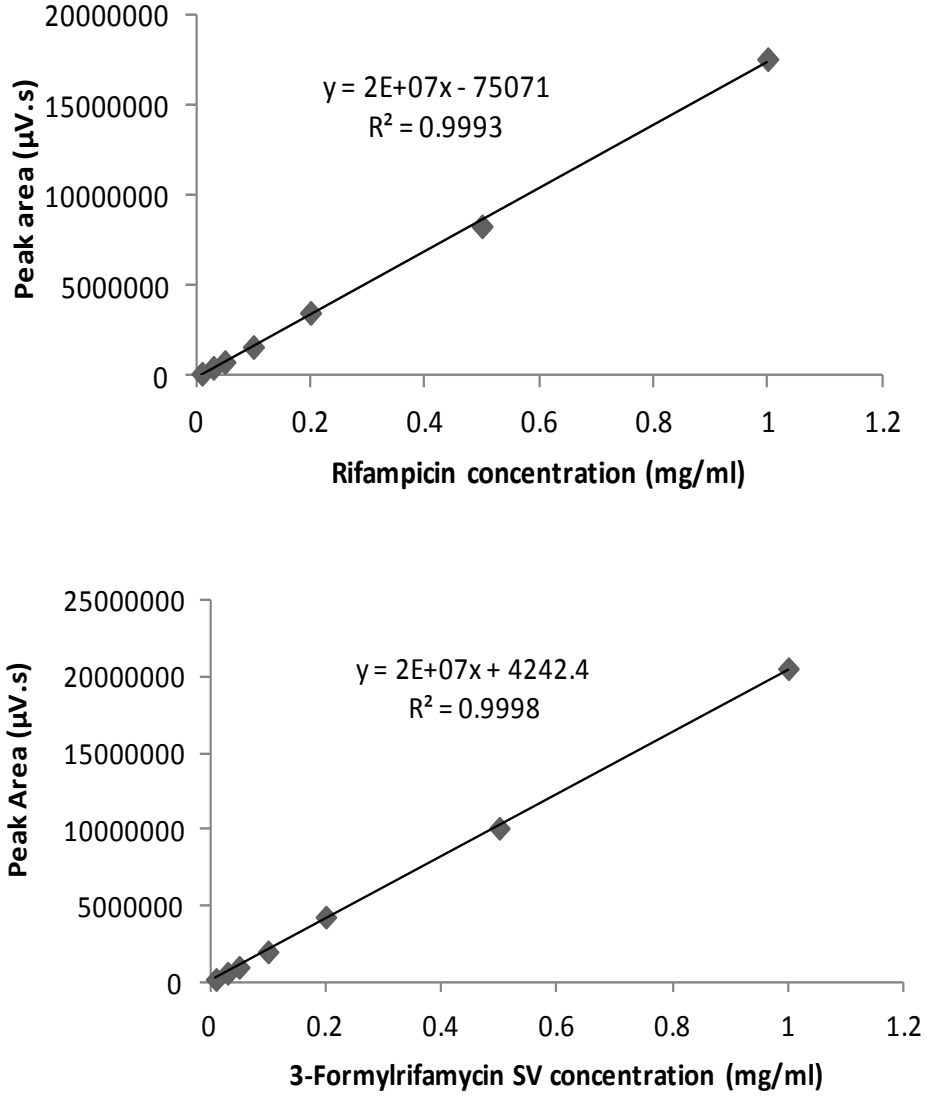

Figure 2.5. Summation of the area of five calibration curves (*n=6* for each concentration of each calibration curve) for the peak area calculations for rifampicin and RSV (data represent mean ± sd, *n*=5)

Calibration standards (mg/ml)	Intra-day precision and accuracy		Inter-day precision and accuracy	
	R.S.D %	Recovery %	R.S.D %	Recovery %
1	0.87	101.3	0.99	101.8
0.5	1.02	99.3	1.53	102.5
0.2	0.92	100.1	2.43	100.4
0.1	0.97	99.2	2.15	102.2
0.05	1.12	100.9	1.45	97.4
0.03	0.84	97.3	1.56	96.4

Table 2.6. Inter- and intra-day variation in the rifampicin assay based on peak area (intra-day: 3 x calibration curves on day 1, inter-day: 3 x calibration curves on days 1, 2 and 3 respectively, *n=6* at each concentration).

Calibration standards (mg/ml)	Intra-day precision and accuracy			Inter-day precision and accuracy		
	Mean Conc. (mg/ml) (n=18)	R.S.D %	Recovery %	Mean Conc. (mg/ml) (n=18)	R.S.D %	Recovery %
1	0.981	1.44	99.6	0.996	2.57	99.9
0.5	0.492	1.68	101.1	0.484	1.38	101.9
0.2	0.199	2.17	98.7	0.201	1.58	102.6
0.1	0.991	1.68	99.0	0.098	0.91	99.7
0.05	0.048	0.89	98.6	0.049	1.25	98.5
0.03	0.031	1.39	97.3	0.028	0.96	97.9

Table 2.7. Inter- and intra-day variation in the RSV assay based on peak area (intra-day: 3 x calibration curves on day 1, inter-day: 3 x calibration curves on days 1, 2 and 3 respectively, *n=6* at each concentration)

Rifampicin hydrolysis was investigated in PBS buffer (pH 7.4) over 72 h at room temperature. As it can be seen from figure 2.6 rifampicin concentration was decreased from 0.78 mg/ml to 0.65 mg/ml over a 72 h period. In contrast, RSV concentration was increased from 0.05 mg/ml to 0.14 mg/ml.

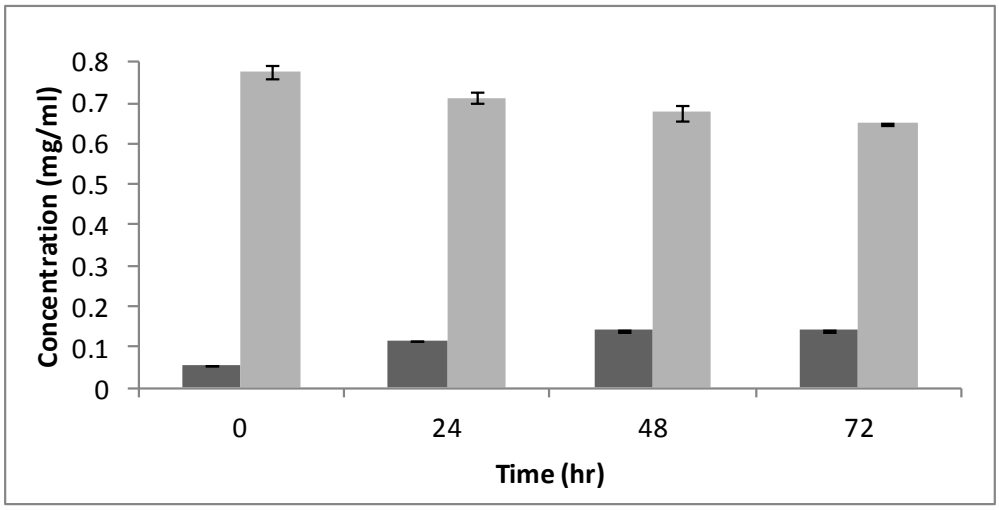

Figure 2.6. The hydrolysis of rifampicin (0.8 mg/ml) in phosphate buffer (pH 7.4) over 72 h at ambient temperature, r*ifampicin (grey) and RSV (black)* (*n=3).*

2.5. Discussion

The aim of the Chapter was to establish HPLC techniques for rifampicin analysis, solubility testing and chemical degradation assessment. In the first HPLC assay, the hydrophobic C_{18} column and the polar mobile phase employed were found to be appropriate for the separation of rifampicin. There was a good linearity for the concentration range studied, acceptable limit of detection and quantification. The mean accuracy, the intra and inter-day variation all complied with the acceptance criteria proposed in harmonised analytical guidelines (R.S.D.: not more 2.0%, recovery: 100 ± 2 %) (Drugs Directorate, 1994). The rapidity, the simplicity and efficacy of the developed method as well as the short retention time of RFP permit the analysis of a large number of samples in a short time period providing a fast and inexpensive method for RFP quantification in this project.

The rifampicin solubility at 37^0C in buffered media of different pHs correlated well with the ionisation profiles of the two functional groups 4-hydroxyl group and piperazine groups. At pH 1 to 4 rifampicin behaves as a base as the number of ionised piperazine groups is higher than the number of ionised 4-hydroxyl groups. At pH range of 4 to 6 both functional groups are ionised which makes the molecule neutral with a low aqueous solubility. Rifampicin exhibited minimal solubility (0.7 mg/ml) at pH 4.5. At pH 6 to 12 rifampicin behaves as an acid. The trend of our solubility data also correlated well with the previous data reported (Mariappan and Singh, 2003; Agrawal and Panchagnula, 2005). The differences in values reported could be due to of the different polymorphic forms used. Additionally, the pH was maintained constant throughout this study, while this was not documented in other studies. This data obtained suggests that pH alteration can be used to modify drug-

solvent interactions. In previous work this has been used to facilitate drug loading into nanocarriers (Govender *et al*., 1999; Zhao *et al*., 2010).

The extent of chemical degradation was investigated in a number of different aqueous matrices over a period of 72 h. These matrices varied in the concentration of the anti-oxidant, drug concentration and temperature. Rifampicin degradation was shown to be accelerated at lower concentrations. The change in temperature also seems to have a significant effect on the rate of rifampicin degradation. The addition of ascorbic acid (0.02% w/v) significantly increased rifampicin recovery by in comparison with the control (without antioxidant) during the 72 h study. This data suggests that ascorbic acid, at a concentration of 0.02% w/v, should be used in aqueous solutions in order to retard drug oxidation. Bain *et al*. (1989) showed that ascorbic acid had the greatest activity ($t_{1/2}$ = 69.3h) in preventing oxidation of rifampicin to RQU in comparison with sodium metabisulphate (($t_{1/2}$ = 4.85h) and the control ($t_{1/2}$ = 2.45h). This previous work showed that 0.1% w/v was adequate for anti-oxidant protection (Bain *et al.,* 1998). High antioxidant was required in the previous study as the experiments were run for few weeks (Bain *et al.,* 1998). Despite the presence of the anti-oxidant, only 88.3 ± 2.14 % was recovered after 72 h storage at ambient temperature, which suggests the presence of second degradation pathway other than oxidation.

For the co-analysis of rifampicin and its hydrolysis degradant RSV, a second HPLC method was developed. The use of a C_{18} stationary phase packing and the simple mobile phase of pH7.5 resulted in adequate resolution of both RFP and RSV whilst maintaining acceptable analysis times. There was a good linearity for the

concentration range studied, with correlation coefficients greater than 0.999. The calculated LOD and LOQ values for rifampicin and RSV were acceptable. The mean accuracies, the intra and inter-day variation all comply with the acceptance criteria proposed (R.S.D.: not more 2.0%, recovery: 100 ± 2 %)(Drugs Directorate, 1994).

Rifampicin hydrolysis is claimed to occur in acidic condition (Gharbo *et al*., 1989; Seydel, 1970; Krubenberg *et al.,* 1996; Nahata *et al*., 1994; Prankerd *et al*., 1992). However, it was shown that the reduced recovery of rifampicin was associated with the formation of RSV at pH 7.4 (37^{o}C) over 72 h period. This provides some evidence that hydrolysis was occurring at pH 7.4 and hence the HPLC method developed for the co-analysis of rifampicin and RSV will be employed in subsequent chapters for the quantification of rifampicin and its degradant. Since rifampicin degrades rapidly rapidly in aqueous solution, fresh calibration standards were prepared on the day of every experiment and constructed calibration curves will be checked for consistency throughout the project.

2.6. Conclusion

This chapter established the methodology for techniques that will be used for the quantification of rifampicin and monitoring its degradation. The developed HPLC methods will be will be applied to address the problems of loading and release of drug from nanomedicines. The rifampicin recovery from several aqueous matrices was also established. Solubility-pH relation was determined and the data obtained will be used at different stages of this project to maximize rifampicin loading in the particles and to control its release.

Rifampicin degradation in aqueous solution could be responsible for the sub-therapeutic concentrations reaching the lung and the variable bioavailability. Therefore the encapsulation into a carrier would provide a protective coat for the drug to reduce its degradation after administration. To achieve that, rifampicin will be encapsulated into new PVA nanocarriers. The loading and release of the drug from these nanocarriers will be also investigated.

CHAPTER THREE

Rifampicin-loaded poly (vinyl alcohol) nanocarriers

3.1. Introduction

Rifampicin is the first-line agent in the treatment of TB, but it requires a high oral dose (600 mg daily) over a long period (4–6 months). Owing to the high incidence of side effects (immunological disturbances, allergic rashes, rheumatoid, or lupoid syndromes, eosinophilia, leukopenia, and other hepatotoxic manifestations) and the need for long-term daily dosing, patient non-compliance, relapse of symptoms and an alarming increase in the prevalence of multidrug-resistant strains are problems associated with TB therapy (Barrow et *al*., 1998; Laura et *al*., 2000). With the aim of maximizing the therapeutic indices and minimizing the associated side-effects, a number of rifampicin-containing delivery systems (liposomes, dendrimers and particulate systems) have been developed and characterized (Barrow *et al*., 1998; Denkbas *et al.,* 1995; Deol and Khuller, 1997; Suarez *et al*., 2001; Sreenivasa *et al*., 2002; Vyas *et al*., 2004). The focus of previous research is the fabrication of a delivery vector for rifampicin, but several systems have been shown to have a the short half life, stability issues, leakage of encapsulated drugs and high production costs (Vyas *et al*., 2004).

Nanoparticles can act as rigid delivery vectors with the potential to enhance drug bioavailability, increase the residence of rifampicin in the lung, may help address issues associated with the problem of non-adherence to prescribed therapy and thus improve patient compliance (Ahmad *et al*., 2008; Gelperina *et al*., 2005; Pandey and Khuller, 2007; Soppimath *et al*., 2001). Several previous studies have documented the use of drug-loaded nanoparticles to modify the pharmacokinetics of anti-tubercular drugs (Gelprina *et al*., 2005). For example, Pandey and co-workers (2003)

investigated the pharmacokinetics and antibacterial effect of nanoparticle-bound anti-TB drugs administered via the respiratory route in guinea pigs (Pandey *et al*., 2003). A single dose of rifampicin, isoniazid and pyrazinamide co-encapsulated in poly(DL-lactide-co-glycolide) (PLGA) nanoparticles administered via nebulization to guinea pigs resulted in sustained therapeutic drug levels in the plasma for 6-8 days and in the lungs for up to 11 days. The elimination half-life and mean residence time of the drugs were significantly prolonged compared to oral administration, resulting in enhanced relative bioavailability (12.7-, 32.8- and 14.7-fold for rifampicin, isoniazid and pyrazinamide, respectively). On nebulization of the drug-loaded nanoparticles to *M. tuberculosis* infected guinea pigs at 10 day intervals, no tubercle bacilli could be detected in the lung after five doses of treatment whereas, 46 daily doses of orally administered drug were required to obtain an equivalent therapeutic benefit. Zahoor and co-workers (2005) also showed that the relative bioavailability of anti-tubercular drugs encapsulated in alginate nanoparticles were significantly higher compared with oral administration of free drugs. A 16.5-fold increase in the relative bioavailability of rifampicin, administered by inhalation, was achieved (Zahoor *et al*., 2005). Sharma and colleagues (2004) demonstrated that the administration of three doses of nebulized rifampicin, isoniazid and pyrrazinamide co-encapsulated in wheat germ agglutinin-functionalised PLG nanoparticles, fortnightly for 45 days, could be sufficient to produce a sterilising effect in lungs and spleen (Sharma *et al.,* 2003). A sterilising effect was also achieved when the drugs were loaded in solid lipid nanoparticles. No tubercle bacilli could be detected in the lungs/spleen after seven doses of treatment of infected guinea pigs with drug-loaded solid lipid nanopraticles (Khuller *et al*., 2005). However, none of these models recapitulates all of the

features of human TB. In addition, the nanoparticulate systems used in these studies were not fully characterised in terms of drug content, nanoparticle yield, stability and drug recovery. The problem of retaining the active form of rifampicin in the particles during formulation storage and the release of the drug upon administration was not addressed in the previous study.

PLGA has previously been used to manufacture nanocarriers in which the anti-tubercular drugs were encapsulated (Esmaeili *et al*., 2007; Pandey *et al*., 2003; Sharma *et al.,* 2003; Tomoda *et al.,* 2008). However, the long residence of PLGA in the lung due to its slow degradation (Dunne *et al*., 1996), can lead to pulmonary accumulation of the polymer, especially with chronic daily administration. Other biocompatible polymers for the encapsulation of anti-TB drugs are therefore necessary.

Poly (vinyl alcohol) (Figure 1), is a synthetic semi-crystalline co-polymer prepared by the polymerisation of vinyl acetate and the subsequent hydrolysis of poly (vinyl acetate). PVA with different physicochemical properties can be produced by varying the length of the initial vinyl acetate polymer, the degree of hydrolysis and the method used to obtain the hydrolysis i.e under alkaline or acidic conditions (Wong *et al*., 1996). The polymer's biocompatibility has made it an excellent material for use in a wide range of industrial, commercial, medical and food applications. PVA is currently used globally for coating pharmaceutical products and dietary supplement products regulated as pharmaceuticals. It is also approved by the Food and Drug Administration (USA) for ocular, topical and oral drug delivery (Hyon et *al*., 1994;

Thanoo et *al*., 1993; Ficek and Peppas, 1993). Published studies on the absorption, distribution, excretion, acute, subchronic and mutagenicity of this co-polymer indicate that it is relatively non-toxic by the oral route (DeMerlis and Schoneker, 2003).

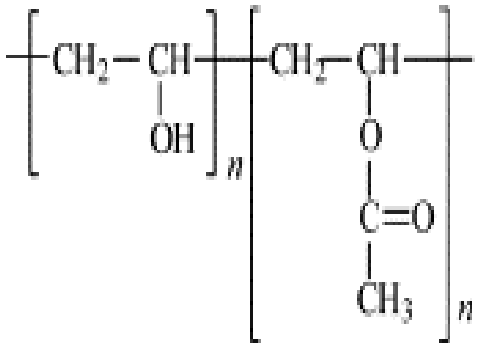

Figure 3.1. Chemical structure of poly (vinyl alcohol)

The aim of the experimental work presented in this chapter was to develop and characterize new rifampicin-loaded PVA nanocarriers. PVA had not previously been used to deliver a therapeutic agent and was selected for the preparation of the nanocarriers because of its biocompability and its potential to modify drug release. A hydrophobic grade of PVA (40 % hydrolysed) was used in this work for the manufacture of nanospheres (NS) and nanocapsules (NC) using solvent displacement technique (Fessi et *al.*, 1989). The specific objectives of the experimental work in this chapter were to:

- Manufacture polymeric nanoparticles of reproducible size with a narrow size distribution.

- Perform nanoparticle characterization by determining the particle size and polydispersity, zeta potential, physical stability (4^{o}C and 25^{o}C) and morphological evaluation of the particles.
- Load the nanoparticles with rifampicin and determine drug encapsulation efficiency, drug content.
- Determine the *in vitro* release kinetics of rifampicin from the PVA nanocarriers.

3.2. Materials

Rifampicin (95% pure) was purchased from Sigma-Aldrich (UK) and PVA 40% hydrolyzed (PVA-40) (MW 72,000) was from polysciences (UK). PVA 80% hydrolyzed (PVA-80) (MW 9,000-10,000) was supplied by Aldrich (USA) and Fluka (Switzerland), respectively. Acetonitrile (HPLC grade) and methanol were purchased from Rathburn Chemicals Ltd (UK) and VWR International Ltd (UK). Sodium citrate dehydrate, citric acid and butylhydroxytoluene were obtained from Sigma-Aldrich (UK). Phospholipids (Epikuron 200) were supplied by Degussa Texturant Systems (UK).

3.3. Methods

3.3.1. Preparation of PVA nanocarriers

The rifampicin-loaded NSs were prepared according to a modified solvent displacement technique (Fessi *et al.,* 1989). This method required 50 mg PVA-40 to be dissolved in 5 ml of methanol using stirring for 12 h for complete dissolution of the polymer. Different amounts of rifampicin (5, 10, 25 and 50 mg) were dissolved in this polymeric solution and injected into a dispersing phase (30 ml) containing citrate buffer (pH 4.8), 1 % w/v of PVA-80, at a speed of 0.5 ml/min using a 5 ml syringe housed in a syringe driver (Precidor, Infors, Basel, Switzerland). PVA nanocapsules were prepared using a similar method, with few modifications (Fessi *et al*., 1989). PVA (50 mg), phospholipids (75 mg) and rifampicin (5, 10 and 25 mg previously dissolved in 0.33 ml of benzyl benzoate) was added to 15 ml of acetone to form the organic phase. To form the nanocapsules the acetone mixture was injected into 30 mL of an aqueous solution composed of poloxamer 188 (0.5 % w/v in citrate buffer, pH 4.8) under moderate homogenization (5,000 rpm). Both mixtures used to form NSs and NCs were homogenized at 5000 rpm for 10 min using a Silverson L4RT laboratory mixer (Silverson Machines Ltd, Waterside, UK), stirred overnight in the fume hood for complete evaporation of the organic solvent and filtered through 1 µm cellulose filter to remove any large aggregates. Drug-free nanoparticles were prepared according to the same procedure omitting the drug.

The drug-loaded nanoparticles were separated from the free drug by an ultrafiltration/centrifugation technique using 15 ml centrifugal filter devices (Amicon

ultra 15®) with MWCF (molecular weight cut-off) of 100 kDA (Fisher Scientific, UK) at 3000×*g* for 1 h (MSC centaur 2 centrifuge, DJB Labcare Ltd., UK). In this system, the non-encapsulated rifampicin is passed through the filter and the nanoparticles retained on the filter are re-suspended in 1 ml of water.

In order to determine the mass of nanoparticles recovered from the process, several batches of concentrated nanosuspensions were freeze-dried for 24 h. The nanoparticle recovery (nanoparticle yield) was calculated according to equation 3.1:

$$\text{NP yield } (\%) = \frac{W_n}{W_t} \text{ x } 100 \qquad (3.1)$$

Where W_n is the mass of nanoparticles recovered and W_t is the mass of particle forming excipients used in the fabrication process.

A second sequence of concentrated nanosuspensions was diluted with ethanol and drug encapsulated was quantified using the validated HPLC assay. A mass balance of the drug was calculated from the process to get the total drug recovery after encapsulation and purification.

The drug content (DC), encapsulation efficiency (EE), Concentration (CC) and drug recovery were calculated (equations 3.2 to 3.5):

$$\mathrm{DC}\ (\%) = \frac{W_1}{W_n}\ \mathrm{x}100 \qquad (3.2)$$

$$\mathrm{EE}\ (\%) = \frac{W_1}{W_0}\ \mathrm{x}\ 100 \qquad (3.3)$$

$$\mathrm{CC}\ (\frac{\mathrm{mg}}{\mathrm{ml}}) = \frac{W_1}{V} \qquad (3.4)$$

$$\mathrm{Drug\ recovery}\ (\%) = \frac{W_1 + W_2 + W_3}{W_0}\ \mathrm{x}100 \qquad (3.5)$$

Where V is the final volume of purified nanosuspension, W_1 is the mass of the drug in the purified nanoparticles, W_2 is the mass of the drug in aqueous filtrate, W_3 is the mass of the drug in the wash, W_0 is the mass of initial drug input and W_n is the mass of nanoparticles on the filtrate.

3.3.2. Physicochemical characterisation of nanocarriers

3.3.2.1. Photon Correlation Spectroscopy

The average volume diameters and the polydispersity index of nanoparticles were determined by Photon Correlation Spectroscopy (PCS) (Zetasizer Nano, Malvern). PCS measurements enable the determination of a diffusion coefficient (D) of a

particle or droplet in solution (Finsy, 1994). By assuming spherical aggregates, the measured D can be used to calculate the hydrodynamic diameter, *d(H)*, of the particle/droplet using Stokes-Einstein equation:

$$d(H) = \frac{kT}{3\pi\eta D} \qquad (3.6)$$

Where *d(H)* is the hydrodynamic diameter, *D* is the translational diffusion coefficient, *k* is Boltzman's constant, *T* is the absolute temperature and *π* is the viscosity. To determine the absolute diameter, serial dilutions (1 in 8, 1 in 16, 1 in 32 and 1 in 64) of each sample were made with filtered water. The analysis was performed at a scattering angle of 90° and at a temperature of 25°C. For each diluted sample, the mean hydrodynamic diameter ± standard deviation of ten determinations were calculated. The obtained diameters were plotted against the concentration and the intercept (zero concentration) was taken as the absolute diameter.

3.3.2.2. Zeta potential

Samples were analyzed following appropriate dilution with 1 mM NaCl and filtration through 0.2 µm filter, using a Zetasizer Nano, Malvern. Values reported are the mean ± SD of three different batches of the nanocarrier formulation.

3.3.2.3. Morphological evaluation

The morphology of the nanoparticles was examined by cryo electron microscopy (cryo-EM). A drop of nanoparticle suspension (10 µl) was placed on a copper grid covered with carbon support film. Liquid nitrogen was used for freezing the specimen grid which was then maintained at a temperature of −176 °C using a Gatan 626 side-entry cryo holder (Gatan Inc., Pleasanton, USA). Images were acquired using an FEI Tecnai G^2 T20 electron microscope (FEI Company, USA) operating at 200 kV. The microscope is equipped with a Gatan Ultrascan 2k × 2k CCD camera (Gatan Inc., Pleasanton, CA, USA). Samples were viewed under low-dose conditions at a constant temperature around −170 °C.

3.3.2.4. Physical stability

Four formulations were selected for this study: blank NS, blank NC, NS-3 and NC-3 (Table 3.2). Physical stability was assessed by comparing the initial particle size with those obtained after 1, 3 and 7 d storage at 25°C and 4°C. The results were analysed for statistical significance using the statistical analysis (Student's t-test) where the differences are considered insignificant when $p > 0.05$.

3.3.3. *In vitro* rifampicin release

To characterize rifampicin release from the particles**,** a 30 ml batch of freshly prepared nanosuspension loaded with 25 mg of rifampicin (NS-3 and NC-3, Table 3.2) was concentrated to 1 ml using the Amicon Ultra YM-100 centrifugal concentrators. At t=0, the concentrated nanosuspensions were spiked into a 5 ml pre-warmed solution of either PBS buffer (pH 7.4) or citrate buffer (pH 4.2). The

suspensions were stirred in a water bath at 37^{o}C and drug release was determined over a series of time points. The pH values were selected to simulate physiological (pH 7.4) and endosomal pH of alveolar macrophages (pH 4.2). At t=0, 2, 4, 6, 24 and 48 h a 0.2 ml sample was withdrawn from the suspensions. The nanoparticles were separated from the free drug using 0.5 ml centrifugal concentrators with MWCF of 100 kDA (Amicon Ultra 0.5 ml) at 3000×*g* for 5 min. The drug content in the nanoparticles and the dispersing medium and were analysed by HPLC. Drug remaining in the nanoparticles was calculated at each time point (*n* = 3) according to equation 3.7 and plotted againt time (h)

$$W_d\,(\%) = \frac{M_t}{M_0} \text{x } 100 \qquad (3.7)$$

Where W_d is the percentage mass of the drug remaining in the nanoparticles, M_t is the mass of drug in the nanoparticles at a time point and M_0 is the mass of drug in the nanoparticles at t_0.

In order to trigger the release of rifampicin from the PVA nanocarriers using an exogeneous triggering system, the drug-loaded nanoparticles were resuspended in two different media: glycine-NaOH buffer (pH 10) and glycine-NaOH buffer: ethanol (80:20) mixture. The release experiment was repeated as described previously.

3.3.4. Rifampicin assay

HPLC quantification of rifampicin was performed using a 600 HPLC pump (Waters, UK) with a 717 auto-sampler (Waters, UK) and a 2487 λ absorbance detector (Waters, UK). The column used was a reversed-phase C18 (250 x 4.6 mm). UV-photodiode array detection was performed at 240 nm. The mobile phase consisted of acetonitrile: PBS buffer (36:64 % v/v) at a flow rate of 1.4 ml/min. Final pH of the mobile phase was adjusted to 7.5 by diluted hydrochloric acid. Column temperature was set to 28°C and 10 µl of samples was injected to the HPLC system. The method was proved to be 'fit for purpose' in the concentration range of 1-0.01 mg/ml (Section 2.4.2).

3.3.5. Data analysis and statistics

All data was expressed as mean ± standard deviation (S.D.) Statistical analysis was performed in SPSS, version 16.0, using either student *t*-test or an analysis of variance (ANOVA) with the chosen level of significance at $p \leq 0.05$.

3.4. Results

3.4.1. Characteristics of the nanoparticulate systems

The blank PVA NSs had a mean diameter of ca. 210 nm and a very low polydispersity index of 0.08 ± 0.01 indicating a very narrow particle size distribution (Table 3.1). They had a zeta potential of - 7.46 ± 1.18 mV (*n* = 3). The plots of hydrodynamic diameter versus concentration showed a linear profile and a a relatively shallow gradient (Figure 3.2). The PVA NCs were significantly smaller than the NSs with a mean diameter of ca. 150 nm, a polydispersity index of 0.14 ± 0.02 and a monomodal size distribution (Figure 3.3). The NCs exhibited a negative charge (- 7.43 ± 2.34 mV). The cryo-EM images demonstrated that the particles had a spherical morphology and their volume diameter observed visually correlated well with the hydrodynamic size measured by PCS (Figure 3.4). The recovery of PVA nanospheres was significantly higher (60.2 ± 5.4 %) than the nanocapsules (24.6 ± 1.8 %), (Table 3.1). Both nanoparticle formulations exhibited good physical stability and no significant changes ($p > 0.05$, ANOVA) to the nanoparticle size occurred after storage at 4^{o}C or 25^{o}C for 7 days (Table 3.3).

(A)

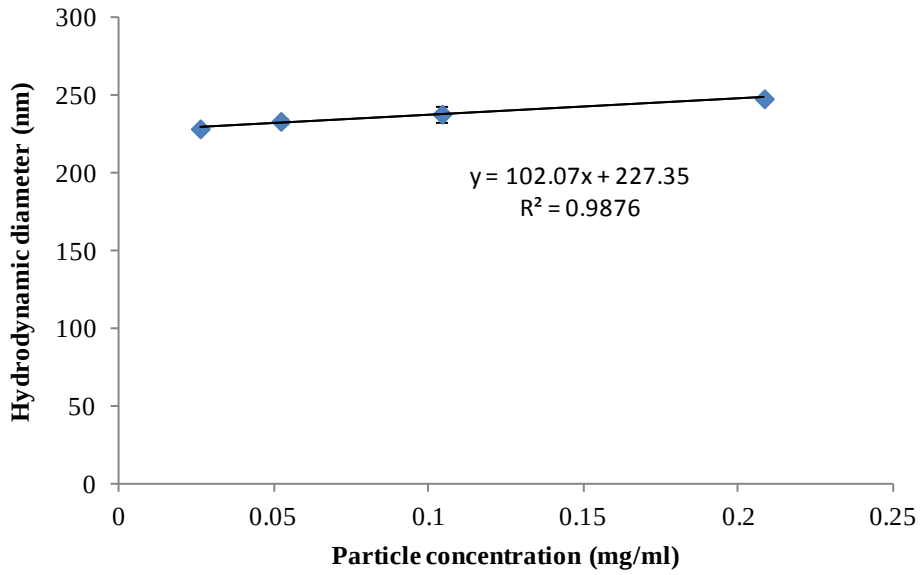

(B)

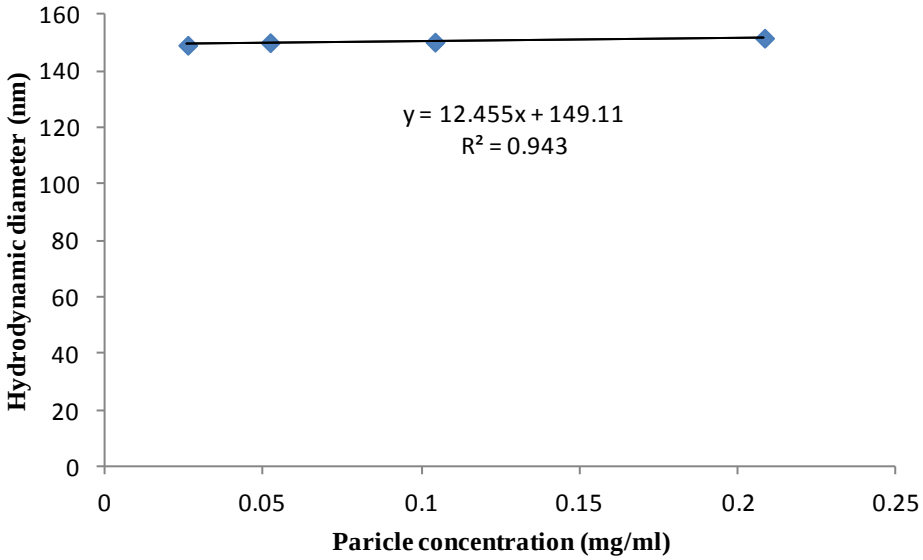

Figure 3.2. A representative nanoparticle hydrodynamic diameter versus plot used to determine the absolute diameter of the PVA nanospheres (A) and nanocapsules (B) (all data are represented as mean ± sd, *n = 3*)

(A)

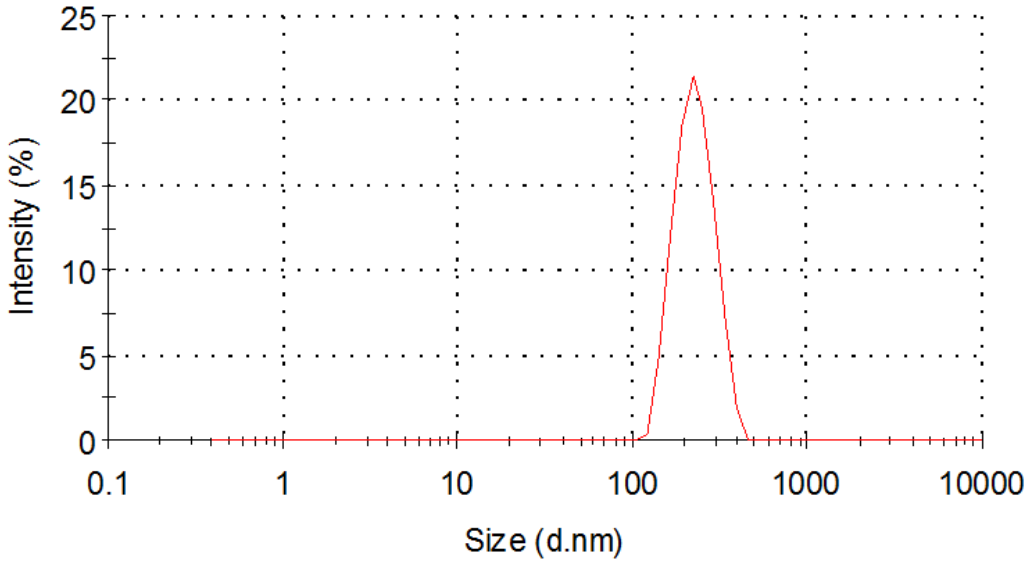

(B)

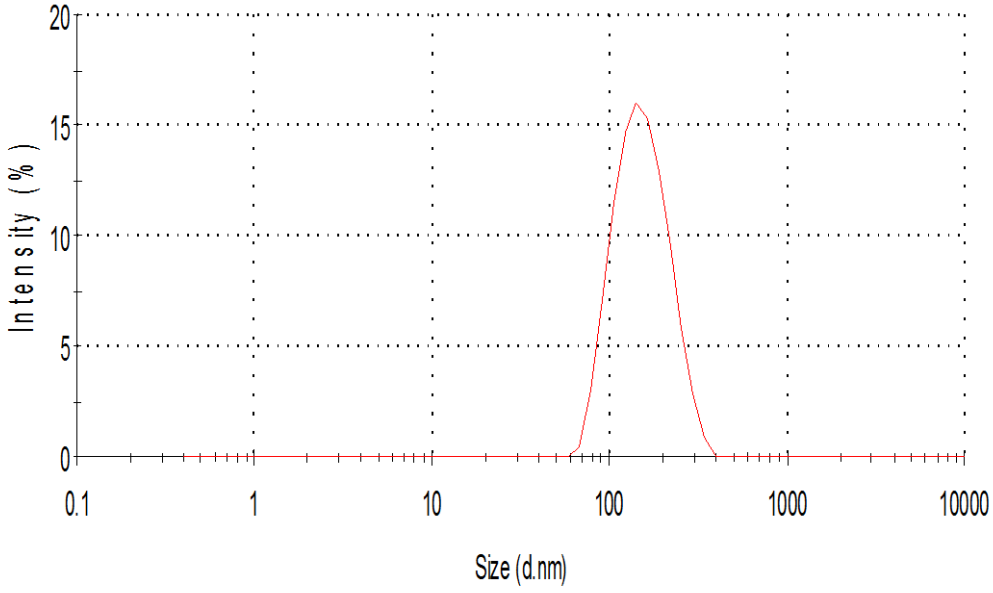

Figure 3.3. Representative size distribution plots of blank PVA nanospheres (A) and nanocapsules (B)

(A)

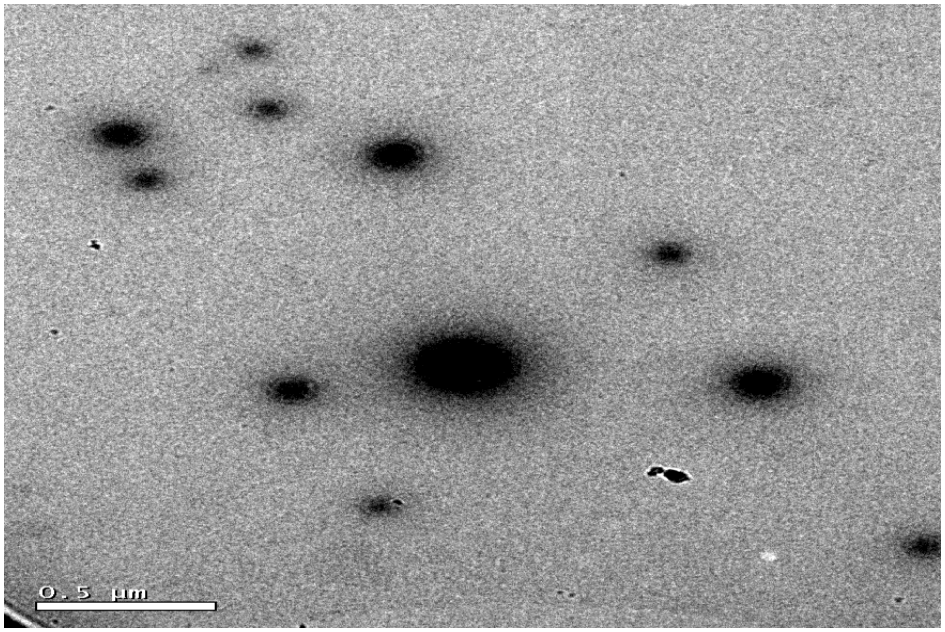

(B)

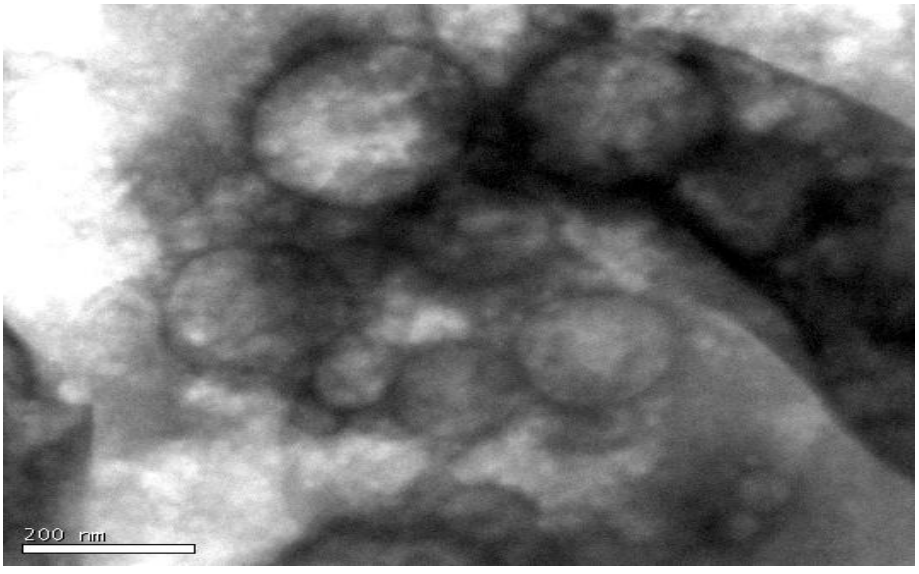

Figure 3.4. Cryo-EM photographs of blank poly (vinyl alcohol) nanospheres (A) and nanocapsules (B)

	NS	NC
Size (nm)	**208.7 ± 7.9**	**151.6 ± 12.4**
PI	**0.08 ± 0.01**	**0.14 ±0.02**
Zeta potential (mV)	**- 7.46 ± 1.18**	**- 7.43 ± 2.34**
Yield (%)	**60.2 ± 5.4**	**24.6 ± 1.8**

Table 3.1. The particle size, polydispersity index (PI), zeta potential and yield of blank PVA nanospheres (NS) and nanocapsules (NC). (all data are represented as mean ± sd, *n* = *3*).

3.4.2. Rifampicin loading

With the increase of rifampicin input from 5 to 25 mg, the drug content in the NS significantly increased from 06.5 ± 0.5 to 22.9 ± 0.5 % (table 3.2). As the loading of rifampicin increased the NS encapsulation efficiency slightly reduced from 38.6 ± 1.1 to 29.3 ± 0.7 %. The drug recovery was significantly lower with low drug input and this correlated with the presence of drug crystal nanosuspensions with a high drug loading. The size of rifampicin-loaded NS ranged from 200 nm to 226 nm. As the drug input increases there was a slight increase from 209 m to 217 nm. The polydispersity index was low for NS batches (PI<0.1) indicating a very narrow size distribution.

When the NC drug input increased from 5 to 25 mg, the drug content of the nanocapsules increased from 2.1 ± 0.1 to 8.1 ± 0.5 % (Table 3.2). Rifampicin-loaded NC were significantly smaller than than the placebo samples ($p < 0.05$, ANOVA). However, as the rifampicin input increase there was not a significant increase ($p > 0.05$) (Table 3.2). The polydispersity index of the rifampicin-loaded NC ranged between 0.1 and 0.25 but the size distribution was consistently monomodal.

Nanoparticles	Drug input (mg)	Drug content (%)	Encapsulation efficiency (%)	Drug recovery (%)	Particle size (nm)
NS-1	5	06.5 ± 0.5	38.6 ± 1.1	73.6 ± 3.1	209.2 ± 4.7
NS-2	10	11.7 ± 0.6	34.5 ± 0.5	81.1 ± 0.8	212.1 ± 5.2
NS-3	25	22.9 ± 0.5	29.3 ± 0.7	86.2 ± 1.5	217.3 ± 9.9
NS-4	50	-	-	-	-
NC-1	5	2.1 ± 0.1	39.3 ± 0.5	72.6 ± 0.9	134.6 ± 4.1
NC-2	10	3.6 ± 0.1	35.5 ± 0.8	78.5 ± 2.2	132.1 ± 7.7
NC-3	25	8.1 ± 0.5	32.3 ± 0.3	85.7 ± 7.4	130.4 ± 5.3

Table 3.2. Rifampicin loading in PVA nanospheres (NS) and PVA nanocapsules (NC). The drug content, encapsulation efficiency, rifampicin recovery and particle size were presented. Each formulation was manufactured in triplicate, (values represent mean ± sd, *n = 3*).

Temperature (^{o}C)	25			4		
Time (d)	1	3	7	1	3	7
B-NS	212.5 ± 7.5	230.3 ± 10.1	234.0 ± 8.5	211.3 ± 6.7	217.2 ± 3.4	221.9 ± 3.5
NS-3	228.5 ± 6.2	231.6 ± 5.6	243.7 ± 12.7	215.7 ± 3.5	227.1 ± 4.8	239.1 ± 17.6
B-NC	146 ± 8.7	148.5 ± 5.01	151.3 ± 5.4	154.8 ± 7.5	155.9 ± 3.8	159.1 ± 8.8
NC-3	137.1 ± 1.9	135.5 ± 3.2	132.8 ± 14.9	128.9 ± 8.1	137.1 ± 7.6	136.4 ± 15.5

Table 3.3. The stability of the nanoparticulate systems: blank PVA nanospheres (B-NS), rifampicin-loaded PVA nanospheres (NS-3), blank nanocapsules (B-NC) and Rifampicin-loaded nanocapsules (NC-3) over 7 d. (values represent mean ± sd, *n* = *3*).

3.4.3. *In vitro* rifampicin release

The *in vitro* release of the two rifampicin-loaded nanocarriers, measured as the percentage of drug remaining in the nanosystems, showed that the two PVA nanocarriers exhibited different behaviours at different pHs (Figures 3.5 and 3.6). The initial burst release was prominent for the particles during the first 2 h. This was followed by gradual reduction of release. At pH 7.4, approximately 10 % and 25 % of drug was released in the first 2 h, for NS and NC, respectively. At pH 4.2, approximately 35 % and 25 % of drug was released in the first 2 h, for NS and NC, respectively. The release rate gradually decreased for both particles at pH 7.4 with the amount of drug released reaching 35 % (NS) and 40 % (NC) at 48 hr. The same pattern was observed at pH 4.2 with 75 % drug released from NS and 80 % from the NC (Figure 3.4). Resuspending the nanoparticles in glycine-NaOH: ethanol mixture (80:20) had a pronounced effect on the amount of drug released after 2 h.

Approximately 40 % and 60 % of drug was released in the first 6 h, for NS and NC, respectively (Figure 3.4).

(A)

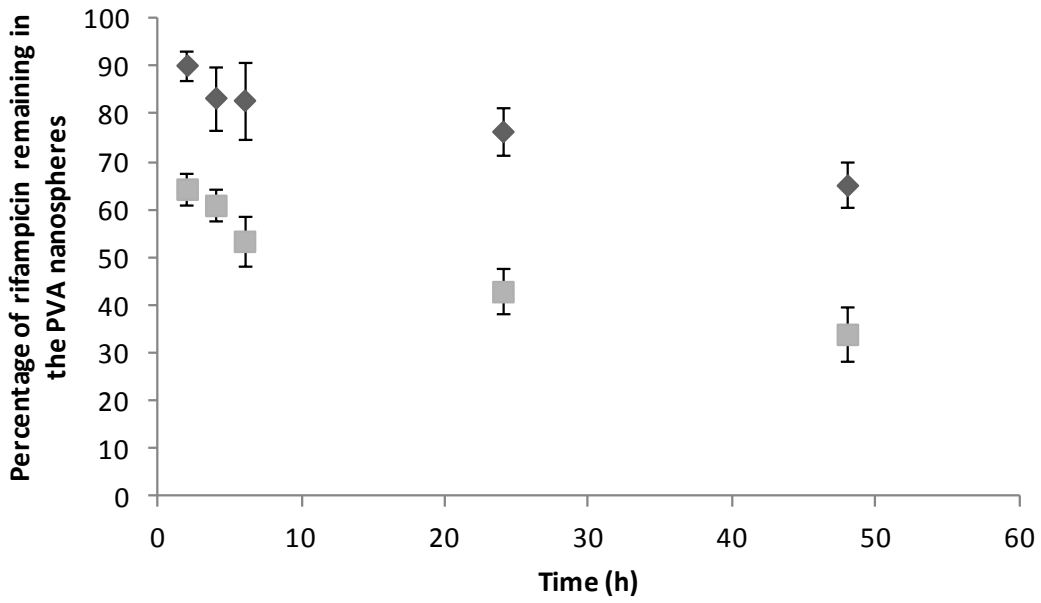

(B)

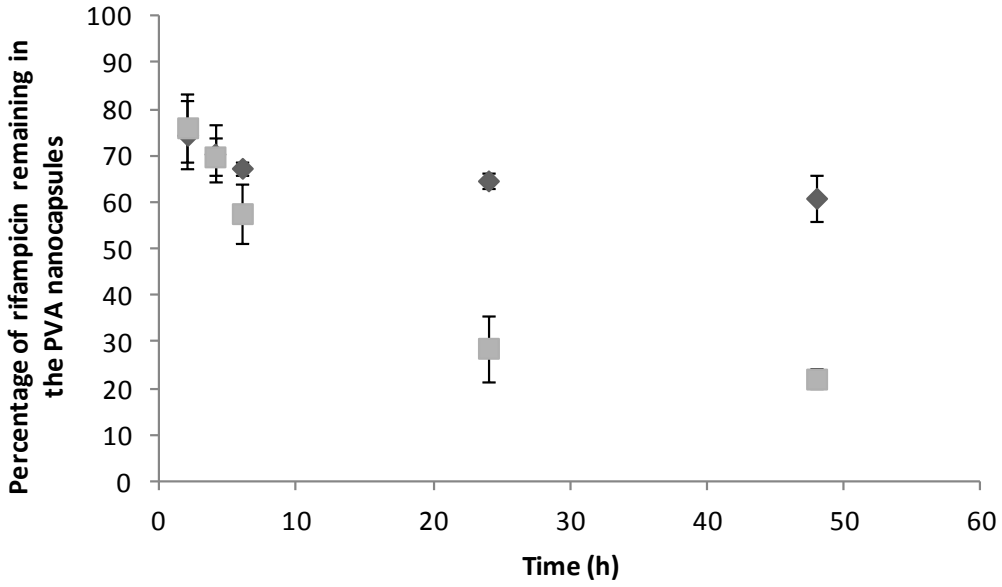

Figure 3.5. Release profile of rifampicin from the PVA Nanospheres (A) and PVA Nanocapsules (B) in PBS buffer (pH 7.4) (diamond) and at citrate buffer (pH 4.2) (square) (data are represented as mean ± sd, *n = 3*).

(A)

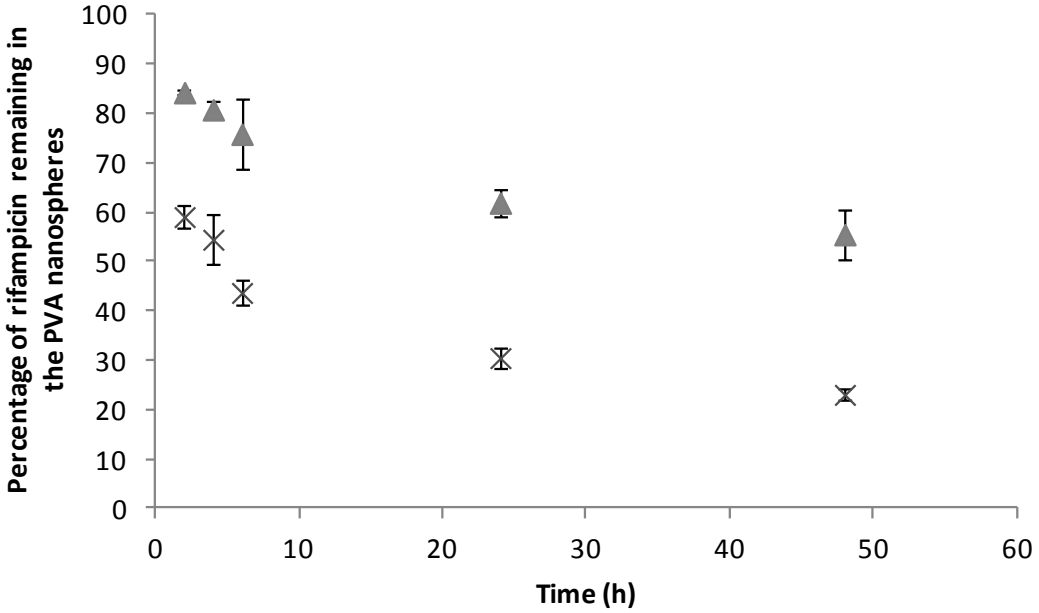

(B)

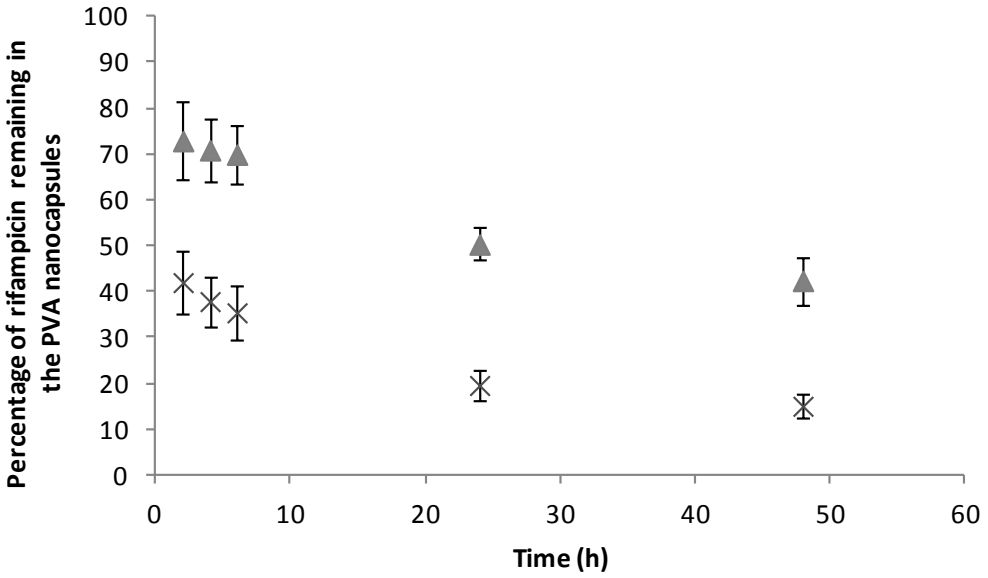

Figure 3.6. Release profile of rifampicin from the PVA nanospheres (A) and PVA nanocapsules (B) at glycine-NaOH (pH 10) (triangle) and at glycine-NaOH buffer (pH 10): ethanol (80: 20). All data are represented as mean ± sd, (*n* = *3*).

3.5. Discussion

It was previously demonstrated that rifampicin was prone to degradation in aqueous solutions. This could be one of the reasons for the variable bioavailability of the drug and the sub-therapeutic concentrations reaching the lung after oral administration. Therefore, the aim of this Chapter was to encapsulate rifampicin into new polymeric nanocarriers that can protect the drug from degradation after administration and reduce its toxicity. PVA was selected for the preparation of the nanocarriers because of its biocompability and its potential to control drug release.

PVA nanocarriers were manufactured using solvent displacement method which was previously used successfully to prepare polymeric nanoparticles in an efficient and reproducible manner (Thioune *et al*., 1997 and Chorny *et al*., 2002). This method, first developed by Fessi *et al*., (1989) has the advantages of being a straightforward technique, rapid and easy to perform. In addition, extended shearing, sonication or very high temperatures are not required. Moreover, the use of potentially toxic components (including chlorinated solvents) may be minimised or avoided in this procedure (Fessi et *al.*, 1989). With appropriate modifications, this method was suitable for producing both vesicle and matrix type nanoparticles, NSs and NC, respectively.

The size and recovery yields of the nanoparticles fabricated were highly reproducible. The particle size distribution measured by PCS demonstrated a homogeneous population characterised by a narrow size distribution. The theory of PCS is based on the “Brownian motion” that is caused by elastic impacts between molecules in the supporting liquid and particles suspended in it (Finsy, 1994).

However, the light-scattering process always presupposes that the scattered light reaches the detector without any further interference by other particles. Such multiple scattering can only be avoided by carrying out the analysis at the highest possible dilution where, unfortunately, signal strength is likely to be very weak and there will be a low signal-to-noise ratio. For that reason, it was important to plot the hydrodynamic particle size against the concentration and the intercept (zero concentration) was taken as the absolute diameter. These plots showed a good linearity and a shallow but significant gradient. This can occur as a result of the interference of the high molecular weight stabilizing polymer with light scattering. Cryo-EM was also to verify the results obtained by PCS. The nanoparticle size as observed by Cryo-EM correlated well with the hydrodynamic size measured by PCS. Cryo-EM analysis also showed that the nanoparticles were spherical in shape.

The encapsulation efficiency of the two particles using PVA was comparatively high. Ismaeili *et al*., (2007) investigated the effects of a number of parameters on the encapsulation efficiency of rifampicin in PLGA nanoparticles such as: concentration of polymer in aqueous phase, solvent nature, and saturation of the outer phase with drug **(**Esmaeili *et al*., 2007). However, 3.2% was the highest encapsulation efficiency achieved in their study. This was due to the ionisation of rifampicin and its diffusion to the aqueous phase. In order to increase the amount of drug that could be incorporated into nanoparticles, an increase of the theoretical loading (amount of drug used in the formulation) was used along with a modification of the pH (Govender *et al*., 1999; Ueda and Kreter., 1997; Zhao et al., 2010). The lowest degree of ionisation of rifampicin is achieved at pH 4.8 and the diffusion of the drug to the external phase is reduced. Therefore, in our studies the pH of the aqueous

phase was maintained at 4.8 to suppress the diffusion of the drug to the external phase and improve encapsulation efficiency.

The hypothesis behind loading rifampicin into the nanocapsules was that the higher affinity of rifampicin to the benzyl benzoate would result in the drug being retained in the oily droplets during their formation instead of diffusing out with the organic solvents. However, due to the complexity of the system, significant amounts of rifampicin were bound to the excess phospholipids and only 32 % of the drug was retained in the nanodroplets.

The *in vitro* release of the two rifampicin-loaded nanocarriers showed that the two PVA nanocarriers exhibited different behaviours at different pHs. For all formulations, there was an initial burst release during the first 2 h followed by a gradual reduction of release. The initial burst could be due to the diffusional release of rifampicin distributed at or just beneath the surface of the nanoparticles. Rifampicin release from the nanoparticles happens either by diffusion through the polymer barriers or by the erosion of the polymer. When the pH was altered to 4.2 or 10, there was a significant increase in the drug release. The mechanism of polymer hydrolysis at low pH is unclear. At high pH, and in the presence of ethanol, the mechanism is postulated to involve the adsorption of the alkali catalyst onto the free hydroxyl groups resulting in the hydrolysis of the acetate groups of the polymer, also known as alcoholysis (Chana et *al*., 2008., Katsurya *et al*., 2001., Moritani *et al*., 1977). The release profiles of the drug from PVA nanoparticles are different from the ones reported for PLGA nanoparticles which makes PVA can an interesting material for drug delivery purposes.

3.6. Conclusion

The methodology allowed the rapid and reproducible formation of new PVA NSs and NCs. The successful encapsulation of first line anti-TB drug, rifampicin, into these nanocarriers would protect the drug from degradation and reduce the associated side effects (such hepatotoxicity) after administration. More interestingly, the PVA nanocarriers released rifampicin at different rates in different media. The ability of these vectors to deliver the drug to the lung and release it in a controlled manner would solve a number of anti-TB therapy issues.

Macrophages are known to provide a niche for Mycobacterium tuberculosis. The ability of these nanocarriers to deliver the drug to these infectious reservoirs would reduce the reccurence of the infection. In the next chapter, the uptake of these carriers by macrophage-like cell line will be evaluated. The association of rifampicin with these cells will be monitored using the PVA nanocarriers and drug solutions. The toxicity of these delivery systems will be also evaluated.

CHAPTER FOUR

Uptake of PVA nanoparticles by the macrophage-like cell line, J774A.1

4.1. Introduction

TB is transmitted by inhalation of *Mycobacterium tuberculosis* in fresh airborne droplets emitted by the coughing pulmonary TB patient (Pratt *et al*., 2005). Upon deposition in the alveolus, the tubercle bacilli are taken up and destroyed by AMs. However, in some instances, virulent bacilli continue to grow within the AMs, eventually releasing additional bacilli until, in an immune-competent host, cell-mediated immunity develops (Dannenberg, 1993; Ferrari *et al*., 1999). At this time granulomas are formed and growth of the virulent bacilli is inhibited. However, the *mycobacterium* can persist for decades in a dormant state inside in the granulomas for years, either inside macrophages or in the central necrotic core of the lesions (Figure 1.2) (Ulrichs *et al*., 2006). Reactivation of these latent organisms can also lead to post-primary disease, even in persons who successfully fought their initial battle against TB (section 1.1).

In the current TB therapy, high drug doses are required to be administered as only a small fraction of the total dose reaches the lungs after oral administration. The recurrence of the infection could be related to the insufficient drug concentrations achieved in macrophages and in granulomas for full eradication of dormant mycobacteria. Moreover, the granulomas are believed to be isolated from the outside environment due to a thick, calcified stratum surrounding them. The inability of drugs to penetrate these lesions could be another factor in the failure of current therapy to kill the virulent bacilli residing these lesions. Recently, Takaki *et al*., (2011) monitored the movement of individual macrophages from a particular granuloma and observed that these macrophages could leave the granuloma and

recruit other macrophages to create new granulomas, often at sites distant from the original (Takati *et al*., 2011).

In the previous chapter, rifampicin was encapsulated in PVA nanoparticles. The ability of these PVA nanocarriers to deliver the drug to macrophages would not only kill the intracellular mycobacteria in these cells, but it would also have the potential to target the bacilli occupying the granulomatous lesions. Therefore, the aim of this study was to investigate the uptake of PVA nanoparticles by a macrophage-like cell line, J774A.1. This model was chosen because it is a standard cell line used in phagocytosis studies that faithfully mimics many aspects of macrophage function.

The potential of a macrophage-targeting strategy using nanoparticle-encapsulated TB drugs is supported by *in vitro* data from a number of studies. For example, incorporation of isoniazid and streptomycin in poly(butyl cyanoacrylate) PBCA nanoparticles not only increased intracellular accumulation (or association) of these drugs in the cultivated human blood monocytes but also produced enhanced antimicrobial activity of these agents against intracellular *M. tuberculosis* compared with their activity in extracellular fluid (Anisimova *et al*., 2000). Kisich *et al*. (2007) showed that the encapsulation of moxifloxacin in PBCA nanoparticles resulted in a pronounced increase in the intracellular concentration of infected macrophages. In addition, encapsulated moxifloxacin was more effective than the free form to kill intracellular bacilli (Kisich *et al.,* 2007). However, the non-biodegradability of the polymer PBCA employed in their study constitute a main limitation. More, recently, Ohashi *et al*. (2009) demonstrated that the encapsulation of rifampicin in PLGA nanoparticles improved the in vivo uptake of the drug by alveolar macrophages in rat

lungs as compared to rifampicin-containing PLGA microparticles (Ohashi *et al*., 2009).

The physicochemical characteristics of particles and media properties have a significant effect on the transport of nanoparticles to cells *in vitro* (Limbach *et al*., 2005). The dynamics that dictate particle transport include: diffusion, gravitational settling and agglomeration. It is hypothesized that cells exposed to a nanoparticle suspension in vitro, will not receive a drug payload nor will be able to interact with the nanoparticles (e.g. exhibit internalization or toxicity-related responses) unless the nanoparticle comes into physical contact with the cell monolayer through the processes of gravitational settling and diffusion. Therefore, it is proposed that a new dose metric, the cellular dose, be used to describe the number or surface area of nanoparticles that reaches the cell layer during a given experimental duration (e.g. number/cm^2, surface area/cm^2; Equation 4.1). The advantage of the cellular dose compared to the nominal dose (defined as the mass, number or particle surface area per total volume of suspension medium added to the cells) is that it takes into account not only the nominal concentration of particles added to the *in vitro* experiment, but also the exposure time, and is therefore a more description metric.

Gravitational settling is the result of opposing forces: gravity, drag and buoyancy. Drag, which is due to viscous forces of the fluid on the moving particle, is a function of particle diameter, fluid viscosity and particle velocity. Buoyancy (force exerted by the displaced fluid) is a function of particle diameter and the density of the medium (Bird *et al*., 1960). The gravitational force is a function of mass (particle diameter and density). Therefore, the rate of delivery of particles by gravitational settling is

dependent on particle size and density. The terminal settling velocity can be calculated from Stoke's law as:

$$V_s = \frac{2(\rho_s - \rho_m)gr^2}{9\mu} \qquad (4.1)$$

Where V_s is the particle's settling velocity (m s^{-1}); g is the gravitational acceleration (m s^{-2}); ρ_s is the mass density of the particles (kg m^{-3}); ρ_m is the mass density of the fluid (kg m^{-3}); μ is the fluid's viscosity (kg m^{-1} s^{-1}) and r is the radius of the particle (m).

By inserting values for the incubation time, estimated particle density, density and viscosity of the cell culture medium at 37°C, and the radius of the particle (based on the measured hydrodynamic diameter in cell culture medium), the maximum sedimentation distance can be calculated. Assuming that this value (converted from m to µm for ease of understanding) represents the height of a suspension-filled cylinder directly above the cell monolayer in which all particles suspended therein will sediment onto the cell surface within the duration of the experiment, it is possible to estimate the number of particles that will be present within this particular volume of medium and therefore the sedimentation fraction of the cellular dose.

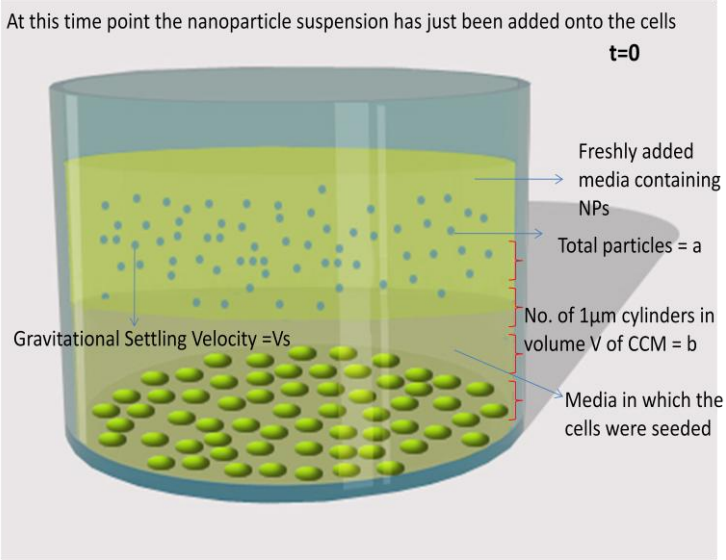

Figure 4.1. Schematic representation of nanoparticle distribution in cell culture model at t=0.

Agglomeration is the combination of individual particles into larger masses due to attractive forces or chemical binding (Maeakin, 1988). Agglomeration shifts the size distribution of particles from that of the primary particles to a distribution with larger mean and usually greater dispersity. Agglomerates have a higher mass and volume than individual particles they are composed of and have correspondingly higher gravitational and buoyant forces acting on them.

Diffusion is the spontaneous, passive movement of particles from high chemical potential areas to low chemical potential ones. When a suspension is applied to an adherent cell culture, a concentration gradient, which drives diffusional transport of these particles, may be created when particles adhere to or are taken up by cells. Since rates of diffusional transport are a function of particle size and the viscosity of the media, smaller particles tend to diffuse more rapidly than larger particles. Diffusional transport processes can be represented by Fick's second law:

$$\frac{\partial c}{\partial t} = \frac{D\,\partial^2 c}{\partial z^2} \qquad (4.2)$$

Where *c* is the particle's concentration (kg m^{-3}); *D* is the diffusion coefficient (m^2 s^{-1}); *t* is the time (s) and *z* is the spatial coordinate (from bottom to top of the culture well) (m).

To calculate the diffusional component of the cellular dose, the assumption must be made that particles will diffuse from the liquid toward the cells in one dimension (top to bottom of the culture well). Although this assumption is not representative of true vectorial movement in a suspension, the approximation has been used by other authors (Teeguard and Limbach). The diffusion coefficient *D* of a small particle can be derived using the Stokes-Einstein (equation 4.3).

$$Diffusion_{coefficient} = \frac{RT}{N 6\pi\mu d} \qquad \text{(Equation 4.3)}$$

Where *R* is the gas constant (8.314 J/K/mol); *T* is temperature (K); *N* is Avogadro's number; μ is the solution viscosity (kg/m/sec) and *d* is the particle diameter (m).

Assuming that at t+Δt the concentration at any other given position z (z = ∞)would be equal to the initial concentration of particles $C_{initial}$ (Figure 4.2).

t=0, all z: $C=C_{initial}$

t>0, z=0: C=0

z=∞: $C=C_{initial}$

The number of particles reaching the cells can be determined by calculating the flux of particles diffusing towards the cell layer *j* (kg m^{-2} s^{-1}) using Fick's law:

$$j = \sqrt{\frac{D}{\pi t}}(0 - Cinitial) \qquad (4.4)$$

Where D is diffusion coeffiecient; t is time and $C_{initial}$ is the initial particle concentration.

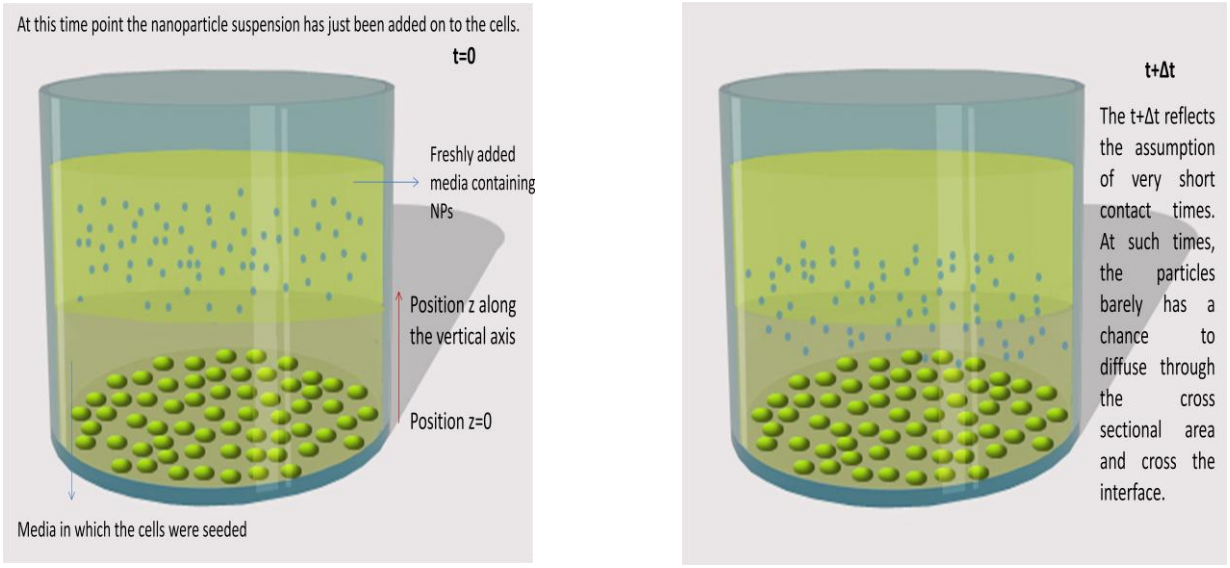

Figure 4.2. Schematic representation of particle distribution in cell culture model at t=0 and t= t+Δt.

The net impact of these processes has been ignored by studies relying on simple metrics such as nominal media concentration or nominal number of particles (Chitrani *et al*., 2006; Desai *et al*., 1996; He *et al*., 2010; Schwarze *et al*., 2007; Zauner *et al.,* 2001). This can obscure the relationships between response and particle characteristics, leading to misleading conclusions regarding the dynamics of cellular uptake. Ideally, to investigate the effect of a specific parameter, e.g. particle

size, on the uptake, particles of different sizes should be delivered to a standardised cell culture system at the same dose of a specific number of particles or particle surface area. This allows the examination of particle size as a determinant of response when other variables are controlled.

The aim of this study was to investigate the uptake of PVA nanoparticles by a murine macrophage-like cell line, J774A.1 cells. The objectives were to:

- Evaluate any toxicity of the PVA nanocarriers towards the J774A.1 cells.
- Verify the stability of PVA nanoparticles in cell culture media.
- Establish assays for the quantification of proteins recovered from cells and to quantify rifampicin in cell lysate.
- Compare the association of rifampicin with the J774 macrophage-like cell line after incubation with PVA nanospheres, nanocapsules and free drug in solution.
- Develop a model to determine the delivered doses (according to rate of transport) and examine the effect on the uptake of nanoparticles.

4.2. Materials

Cell culture reagents including Dulbecco's Modified Eagle Medium with phenol red (Lonza) cell culture medium, Fetal Bovine Serum (FBS), L-Glutamine, Sodium pyruvate, Sodium Dodecyl sulphate and HEPES were purchased from Sigma-Aldrich (UK). Coomasie plus assay kit was supplied by Thermo Scientific (UK).

4.3. Methods

4.3.1. Preparation of nanoparticle suspensions

PVA NS and NC (NS-3 and NC-3, Table 3.2) were manufactured according to section 3.3.1. The 30 ml nanosuspension batches produced were concentrated to 1 ml by an ultrafiltration/centrifugation technique using 15 ml centrifugal filter devices (Amicon ultra 15®) with MWCF (molecular weight cut-off) of 100 kDA (Fisher Scientific, UK) at 3000×*g* for 1.

4.3.2. Particle size and colloidal stability of PVA nanocarriers in biological fluids

The particle size and colloidal stability physical stability of the nanoparticle suspension were assessed in cell culture medium using photon correlation spectroscopy at predetermined time points (t=0 and 6 h). Nanoparticle suspensions were measured at the different concentrations used in this study as test solutions. The hydrodynamic diameter of particles was determined for each batch in triplicate.

4.3.3. Cell culture methodology

The J774A.1 cell line was obtained from Dr H. Collins (Department of Infectious Diseases, King's College School of Medicine, UK) and the cells were used up to passage 24.

4.3.3.1. Cell maintenance

Cells were grown in 162 cm^2 cell culture flasks using cell culture medium (DMEM suplemented with 10% v/v FBS, 1% v/v L-glutamine, 1% v/v Sodium pyruvate and 1 % v/v HEPES. Cells were grown in a humidified environment in an atmosphere of 5% CO_2 at 37^oC. Medium was changed twice a week. After aspiration of old media, 20 ml of warmed fresh medium was added to cell layers.

4.3.3.2. Cell passage

Cells were subcultured when 90-100 % confluency was reached, approximately once a week. This was confirmed by examining the flask surface under light microscope. After aspiration of old medium, cells were detached by scraping cell layers from the surface of flask in 1 ml of warmed fresh cell culture medium. After repeat pippeting to generate a suspension of single cells, the cell suspension was divided into new culture flasks (at a split ratio of 1: 5) and 20 ml of cell culture medium was added to each flask.

4.3.3.3. Cell counting

After detachment of cells, 20 µl of the cell suspension was removed and mixed with 20 µl tryptan blue. This was placed on the haemocytometer after affixation of cover slip. Six large squares from each of the top and bottom sections were counted at random and number of cells per ml was calculated as follows:

$$Number_{cells/ml} = \frac{N * d_{factor}}{V} \qquad (4.5)$$

Where N is the mean number of cells per large square; d_{factor} is the dilution factor of cell suspension and V is the volume of square

4.3.4. Biocompatibility of PVA nanoparticles with J774A.1

4.3.4.1. Metabolic activity test (MTT)

The biocompatibility of nanoparticle formulations was determined in J774A.1 cells in 96-well plates using an MTT assay (Mosman, 1983). The MTT is a colourimetric method for the determination of cell viability based on the reduction of the yellow tetrazolium salt MTT to a purple formazan dye by mitochondrial sccinate dehydrogenase in viable cells.

Cells were seeded in 96-well plates at a density of 5×10^4 cells/well in 100 µl of cell culture medium and used in experiments after 12 h. Concentrated nanosuspensions prepared in section 4.3.1 were diluted with cell culture medium (1 in 4, 8, 16, 32, 64, 128, 256 and 512) . To initiate the assay, the medium was removed and 100 µl of each test suspension was added to the cells and incubated for 6 h. Cell culture medium was used as negative control and cell culture medium supplemented with 2% SDS was used as a positive control. After removal of solutions, the cells were incubated with 50 µl of MTT (0.5 mg/ml in PBS) for 4 h. Afterwards, 100 µl of 10% SDS in was added to solubilise the water insoluble formazan crystals overnight. Upon complete solubilisation of the crystals, the absorbance of each sample was measured at 570 nm and corrected for background absorbance at 650 nm. The cell viability was calculated as the ratio of treated cells and the untreated cells. Each experiment was carried out in triplicate on six different well-plates.

4.3.4.2. Determination of monolayer protein content using the Bradford assay

Protein concentrations in cell monolayer can provide an indication of the total number of adherent cells remaining on the plate after the incubation period. Changes to the total protein concentration in nanoparticle or drug treated cells, as compared to non-treated cells, can provide information on cell detachement as caused by 1) excessive particle uptake or 2) cell death. Total monolayer protein concentration was determined by a modified Bradford assay using BSA as the standard (Bradford, 1976). Standard solutions containing 1000, 750, 500, 250, 125 and 25 µg/ml of BSA were prepared by diluting the BSA stock solution (2000 µl/ml) in water. Each standard (10 µl) was transferred into a microplate and 300 µl of the coomassie plus reagent (Contains coomassie G-250 dye) was added. The solutions were mixed in a plate shaker for 30 seconds and incubated at room temperature for 10 minutes. The absorbance was measured at 595 nm with a plate reader. After substracting the average absorbance for the blank (water) from the measurements of all standards, a calibration curve was created by plotting the average blank-corrected absorbance versus concentration. The linearity was evaluated by linear regression analysis, which was calculated by the least square regression method. Accuracy was calculated according to equations 4.6:

$$Accuracy = \left(\frac{A}{T}\right) \times 100 \qquad (4.6)$$

Where T is the theoretical concentration of analyte and A is the actual concentration of analyte. To measure the quantity of proteins recovered from cell homogenates, 10 µl of cell lysate was diluted with 300 µl of the dye and the absorbance was measured at 595 nm with a plate reader. The calibration curve of BSA in water displayed a good linearity over the concentration range of 25-1000 µg/ml, with correlation coefficient of >0.99 (Figure 4.3). The recovery values ranged between 93.8 and 97.3 % (*n*=3).

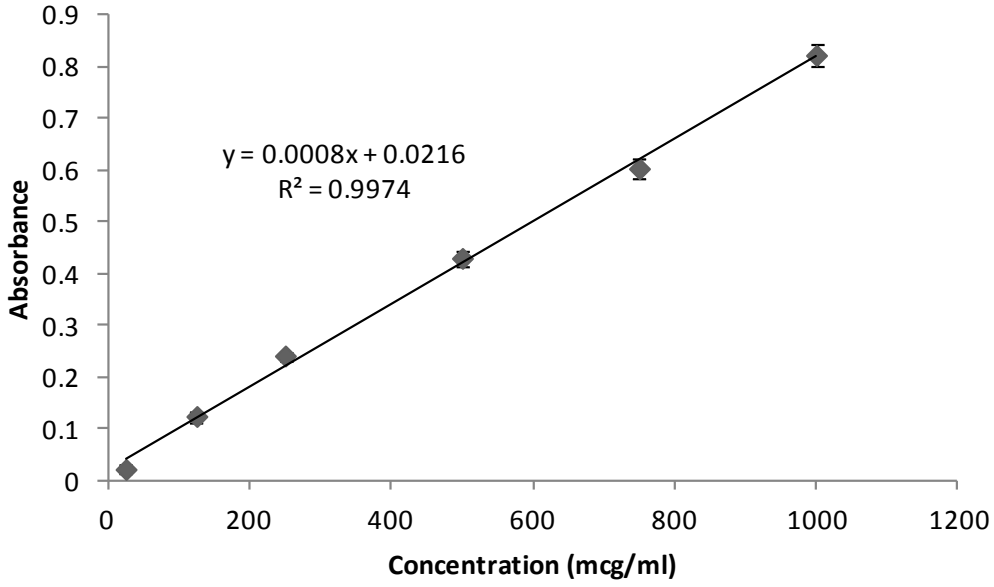

Figure 4.3. Calibration curve for the Bradford assay for BSA. Data represent mean ± sd, *n*=3 calibration curves (each each calibration curve having 3 analyses at each concentration).

4.3.5. Cell association and uptake of PVA nanoparticles by J774A.1 cells

4.3.5.1. Rifampicin quantification in the presence of cell homogenate

Cell homogenates were spiked with different concentrations of rifampicin (250, 100, 40, 10, 4 and 4 µg) and centrifuged at 10,000 *g* for 10 minutes. The supernatants

were filtered and the amount of drug was quantified using HPLC developed in section 2.3.2. The calibration curve of rifampicin in cell lysate was compared to the one of rifampicin in water: ethanol mixture (50: 50).

4.3.5.2. Rifampicin uptake by J774A.1 cells

Cells were seeded in 24-well plates at a density of 5 x 10^5 cells/well in 500 µl of cell culture medium and used in experiments after 12 h. Upon reaching confluence, cell uptake of nanoparticles was initiated by exchanging cell culture medium with 500 µL of specified nanoparticle suspension and incubating the cells at 37^{o}C for 6 h. PVA nanoparticles containing 100, 200, 500 and 1000 µg /ml of RIF were suspended in the medium and were added separately into the well containing cells. Control rifampicin solutions contained 100, 200, 500 and 1000 µg /ml of drug. The experiment was terminated by washing the cell monolayer three times with phosphate-buffered saline (PBS, pH 7.4) to eliminate excess particles which were not strongly associated to the cells (i.e. either internalized or adhering to cells). The cell membrane was permeabilized using probe sonication to expose the internalized nanoparticles for quantitative measurement. Cell-associated nanoparticles were dissolved in ethanol and quantified by analyzing the cell lysate using HPLC. The quantification method was shown to be “fit for purpose” in the presence of cell homogenates as described in section

4.3.6. The predicted cellular dose

The predicted cellular dose was determined by combining the mumber of particles reaching the cell monolayer after 6h via both sedimentation and diffusion (Equation 4.7)

$$Cellular\ dose = \frac{(Particles\ sedimented* [\#] + Particles\ diffused\ [\#])}{(Monolayer\ surface\ area\ [cm^2])} \quad (4.7)$$

* *Taking agglomeration behavior into consideration*

Number of particles reaching the cells via sedimentation and diffusion were calculated using equations 4.1 to 4.4.

Note: This particokinetic model for calculating the predicted cellular dose was develop by Abhinav Kumar (Pharmaceutical Research Science division, King's College London, Uk) as part of his PhD project and was used in this work with his permission.

4.3.7. Data analysis and statistics

All data was expressed as mean ± standard deviation (S.D.) Statistical analysis was performed in SPSS, version 16.0, using either student *t*-test or an analysis of variance (ANOVA) with the chosen level of significance at $p \leq 0.05$.

4.4. Results

4.4.1. Stability of PVA-VAc nanocarriers in biological fluids

The rifampicin-loaded PVA nanospheres and nanocapsules showed size increases at different concentrations after incubation in cell culture medium at 37^{o}C over 6 h (table 4.1). As it can be seen for both formulations; the particle size increases both over time and as the concentration increases. The increase for the nanocapsules was higher than the increase for the nanospheres.

.

Rifampicin concentration in the NP (μg/ml)	R-PVA NS		R-PVA NC	
	0	6	0	6
100	211.7 ± 5.4	257.1 ± 14.8	141.5 ± 7.7	281.2 ± 15.7
200	225.4 ± 7.1	268.2 ± 18.1	144.6 ± 3.8	308.7 ± 25.3
500	220.5 ± 11.7	274.3 ± 21.3	152.5 ± 5.7	325.1 ± 31.7
1000	224.4 ± 9.4	288.2 ± 10.9	151.9 ± 11.7	345.9 ± 19.8

Table 4.1. The stability of rifampicin-loaded PVA nanospheres and rifampicin-loaded PVA nanocapsules in cell culture medium at 37 ^{o}C (*n*=3).

4.4.2. Biocompatibility of PVA nanoparticles with J774A.1

The metabolic activity of the PVA nanoparticles was higher than 80% at all concentrations for the rifampicin loaded nanoparticles lower than 10 mg/ml (Figure 4.4 and 4.5). As the nanoparticle concentration increased the viability decreased reaching approximately 60 % at 50 mg/ml.

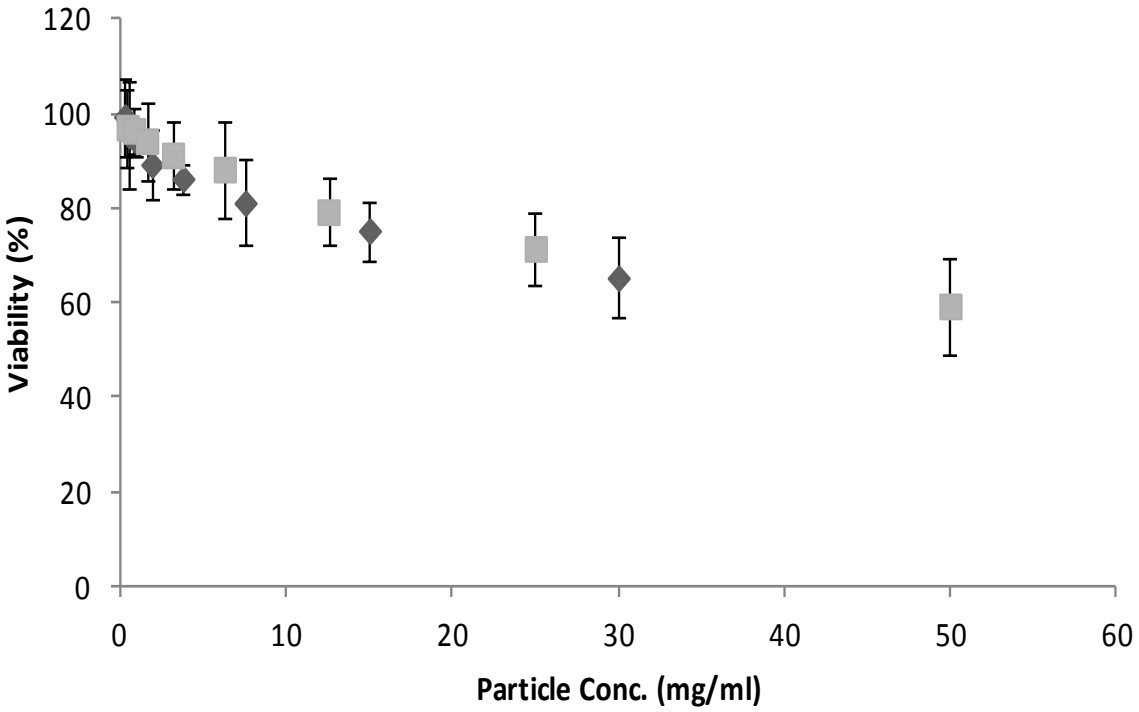

Figure 4.4. Viability of J774A.1 cells after incubation with blank PVA nanospheres (diamond) and Blank PVA nanocapsules (squares) and for 6 h at different concentrations (*n*=6).

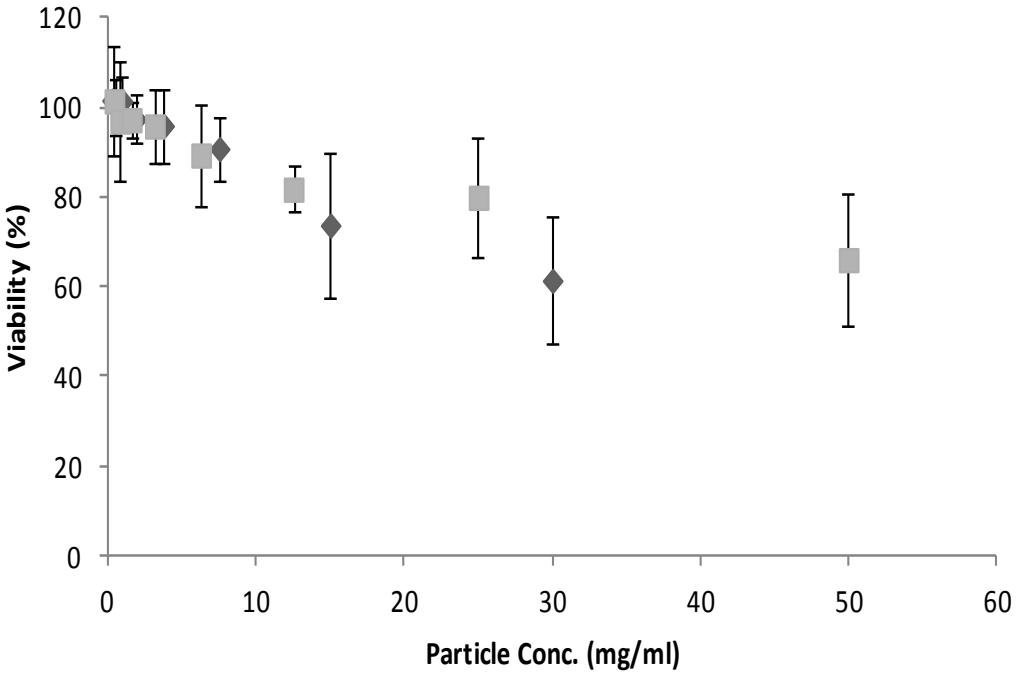

Figure 4.5. Viability of J774A.1 cells after incubation with rifampicin-loaded nanospheres (diamond) and rifampicin-loaded nanocapsules (squares) for 6 h at different concentrations (n=6).

The amount of protein recovered from the J774 cells after 6 h incubation with rifampicin-loaded nanospheres, Rifampicin-loaded nanocapsules and free rifampicin varied (Fig 4.6). As it can be seen, the amount of protein recovered in the homogenate decreased as the amount of nanoparticles presented in the test solution or suspension increased. There was also significant difference between the amounts of protein recovered after exposure to nanospheres and nanocapsules ($p < 0.05$, ANOVA). For example, when exposed to PVA nanoparticles containing 500 µg of rifampicin, the amount of proteins recovered was 404.3 ± 81.7 and 201.8 ± 39.1 µg, for nanospheres and nanocapsules, respectively. Statistical analysis also show that drug encapsulation in nanospheres significantly increase cell recovery compared to free drug ($p < 0.05$, ANOVA).

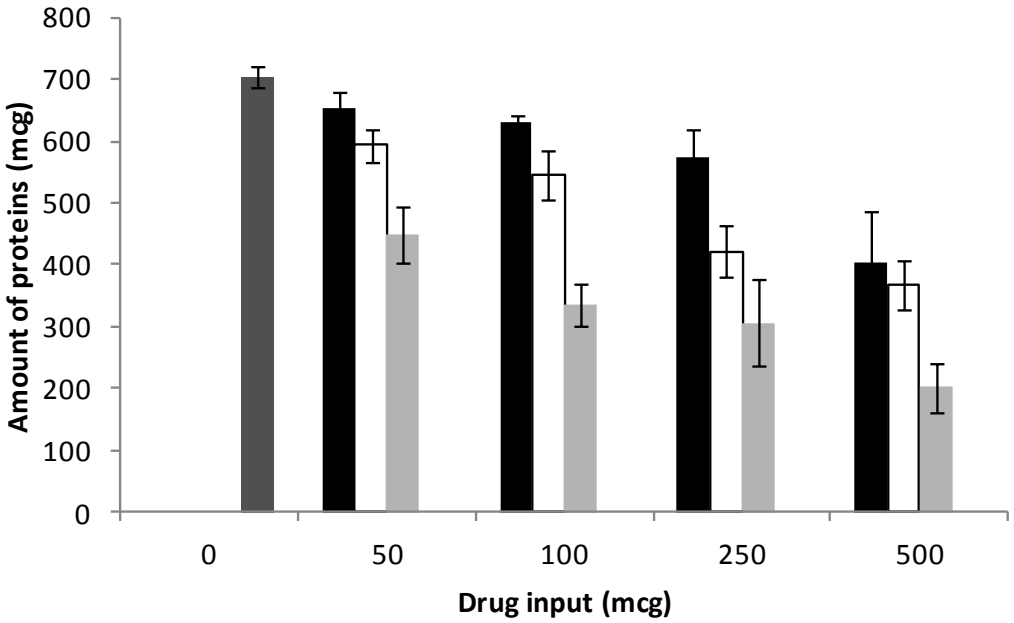

Figure 4.6. The amount of protein recovered from the untreated J774A.1 cells after 6h incubation with rifampicin-loaded nanospheres (black), rifampicin-loaded nanocapsules (grey), free rifampicin (white) and untreated cells (dark grey) (*n*=3).

4.4.3. Rifampicin quantification in the presence of cell lysate

In order to rule out interference by cell lysate components, the rifampicin extraction and quantification procedure was validated by spiking known amounts of rifampicin into representative volumes of cell lysate and evaluating recovery and signal intensity using the HPLC method described in Chapter 2.3.2. The calibration curve of rifampicin in cell lysate displayed excellent linearity over the concentration range of 0.1-0.001 mg/ml, with correlation coefficient of >0.999 for the peak area calculations (Figure 4.7). The calculated LOD value was 0.8 µg/ml while the LOQ was 3.2 µg/ml using peak area. The recovery values ranged between 99.4 and 96.1

% (n=3). The calibration curve of rifampicin in ethanol: water (50: 50) mixture is displayed in Figure 4.4 as a reference.

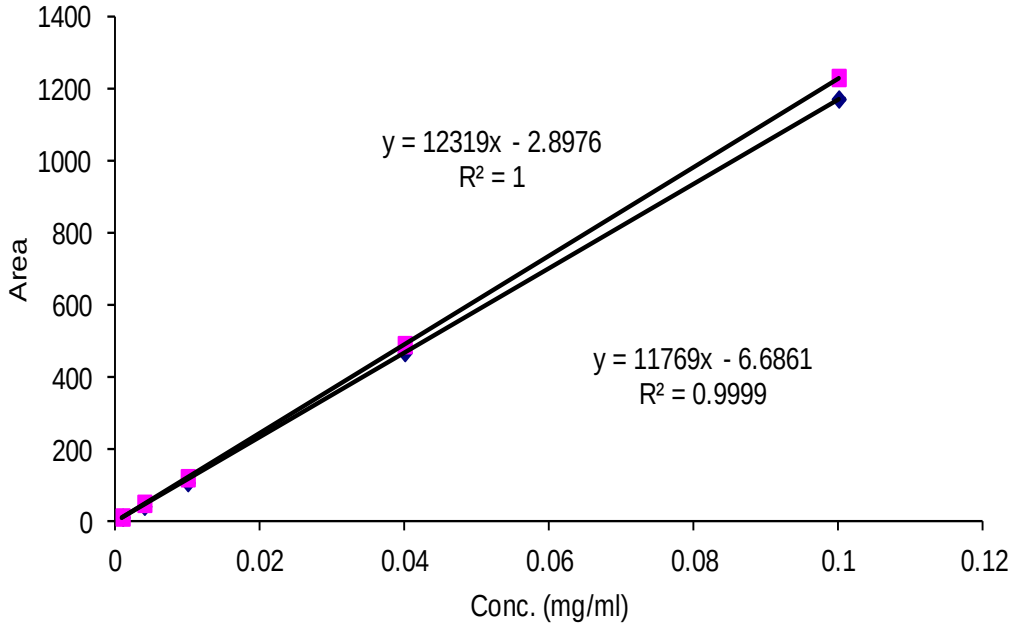

Figure 4.7. Calibration curve for HPLC assay for Rifampicin in Ethanol: water (50:50) mixture (Square) and Cell lysate (Diamond). Data represent mean ± sd, *n*=3 calibration curves (each each calibration curve having 3 analyses at each concentration).

4.4.4. Delivery of Rifampicin to J774 cells

The amount of rifampicin associated with the J774A.1 increased as the amount of drug administered increased (Figure 4.8). As the drug input increases from 50 to 500 µg, the amount of drug accumulating in the cells increases from 3.9 to 10.2 µg and from 3.8 to 7.5 µg for PVA nanospheres and nanocapsules, respectively. In

contrast, the amount of free rifampicin accumulated in the cells was significantly lower ($p < 0.05$, ANOVA). The increase was only from 2.7 to 3.3 µg over the 6 h incubation time.

Since the Bradford assay results showed that the mass of proteins recovered was different for the three formulations (Fig 4.9), the uptake results were normalised and presented as mass of drug per mass of proteins (Figure 4.6). The same trend was observed as in figure 4.6. The amount of the dug associated with the cells was significantly higher for the PVA nanocarriers than the free drug ($p < 0.05$, ANOVA). However, the PVA nanocapsules were shown to be more efficient in terms of delivering the drug to the cells. When the cells were incubated with the same dose of drug e.g 1000 µg, the drug concentration reached 0.6, 0.5 and and 0.06 µg/ µg (drug/protein) for the NC, NS and free drug, respectively (Figure 4.9).

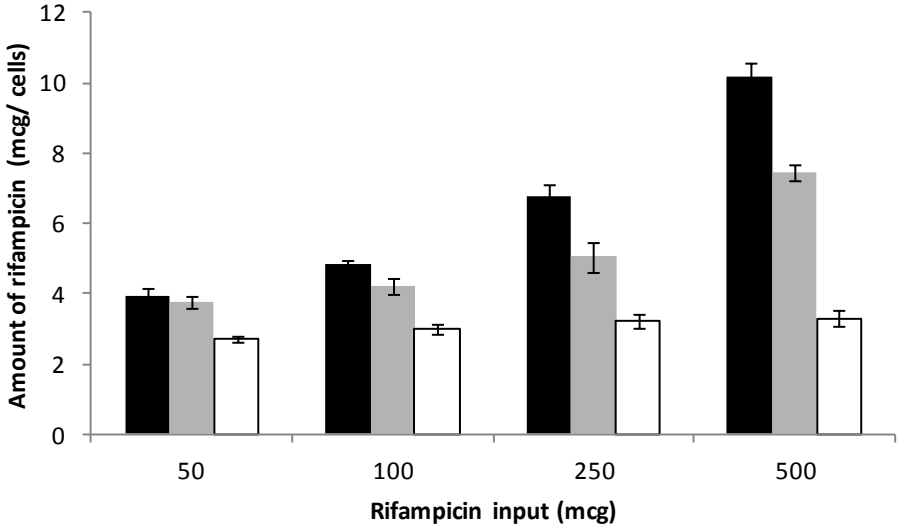

Figure 4.8. The amount of rifampicin accumulated inside the J774A.1 cells after 6h incubation with rifampicin-loaded nanospheres (Black), rifampicin-loaded nanocapsules (grey) and free rifampicin (white) at four different concentrations (n=6).

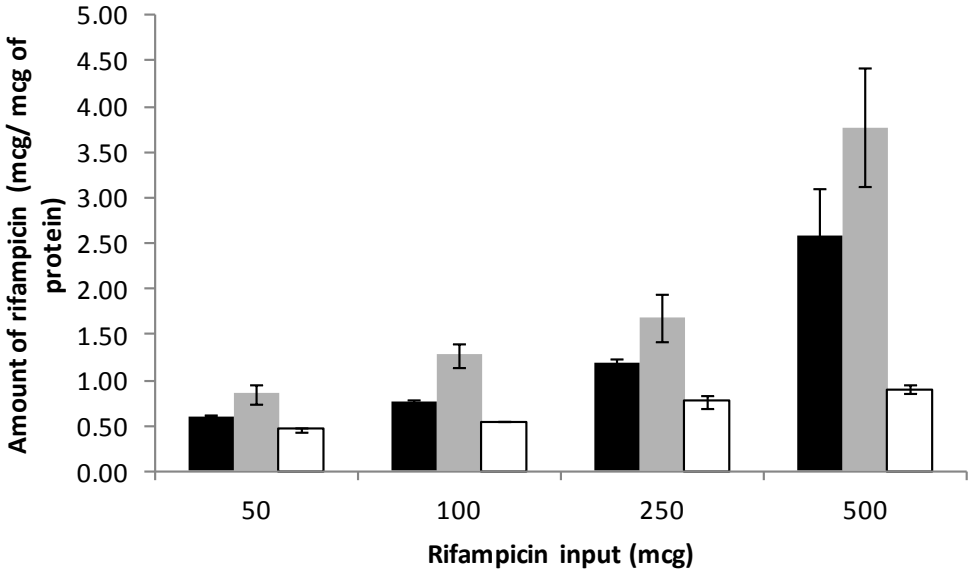

Figure 4.9. The amount of rifampicin per mass of protein recovered from J774A.1 cells after 6h incubation with rifampicin-loaded nanospheres (black), rifampicin-loaded nanocapsules (grey) and free rifampicin (white) at four different concentrations. (n=6).

4.4.5. The predicted cellular dose

Particokinetics calculations show that the percentage of nanoparticles reaching the cell monolayers was between 13.6 and 19.6 % (Table 4.2). It can also be seen that the predicted dose for the PVA nanocapsules was approximately double the predicted dose for the PVA nanospheres at all four concentrations.

Mass of rifampicin in the nanoparticles (µg)	NS				NC			
	Nominal dose (µg)	Nominal number of particles ($x10^9$)	Predicted number of particles ($x10^9$)	Particles reaching the cells (%)	Nominal dose (µg)	Nominal number of particles	Predicted number of particles	Particles reaching the cells (%)
50	218	21	2.9	13.6	617	45	6.7	15
100	436	37	5.2	14.2	1234	68	11.4	16.8
250	1091	86	12.5	14.6	3086	146	26.1	17.9
500	2183	148	22.8	15.4	6172	241	47.2	19.6

Table 4.2. The nominal and predicted dose of rifampicin-loaded nanospheres (NS) and rifampicin-loaded nanocapsules (NC) after 6 h incubation with J774 cells.

4.5. Discussion

The aim of this study was to investigate the uptake of PVA nanoparticles by a macrophage-like cell line, J774A.1. This model was chosen because it is a standard cell line used in phagocytosis studies that faithfully mimics many aspects of macrophage function. In this regard, a study using mouse macrophage cell line J774A.1 showed that certain combinations of antimicrobial agents are able to kill the Mycobacterium avium complex (MAC) inside macrophages and suggested that this cell line could be used as a model for screening of drugs for intracellular activity against MAC (Yajko *et al*, 1989). As a test of the validity of this model, alveolar macrophages isolated from the bronchoalveolar lavages of 36 patients were used for the same experiment. The good agreement between the alveolar macrophages results and those obtained with J774A.1 cells gave further evidence that mouse macrophage continuous cell line J774A.1 is a valid alternative to the use of alveolar macrophages to screen antimicrobial agents for intracellular activity against MAC (Yajko *et al*., 1991).

The cell viability was measured by quantification of mitochondrial dehydrogenase activity. The blank and rifampicin-loaded PVA nanoparticles showed negligible cytotoxicity in the J774A.1 cells after a 6h incubation at concentrations of 10 mg/ml or lower. Lherm *et al*., (1992) observed a time-dependent increase in cytotoxicity after incubating different types of poly (alkyl cyanoacrylate) nanoparticles with L929 fibroblasts (Lherm *et al*., 1992). This phenomenon was found to be related to the degradation products of the polymer. In our study, the low toxicity data could be explained by the low degradation products of PVA in the 6 h incubation period.

Bradford assay was employed in this study as a cell recovery-indicating assay. After incubation with the PVA nanocarriers the adherent cells were lysed and proteins released were quantified to determine cell recovery. This assay demonstrated that there was a significant decrease in cell recovery after exposure to the drug ($p< 0.05$). The high toxicity of cells in the presence of free rifampicin has been demonstrated by a number of studies (Barrow *et al*., 1998; Kumar *et al*., 2006). Barrow *et al*., (1998) demonstrated that the incubation of MM6 human monocytic cells with rifampicin solution (2 µg/ml) for 7 days resulted in viability of 42 %. In another study, Kumar *et al*., (2006) showed that rifampicin solution was toxic to VERO cells as only 50% of cells were viable after 72 h exposure. In our study, it was shown the encapsulation of rifampicin in PVA NS was shown to significantly reduce the toxicity of rifampicin for the J774A.1 cells ($p < 0.05$).

Loading rifampicin in the PVA nanocarriers dramatically enhanced the amount of drug associated with the cells. The amount of rifampicin imported into macrophages by drug-loaded nanoparticles, containing 1000 µg/ml of drug, was twice (NC) or three times (NS) greater than that attained with rifampicin solution. Similar results have been reported by Skidan *et al*. (2003) using rifampicin-loaded PBCA nanoparticles. The drug levels in alveolar macrophages 2-3 fold after incubation with with rifampicin-loaded nanoparticles in comparison to the free drug (Skidan *et al*., 2003). However, the polymer PBCA used in their study to produce the nanoparticles is non-biodegradable which limits the potential to use these particles as delivery systems. In addition, PBCA nanoparticles have been shown to exhibit a cytotoxic effect in peritoneal macrophages (Cruz *et al*., 1997). A number of studies have

demonstrated increased efficacy of nano-encapsulated drug in macrophage-infected models (Forestier *et al*., 1992; Balland *et al*., 1996 and pinto-Alphadary *et al*., 1994). It was suggested that the efficacy of nanotargeted therapeutic agents to macrophages, during bacterial infections, can be attributable to the maintenance of higher drug levels inside these cells.

The enhanced accumulation of encapsulated rifampicin relative to free form shows that the encapsulation allows entry of rifampicin into the cells using an additional cellular internalization process, presumably phagocytosis or endocytosis. Vauthier *et al*. (2003) showed that that the uptake of nanoparticles by J774 macrophages occurs via an endocytocis process, after which the particles end up in the lysosomal compartment where they are degraded (Vauthier *et al., 2003).* In another study, wheat germ agglutinin-conjugated PLGA nanoparticles were shown to be taken up up by A549 cells by a receptor-mediated, caveola-dependant endocytic pathway (Mo and Lim, 2004)

Using the developed particokinetics model to calculate the predicted dose it was shown that the number of particles for PVA NCs was approximately twice than for the PVA NSs at all concentrations. This can explain the increased toxicity of the PVA NCs in comparison to the NSs observed in the Bradford assay. This illustrates the importance of taking particokinetics into consideration in the *in vitro* studies for toxicity assessment or particle uptake investigations. For example, the influence of particle size on the phagocytosis by mouse peritoneal macrophages was studies using polystyrene particles of different sizes (Tabata and Ikada., 1988). It was claimed that the maximum phagocytosis took place when their size was in the range

of 1-2 µm. Similar studies have been carried out by Shafer *et al*., using polyalkylcyanoacrylate, polymethylmethacrylate and human serum albumin nanoparticles (Shafer *et al*., 1992). The study claimed that nanoparticles of the same material were taken up to a larger extent if they were of larger diameter, which corroborates the findings of Tabata and Ikada (Tabata and Ikada., 1988). The differences in particle uptake by particles of different sizes in these studies could be due to the differences in the number of particles reaching the cells. Therefore, particokinetics modelling in such studies can be used to adjust the nominal doses for accurate predicted doses so that any change in particle uptake would reflect the effect of the variable under investigation.

4.6. Conclusion

The present work established the suitability of PVA nanoparticles as a drug delivery system for rifampicin. The MTT assay revealed a negligible *in vitro* toxicity of PVA nanoparticles in J774A.1 cells, hence justifying biocompatibility of this delivery system. In addition, the PVA nanocarriers were shown to increase rifampicin uptake substantially in comparison with the free drug. The particokinetics model demonstrated the importance of predicted dose calculations in the *in vitro* studies.

One of the reasons for the failure of anti-TB therapy is the exposure of mycobacteria to sub-therapeutic levels of antibiotics. Conventional therapy by the oral and parenteral routes fails to deliver anti-TB drugs to AMs and granulomas harbouring dormant mycobacteria. Local delivery of the PVA carriers to lungs allows these

carriers to be in contact with AMs and higher drug deliverey to these cells and lung lesions. Therefore, in next Chpater PVA nanocarriers will be incorporated into an inert carrier that can deliver and release these delivery systems in the lung.

CHAPTER FIVE

Inhalable microspheres containing PVA nanocarriers

5.1. Introduction

Since most of the TB manifestations are observed mainly in the respiratory system, treatment by local delivery to the lungs by inhalation has emerged as an attractive alternative to oral dosing (Pandey *et al*., 2005). In Chapter 4, it was demonstrated that encapsulating rifampicin into PVA nanocarriers increased the association of the drug with the macrophages. Pulmonary delivery of the PVA carriers provides an opportunity to optimise the ability of AMs that harbour the mycobacterium to be exposed to higher doses of rifampicin. In addition, the potential of these carriers to release their drug load in a sustained fashion in the lungs, the primary site of infection in TB, could lead to reduced doses and less frequent administration, which will minimise systemic toxicity of the drugs and potentially improve patient compliance (Pandey *et al*., 2005).

The administration of anti-TB drugs-loaded nanoparticles by nebulisation has been shown to be a promising alternative to the oral delivery (Muttil *et al*., 2009). Using nebulisation, Pandey *et al.,* (2003) demonstrated that PLGA nanoparticle-loaded anti-TB drugs have been detected in the lungs 11 days post administration. In addition, five doses of nanoparticles administered every 10 days shown to have the same anti-TB effectiveness as 46 oral daily doses (Pandey *et al*., 2003). In another study, Zahoor *et al.,* (2005) encapsulated rifampicin, isoniazid and ethambutol in alginate nanoparticles which were detectable up to 14, 10 and 14 days, respectively, as opposed to the fast clearance of the free drugs after 12–24 h. Nebulization of drug-loaded alginate nanoparticles (1 dose twice a week, 3 doses) over the course of 45 days was as effective in clearing the lungs and the spleen of M. tuberculosis-

infected guinea pigs as 45 oral daily doses of the free drugs. The ability of nebulization to administer the anti-tubercular drug-loaded nanocarriers is evident from the previous studies but in Chapter 3, it was demonstrated that, upon manufacture of the nanoparticles, rifampicin is continuously released from the nanocarriers. During storage, drug release is a significant problem for nanocarriers as the formulation will revert to activity like a simple solution (Zhao *et al*., 2010a; Zhao *et al*., 2010b).

Successful deposition into deep lung will localise the nanocarriers with AMs, but this requires the particles be large enough to avoid exhalation (Tsapis *et al*., 2002; Gill *et al*., 2007). The optimal particle size for achieving delivery deep into alveolar region has been established to be an aerodynamic diameter between 1 and 3 μm (Byron, 1986). Therefore the nanoparticle carrier must be formulated within large structures for delivery to avoid a large fraction of the inhaled nanoparticles (up to 80%) escaping lung deposition (Finlay *et al*., 1997; Heyder *et al*., 1986; Heyder and Rudolf, 1984).

One way to overcome the challenges of pulmonary delivery of nanosystems is the use of hydrophilic microparticle vector. If the PVA nanoparticles can be encapsulated into an inert microparticle of a suitable particle size it can be deposited in the deep lung. Carbohydrates are widely used as carriers in dry powder formulations as they are approved for inhalation purposes by the Food and Drug Administration (Bosquillon *et al*., 2001). Moreover, their non-toxicity and biodegradability properties made them very popular inhalable drug carriers.

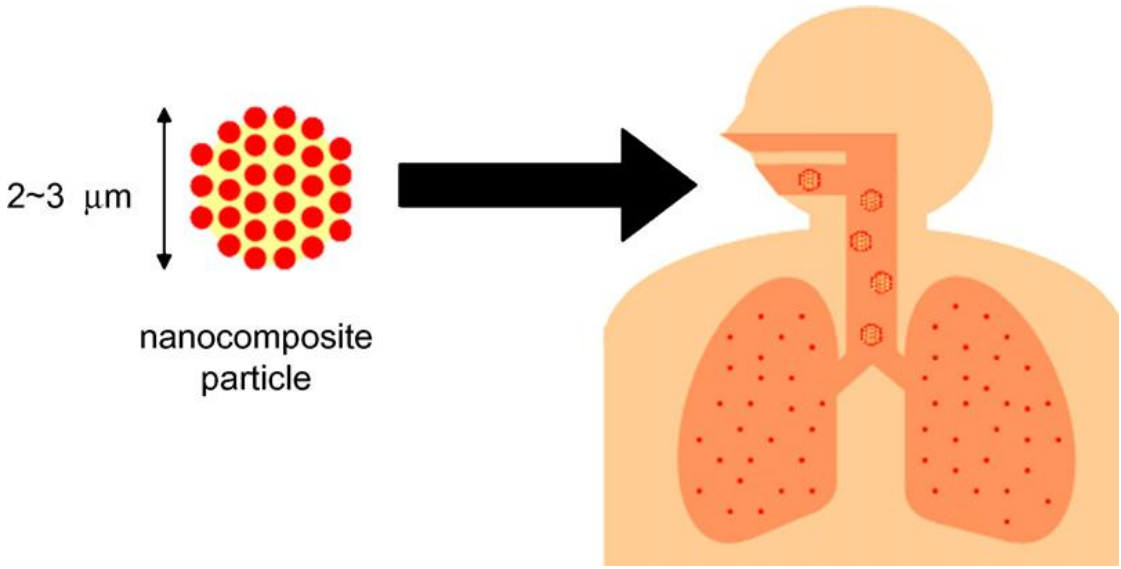

Figure 5.1. Decomposition of microparticles into nanocarriers following their deposition in the lung (Makino *et al*., 2006).

It was previously demonstrated that the rate of rifampicin release from the PVA nanocarriers was dependent on the pH of the release media. PVA hydrolysis is accelerated in the presence of an acidic or alkaline catalyst. To investigate the extent to which the administration of nanocarriers in a dry powder form would reproduce the release profiles observed when nanoparticles were delivered as a suspension the incorporation of a pH-modifier in the nanocarrier-containing dry powder formulation will be attempted.

It was hypothesized that developing nanoparticle-containing microspheres, with an aerodynamic diameter between 1 and 5 μm, would facilitate the co-localization of rifampicin and AMs in alveolar regions of the airways. Therefore, the aim of the work

in this chapter was to investigate the ability of microencapsulated PVA nanoparticles to deliver rifampicin from a dry powder inhaler. To achieve this aim the following objectives were set:

- Spray dry the PVA nanoparticles with lactose to produce microspheres of an inhalable aerodynamic diameter.
- Characterize the formulations with regard to their yield, particle size, dissolution in aqueous solutions, drug content and morphological evaluation.
- Investigate the nature of rifampicin release when presented to a liquid interface using the microparticle vector.
- Investigate the effect of pH modifier inclusion in the dry powder formulation on the release rate of rifampicin from the nanoparticle-containing microparticles.

5.2. Materials

Lactose and succinic acid were purchased from Sigma Aldrich, UK. Other materials were as described in Chapter 3.

5.3. Methods

5.3.1. Preparation of nanoparticle-loaded microsphres

Blank and rifampicin-loaded PVA nanoparticles were prepared and purified according to Section 3.4.1.

5.3.2. Microsphere production by spray drying

Spray drying was performed with a mini-spray drier (Buchi laboratoriums-Technik, Flawil, Switzerland), which operates on the principle of a nozzle spraying in a parallel flow (Table 5.1).

Spray drying parameters	Operational conditions
Inlet air temperature (^{o}C)	180
Aspiration setting (%)	85
Feed flow rate (ml/min)	2
Air flow rate (l/h)	700
Atomising air pressure (psi)	80

Table 5.1. Operational conditions applied for the spray-drying technique

For the preparation of rifampicin- and blank PVA nanoparticle-loaded microspheres, 1 ml of concentrated nanosuspensions was mixed with lactose dissolved in distilled water (3 g in 90 ml of water) using magnetic stirring for 10 min. The mixture volume was adjusted to 100 ml with additional water. For the preparation of microspheres containing a pH modifier, 1g of the pH modifier (either sodium hydroxide or succinic acid) was dissolved in a lactose solution (2 g in 90 ml of water) by magnetic stirring for 10 min. The mixture volume was then adjusted to the desired volume (100 ml) with additional water. Aqueous suspensions of lactose (3 g in 100 ml) were also spray dried in the same conditions as controls. The preparation spray drying feed stock was maintained under moderate agitation and supplied into the spray drier using a peristaltic pump. The dried powders were recovered, weighed and stored at room temperature, protected from light, in the presence of a dessicant potassium pentoxide. For process yield determination the spray-dried powders collected were weighed and the yield was calculated by dividing these quantities by the total mass in the drying feed stock for each batch.

5.3.3. Particle size analysis

The particle size distribution (PSD) of each sample was evaluated using a Sympatec Helos/Rodos laser diffraction particle-size analyzer (Sympatec Inc. Germany). Approximately 20 mg of powder was introduced to the dry dispersion feeder system using a vibratory feed tray. The dispersion pressure was set at 4.0 bar (found optimal to break up any loose agglomerates in the sample). The laser diffraction system, equipped with the appropriate lens for the sample's particle-size range was used to measure the PSD of the sample. The cumulative PSD and D10, D50, D90 were calculated using the Sympatec Windox 4.0 software.

5.3.4. Particle morphology

Microparticles were mounted on 0.5 inch aluminium stubs using double sided adhesive tape discs. The samples were spatter coated operated at an electrical potential of 2.0 kV, a current of 20 mA and at high vacuum (0.02 Torr) for 2 min. This procedure resulted in a film of gold, approximately 15 to 20 nm thick, being deposited on the specimen. The electron micrographs were recorded on 220 size Ilford FP4 film using a scanning electron microscope.

5.3.5. Nanoparticles recovery from dry powders in aqueous medium

A 100 mg aliquot of spray dried powder was dispersed in a bottle containing 5 ml of PBS (pH 7.4) under magnetic stirring at a temperature of 37 ^{o}C. The particle size of released NP from each formulation was measured by PCS.

5.3.6. Drug uniformity content

Drug uniformity content for each formulation was determined by dissolving 100 mg of the spray dried powder in a 20 ml mixture of ethanol: water (50:50) and drug was quantified using HPLC (Section 3. 3. 4).

5.3.7. The preparation of PVA nanoparticle-pH modifier containing powders

Rifampicin-loaded PVA nanospheres-containing microspheres were blended with pH-modifier containing-microspheres at 1: 1 ratio. The two powders were mixed for 30 min using the TURBULA® shaker mixer.

5.3.8. pH measurements

Three powders were used in the experiments: (a) Rifampicin-loaded nanospheres containing-microspheres, (b) Rifampicin-loaded nanospheres containing-microspheres: Sodium hydroxide-containing microspheres (1:1) and (c) Rifampicin-loaded nanospheres containing-microspheres: Succinic acid-containing microspheres (1:1). 5 mg aliquot of each powder was dispersed in 2 ml of PBS (pH 7.4) and maintained under moderate agitation. The pH of the mixture was determined at 0, 6, 12 and 24h.

5.3.9. Deposition characterisation

A Twin Stage Impinger (TSI, Apparatus, British Pharmacopoiea 2000) was adapted to accommodate a filter-containing transwell in the lower chamber where particles with an aerodynamic diameter of less than 6.4 um were normally deposited. A size 3 capsule containing approximately 20 mg of powder was placed in a handheld, breath-activated inhaler device (Aerolizer®, Novartis, Fig. 6.2). The capsule was punctured, a pump was actuated to simulate an inspiration (utilizing an air flow rate of 30 L/min for a duration of 8 s) and the powder was deposited on different stages. The procedure was repeated 20 times for each formulation (n=3). Stage 1 and stage 2 of the impinger contain respectively 7 and 30 mL of collecting solvents (ethanol/water, 50/50 v/v) to dissolve particles.

5.3.10. Mass of powder delivered to the transwell

Deposited powders were recovered from the transwell by removal of the filter membrane which was then placed into a glass bottle containing 1 ml of solvent (ethanol/water 50/50 v/v) and sonicated for 5 minutes. Powder in the device, mouthpiece, stages 1 and 2 was dissolved by rinsing with fresh solvent (ethanol/water 50/50 v/v) and the solutions were then diluted to appropriate volumes. Rifampicin content on each stage was determined using HPLC. Powder deposited on stage 1 corresponds to the amount deposited in the mouth and throat whereas powder deposited on the transwell and stage 2 corresponds to what is actually deposited in the lungs.

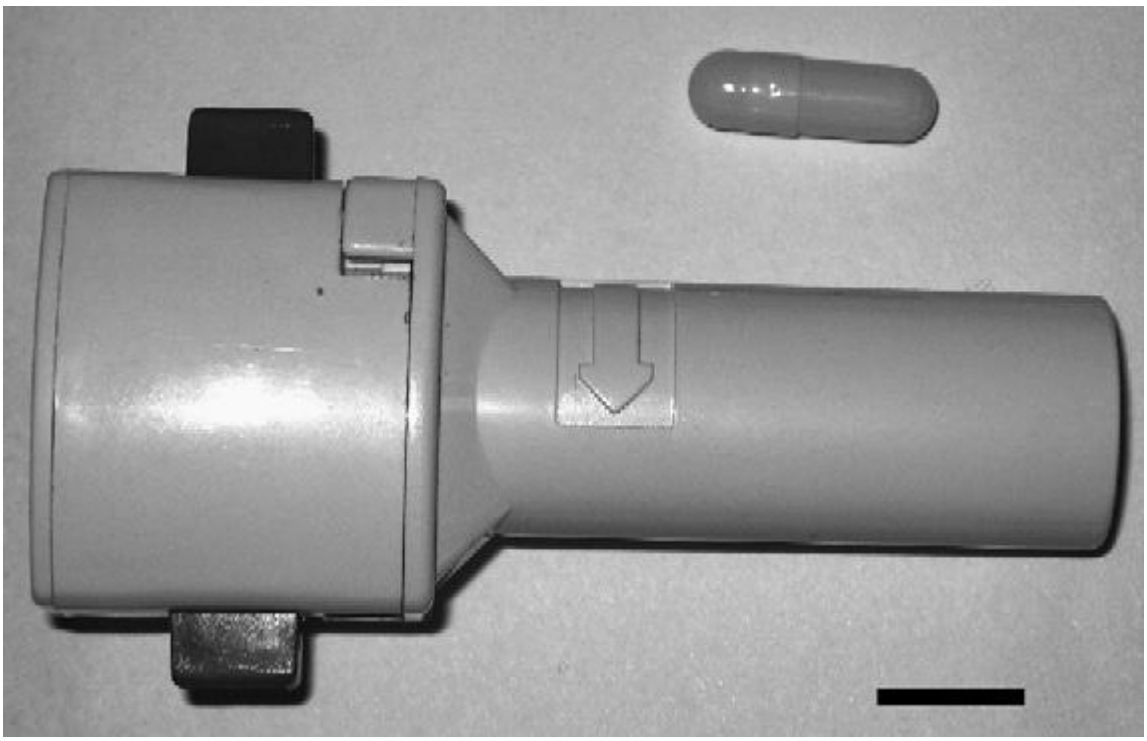

Figure 5.2. Dry powder inhaler (DPI) Aerolizer from Novartis.

5.3.11. Release kinetics of microencapsulated nanoparticles

Four formulations were aerosolised into the TSI containing a filter-containing Transwell placed in the lower chamber as described above. Deposited powders were recovered from the transwell by the removal of the membrane which was then placed into a glass bottle containing 1 ml of phosphate buffer and maintained in moderate agitation at 37 ^{o}C. At 0 and 24 h 0.5 ml samples were withdrawn from the suspensions. The nanoparticles were separated from the dispersing medium by ultrafiltration/centrifugation technique using 0.5 ml centrifugal concentrators with MWCF of 100 kDA (Amicon Ultra 0.5ml) at 3000×*g* for 5 min. The drug content in the nanoparticles and the dispersing medium were analysed by HPLC. Drug remaining in the nanoparticles was calculated after 24 h (*n* = 3) (equation 6.1).

$$W_d\,(\%) = \frac{M_{t24}}{M_0} \text{x}\ 100 \qquad (6.1)$$

Where W_d is the percentage mass of the drug remaining in the nanoparticles; M_{t24} is the mass of drug in the nanoparticles at t_{24} and M_0 is the mass of drug in the nanoparticles at t_0.

5.3.12. Data analysis and statistics

All data was expressed as mean ± standard deviation (S.D.) Statistical analysis was performed in SPSS, version 16.0, using either student *t*-test or an analysis of variance (ANOVA) with the chosen level of significance at $p \leq 0.05$.

5.4. Results

5.4.1. Spray dried microsphere characteristics:

Incorporating blank or rifampicin-loaded PVA nanocarriers into microspheres did not have any effect on particle size (Table 5.2). In contrast, the incorporation of a pH modifier resulted in a significant increase in particle size ($p < 0.05$). The recovery yields ranged from 43.7 to 54.8 % for the nanocarrier-conatining microspheres. The recovery yields were much lower for the pH modifier-containing microspheres resulting in 32.3 ± 8.41 and 35.9 ± 4.25 % yields for NaOH-containing microspheres and succinic acid-containing microspheres, respectively.

	Particle size (µm)			
Formulation	X10	X50	X90	**Yield (%)**
B-NS-MS	0.45 ± 0.023	2.28 ± 0.015	3.84 ± 0.006	46.3 ± 5.23
Rif-NS-MS	0.32 ± 0.015	1.86 ± 0.053	3.61 ± 0.176	43.7 ± 4.78
B-NC-MS	0.36 ± 0.032	2.02 ± 0.049	3.59 ± 0.015	54.8 ± 7.36
Rif-NC-MS	0.33 ± 0.021	1.82 ± 0.114	3.36 ± 0.131	52.6 ± 8.57
NaOH-MS	0.57 ± 0.02	2.65 ± 0.036	6.90 ± 0.064	32.3 ± 8.41
Succ-MS	0.61 ± 0.04	3.42 ± 0.207	23.75 ± 1.551	35.9 ± 4.25

Table 5.2. Particle size of the different spray dried powders: B-NS-MS (blank nanosphere-microspheres; Rif-NS-MS (rifampicin-loaded nanosphere-microspheres); B-NC-MS (blank nanocapsules microspheres; rifampicin-loaded nanocapsules microspheres (Rif-NC-MS); NaOH-MS (blank NaOH-microspheres) and Succ-MS (blank succinic acid-microspheres) using laser diffraction, yield of spray drying. Data represent mean ± SD.

SEM micrographs indicated that the NS- and NC-containing microspheres were spherical in shape with smooth surfaces (Figures 5.3A and 5.3B). The pH-modifier-containing microspheres had a rough surface and appeared to be a little aggregated. The NC-containing powder was very sticky and the presence of big agglomerates of paricles in the powder can be seen (Figure 5.3B).

5.4.2. Drug uniformity content and nanoparticles recovery from dry powders in aqueous medium

The amount of nanoparticles encapsulated in the microspheres was similar for PVA nanospheres and PVA nanocapsules, approximately 820 µg of nanoparticles per 100 mg of powder (Table 5.3). However, Drug content of rifampicin-nanospheres-containing powders was almost three times higher than the rifampicin-nanocapsules-containing powders. The spray dried microspheres dissolved instantly when dispersed in aqueous solution. The mean particle size of the nanoparticles in the resultant suspensions was measured and found to be increased for both formulations (Table 5.3).

Formulation	Particle size before spray drying (nm)	Particle size after release (nm)	Amount of drug in 100mg powder (µg)	Amount of NP in 100 mg powder (µg)
Rif-NS-MS	215.7 ± 5.8	265.3 ± 21.2	187.1 ± 19.4	816.9 ± 84.7
Rif-NC-MS	142.9 ± 7.2	231.8 ± 17.7	66.9 ± 4.3	822.1± 52.5

Table 5.3. Nanoparticle size before spray drying and after microsphere dissolution in aqueous solutions and drug uniformity content of rifampicin-nanosphere-loaded microspheres (Rif-NS-MS) and rifampicin-nanocapsules-loaded microspheres (Rif-NC-MS) (Data represent mean ± SD)

(A)

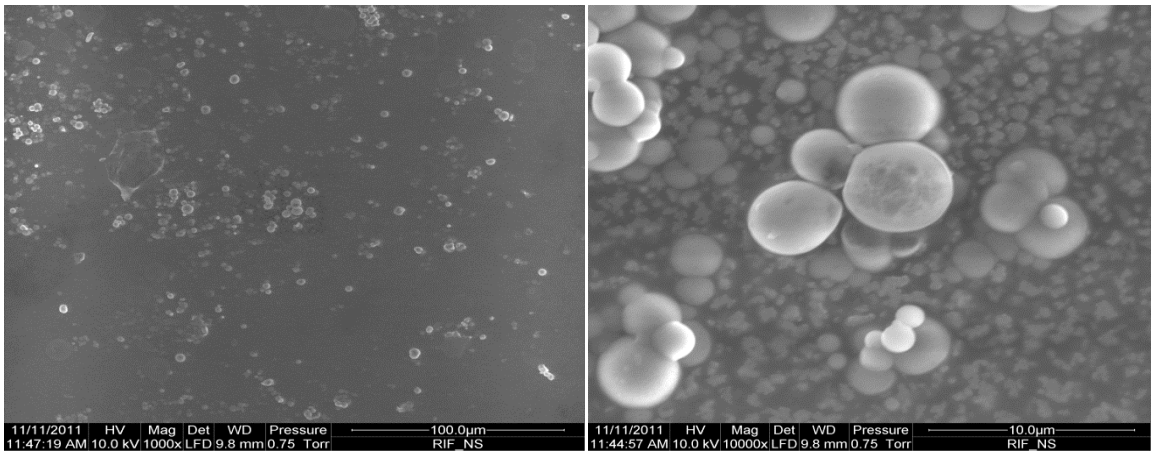

(B)

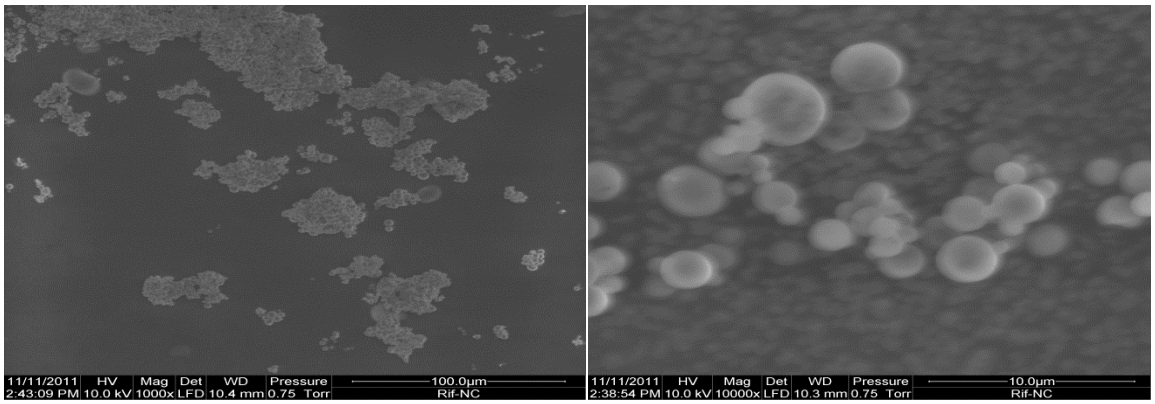

(C) **(D)**

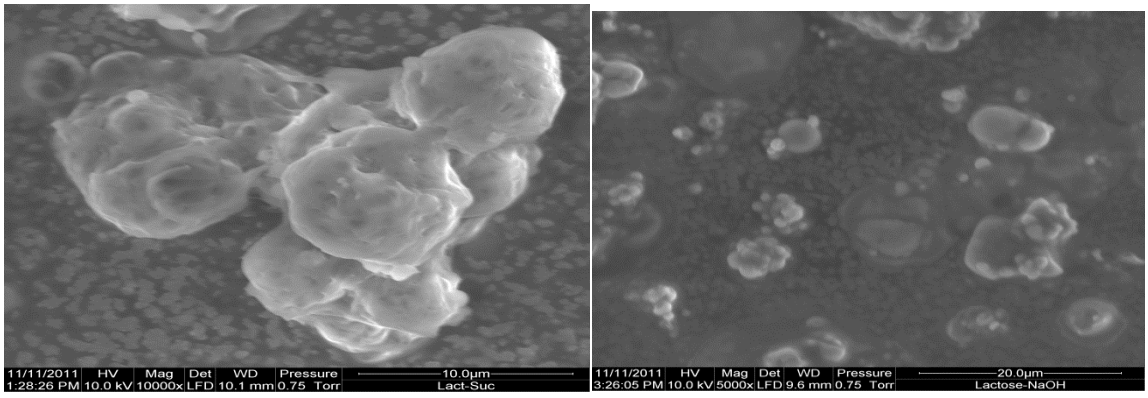

Figure 5.3. Representative scanning electon micrographs of the spray dried formulations: (A) PVA nanosphere-microspheres, (B) PVA nanocapsule microspheres (C) Succinic acid-microspheres and (D) NaOH-microspheres.

5.4.3. pH monitoring of powders at phosphate buffer pH 7.4

The incorporation of a pH modifier in the microspheres and blending it with nanoparticle-containing microsphres had a significant effect on the pH of the incubation media ($p < 0.05$). For sodium hydroxide-containing microspheres, the pH was constantly higher than 10 over the 24 h period. In contrast, the pH of the suspension was constantly lower than 5 when the nanospheres-containing powders were blended with succinic acid containing powders at a 1:1 ratio (Figure 5.4).

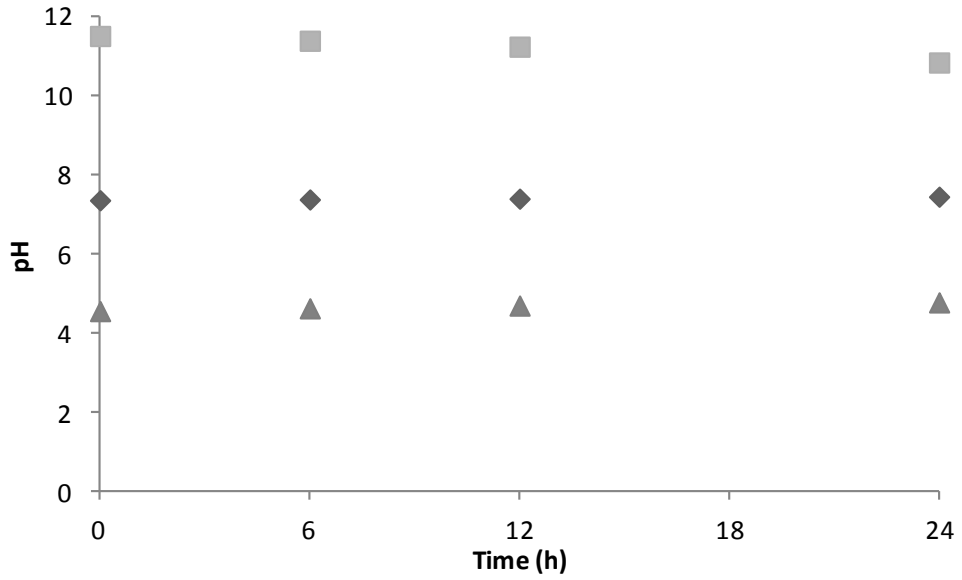

Figure 5.4. pH values of the suspension of Rif-NS-MS (diamond), Rif-NS-MS: NaOH-MS (1:1) (square) and Rif-NS-MS: Succinic acid-NS-MS (1: 1) (Triangle). Data represent mean ± SD.

5.4.4. The deposition of the nanocomposite particles

The recovery of formulations after aerosolisation was high (between 80 and 101 %) for all formulations (Table 5.4). NS-containing powders (R-NS-MS) had a higher deposition than the nanocapsule-containing powders (R-NC-MS) (Figure 5.5). The percentages of powder depositing on the transwell and stage 2 were 5.6 and 22.5 %, respectively, for R-NS-MS, and 0.7 and 6.2 % for R-NC-MS. There was no effect on the deposition pattern when the R-NS-MS were blended with NaOH-MS. However, mixing R-NS-MS with succinic acid-microspheres the percentage of powder depositing on the transwell significantly decreased from 5.6 to 0.1 %.

	Delivered dose (μg)	Transwell	Stage 2	Stage 1	Device	Mouthpiece	Recovery
Rif-NS-MS	730.3 ± 71.4	40.95 ± 5.29	164.8 ± 19.8	328.9 ± 8.4	160.6 ± 10.8	23.6 ± 1.4	98.7 ± 4.6
Rif-NS-MS: NaOH-MS	323.9 ± 18.5	23.97 ± 4.29	79.1 ± 09.3	156.9 ± 9.5	59.1 ± 12.5	10.5 ± 0.9	101.7 ± 0.7
Rif-NC-MS: Succ-MS	293.6 ± 07.6	0.27 ± 0.04	18.2 ± 03.9	202.1± 12.8	10.03 ± 1.5	6.8 ± 3.3	80.9 ± 0.8
Rif-NC-MS	260.6 ± 16.6	1.86 ± 0.29	16.6 ± 02.3	155.3 ± 13.4	55.8 ± 6.6	8.5 ± 1.5	91.2 ± 6.9

Table 5.4. The amount of rifampicin in the delivered dose, the amount of rifampicin on different stages of the TSI after deposition of the different spray-dried powders and % recovery of rifampicin-loaded nanosphere-microspheres (Rif-NS-MS); rifampicin-loaded nanospheres-microspheres: NaOH-microspheres (Rif-NS-MS: NaOH-MS); rifampicin-loaded nanospheres: succinic acid-microspheres (Rif-NSMS: Succ-MS) and rifampicin-loaded nanocapsules microspheres (Rif-NC-MS). Data represent mean ± SD.

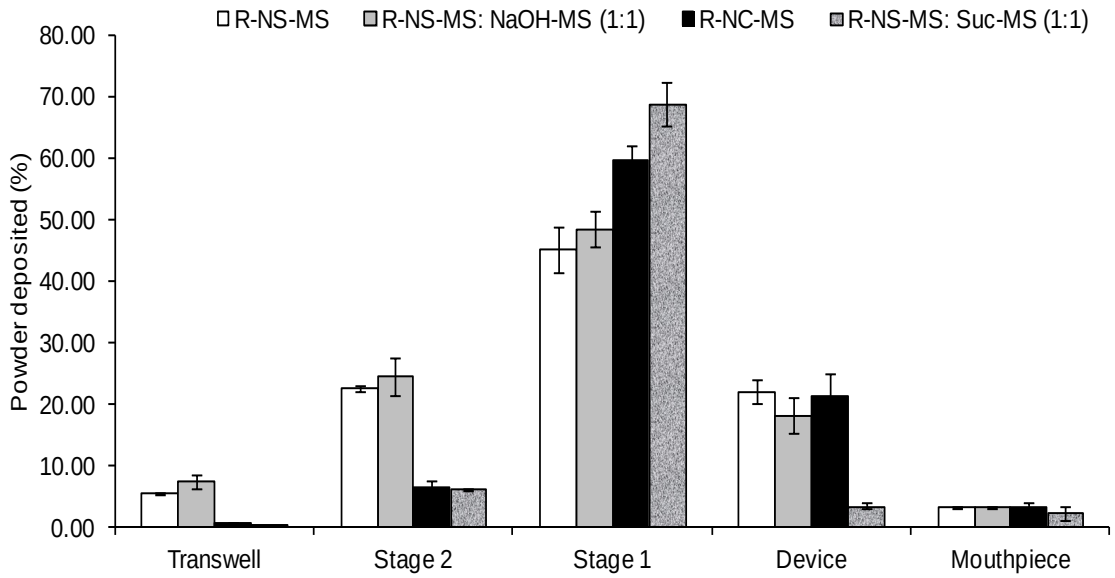

Figure 5.5. Percentage of powder deposited on different stages of the TSI for four different formulations: rifampicin-loaded nanosphere-microspheres (Rif-NS-MS); rifampicin-loaded nanospheres-microspheres: NaOH-microspheres (Rif-NS-MS: NaOH-MS); rifampicin-loaded nanospheres: succinic acid-microspheres (Rif-NSMS: Succ-MS) and rifampicin-loaded nanocapsules microspheres (Rif-NC-MS). Data represent mean ± SD.

5.4.5. Release kinetics of microencapsulated nanoparticles

As it can be seen from figure 5.6, the amounts of rifampicin remaining in the nanoparticles were approximately 85 and 67 %, for nanospheres and nanocapsules, respectively. Once the pH modifier powder was mixed with the R-NS-MS, the release of the drug to the aqueous phase was enhanced. The amount of drug remaining in the particles decreased to 64 and 49 %, after the introduction of sodium hydroxide and succinic acid, respectively (Figure 5.6).

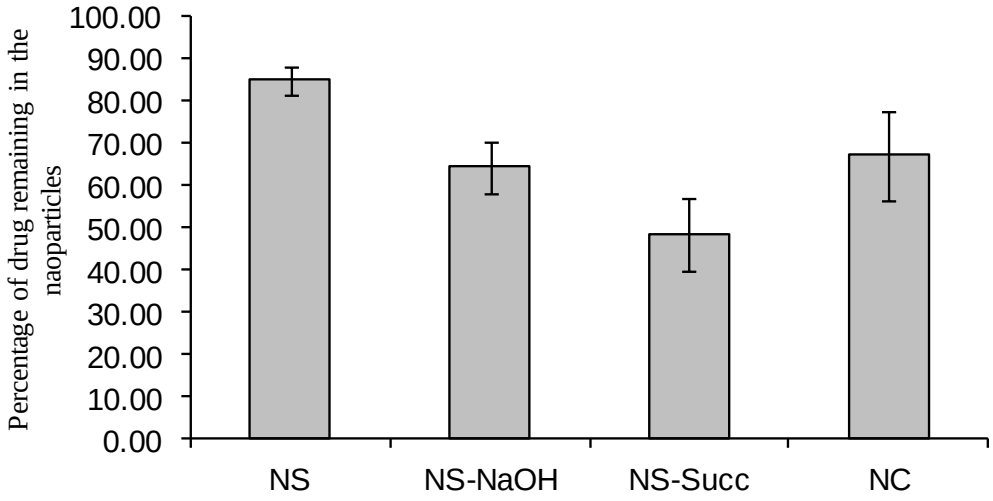

Figure 5.6. The percentage of drug remaining in the nanoparticles after 24 h incubation of rifampicin-loaded nanosphere-microspheres (NS); rifampicin-loaded nanospheres-microspheres: NaOH-microspheres (NS-NaOH); rifampicin-loaded nanospheres: succinic acid-microspheres (NS-Succ) and rifampicin-loaded nanocapsules microspheres (NC) in phosphate buffer pH7.4. Data represent mean ± SD.

5.5. Discussion

It was previously demonstrated that rifampicin was prone to continuous diffusion out the PVA nanoparticles upon manufacture. The incorporation of nanoparticles in a dry powder formulation would increase the shelf life of the formulation during storage and minimize drug diffusion out of the particles before administration. Therefore, in this chapter the feasibility of developing carrier particles to deliver PVA nanocarriers to the lower airways was investigated.

Spray drying was shown to be suitable as a mean to load PVA nanoparticles into a lactose microparticle vector. A carbohydrate was selected for the micropaticle matrix as it is approved by the Food and Drug Administration (FDA) for pulmonary delivery, and widely applied in pulmonary formulations (Bosquillon *et al*., 2001b). The microspheres produced in this work had a diameter of 2 to 4 µm which was considered to be suitable for delivery to the lower airways (Byron, 1986). The yield of PVA nanoparticle-containing microspheres during manufacture ranged from 43 and 55 %. Similar yield values have been reported for spray drying chitosan nanoparticles with lactose/mannitol (Grenha *et al*., 2005). SEM micrographs revealed that nanoparticle-containing microspheres were spherical in shape and had a smooth surface in comparison with the blank lactose microspheres and the pH modifier-containing microsphres. Grenha *et al*., (2005) observed that upon the incorporation of chitosan nanoparticles, the resulting mannitol microspheres showed more defined limits and spherical shape as the nanoparticles amount increased with respect to mannitol. In the previous work it was suggested that the incorporation of

nanoparticles as a solid structure contribute to the enhancement of microspheres morphology, once these can grow around a solid body (Grenha *et al*., 2005). The PVA nanocapsule-containing microspheres were shown to have a high tendency to agglomerate. This could be attributed to the presence of phospholipids in the formulation. The agglomeration of the primary particles and the adhesiveness of agglomerates can be explained by the degradation of the nanocapsules coating the microsphere surface (Tewa-Tagne *et al*., 2006).

Drug uniformity content data show that the encapsulation efficiency for the PVA nanospheres in the microspheres was significantly higher than the PVA nanocapsules ($p < 0.05$). This could be explained by the loss of the nanocapsules during the spray drying procedure. Tewa-Tagne *et al*., (2006) demonstrated that with insufficient concentration of adjuvant spray drying nanocapsules led to strong adhesive products onto the apparatus walls (Tewa-Tagne *et al*., 2006). In this work, lactose concentration was not sufficient to interact with all nanocapsules present in the feed. Therefore, the excess of nanocapsules adhered to the cyclone walls.

.

The ability of the obtained dry powders to release the nanoparticles following incubation in phosphate buffer (pH 7.4) was investigated. This experimental set up was chosen as It was assumed that the airway surface liquid has a pH of approximately 7, close to that of the interstitial fluid and plasma (Walters, 2002). We observed that after incubating the powders in the aqueous medium under low stirring rate, lactose dissolved instantly resulting in a nanoparticle suspension. In spite of

the slight enlargement of the nanoparticles they remain in the nano-range and thus retained the capacity to control drug release effectively. The enlargement of particles size after spray-drying was also found by Sham *et al*. (2004) for powders prepared with lactose and gelatin nanoparticles and the effect was attributed to eventual changes in conformation due to the thermal conditions of the spray-drying process (Sham *et al*., 2004).

A twin-stage impinger was adapted to accommodate a transwel in the lower chamber where particles with an aerodynamic diameter of less than 6.4 um are normally deposited. The amount of powder depositing on the transwell and stage 2 was significantly lower for the PVA nanocapsules-containing microspheres than the PVA nanospheres-containing microspheres ($p < 0.05$). This could be due to the surface active properties of the nanocapsule which induced agglomeration of particles during powder aerosolisation (French *et al*., 1996; Timsina *et al*., 1994).

The release of rifampicin from the PVA nanocarriers is shown to be siginificantly enhanced when particles are incubated in basic or acidic media (Chapter 3). In this chapter, there was an attempt to blend the PVA nanosphere-containing microspheres with pH-modifier-containing nanospheres. The objective was to investigate the extent to which the administration of nanocarriers in a dry powder form would reproduce the release profiles observed when nanoparticles were delivered as a suspension. The introduction of sodium hydroxide and succinic acid to the formulation successfully enhanced the release of the drug from the

nanocarriers. The pattern correlated well with the data obtained when the nanoparticles were presented as suspensions. The difference in the values reported in the two studies could be due the differences in the experimental set up and the lack of the buffering effect in this experiment.

In summary, the present study demonstrates that incorporation of PVA nanoparticles into respirable carrier particles is possible. The spray-dried powders had a suitable size and shape for airway deposition. After reaching alveolar regions, the carrier is expected to dissolve instantly in the alveolar lining fluid (pH 7.4) releasing the nanoparticles. Blending the PVA nanosphere-containing microspheres with pH-modifier-containing microspheres had a pronounced effect on the release of the drug from the PVA particles. This delivery platform opens up a wide of treatment applications of pulmonary and possibly systemic diseases using targerted delivery strategies via nanoparticles.

Chapter SIX

General Discussion

Despite the availability of potentially curative pharmacotherapies, TB remains the leading cause of preventable deaths (WHO, 2011). For new cases of drug susceptible TB, the most effective therapeutic regimen requires 6 months of treatment with first-line drugs (a combination of rifampicin, isoniazid, ethambutol and pyrazinamide for 2 months, followed by a 4-month continuation phase of rifampicin and isoniazid) (BNF, 2011). Despite its high efficacy, with cure rates of around 90 % in HIV-negative patients, the regimen is far from ideal. The long duration of therapy and the associated side effects can hamper patient lifestyle and induces patient non-compliance, treatment failure and development of drug-resistant strains (Chan and Iseman, 2008).

Mycobacterial strains exhibiting resistance to one or more drugs are arising at an alarming rate, requiring the incorporation of more drugs in the increasingly complex combination therapy. The current treatment of multi-drug resistant TB (MDR-TB) comprises of the administration of pyrazinamide simultaneously with second-line drugs such as ethionamide, prothionamide, cycloserine, capreomycin, p-aminosalicylic acid or fluoroquinolones. These second-line drugs are more toxic, more expensive and less active than first-line agents. Also, prolonged treatment (up to 24 months) is required in order to assure therapeutic effectiveness (Smith, 2003). In this context, low patient compliance and adherence to the administration regimens become crucial drawbacks of the pharmacotherapy, leading to increased TB mortality. Therefore, novel and effective anti-TB drugs and delivery systems are urgently required to replace or supplement the current therapies with the aims of shortening the treatment course and overcoming the problem of drug resistance.

For more than 40 years, not a single new drug has been developed and licensed for the treatment of TB. The emergence of MDR and extensively drug-resistant TB (XDR-TB) has spurred interest in the development of new drugs with different modes of action. At present there is a coordinated portfolio of promising new compounds on the horizon, some of which have the potential to become the cornerstone drugs of TB treatment in the future. There are 10 new compounds under clinical investigation (WHO, 2011). The status of the pipeline for new anti-TB drugs is illustrated in table 6.1.

Two of the Phase III trials are evaluating 4-month regimens (in which a fluoroquinolone, gatifloxacin or moxifloxacin, is used in place of ethambutol or isoniazid) for the treatment of drug-susceptible TB. The third Phase III trial is evaluating the use of rifapentine (a rifamycin that has a longer half-life than rifampicin) as part of a 4-month regimen. The use of rifapentine in combination with isoniazid for a shorter (3 months) treatment of latent TB infection is also being evaluated.

Of the compounds in Phase II trials, two are in the advanced stages of being tested for the treatment of MDRTB. These are TMC-207 (bedaquiline) and OPC-67683 (delamanid). Both compounds have been evaluated in Phase IIb trials in newly-diagnosed MDR-TB patients, in which either the investigational drug or a placebo were added to an optimized background regimen. Other compounds in Phase II trials include linezolid, which is being tested for the treatment of extensively drug-resistant TB (XDR-TB) at a dose of 600 mg (in the Republic of Korea) and at a dose of 300 mg for the treatment of MDR-TB (in South Africa) ; PNU-100480 (a close analogue of linezolid); PA-824; and SQ-109 (a derivative of ethambutol). In

November 2010, the first clinical trial of a novel TB drug regimen (NC001), investigating the bactericidal activity of a three-drug combination of PA-824, moxifloxacin and pyrazinamide was initiated.

These major advances in TB drug development mean that multiple trials will be needed in various high-burden countries. This presents several challenges. Trials are lengthy and costly since patients need to be followed for an extended period of time after completing treatment. New drugs have to be tested in specified drug combinations with current and newly re-purposed drugs. Moreover, researchers will be always faced with some of the old challenges of the conventional therapy. The inability of the new drugs to reach the bacilli in alveolar macrophages and lung granulomas can lead to the recurrence of the infection and consequently, in the long term, development of resistance to the new agents. Strategies allowing more efficient delivery of the anti-TB drugs to the infection reservoirs will be needed. Therefore it is not guaranteed to have a new drug in clinical use in the near future. On the other hand, first generation anti-TB drugs, such as rifampicin, are still highly effective. Overcoming the main pharmaceutical drawbacks of the conventional therapeutic agents to improve their effectiveness as well as to enhance compliance and adherence represents an attractive strategy and remains the main goal of the pharmaceutical industry.

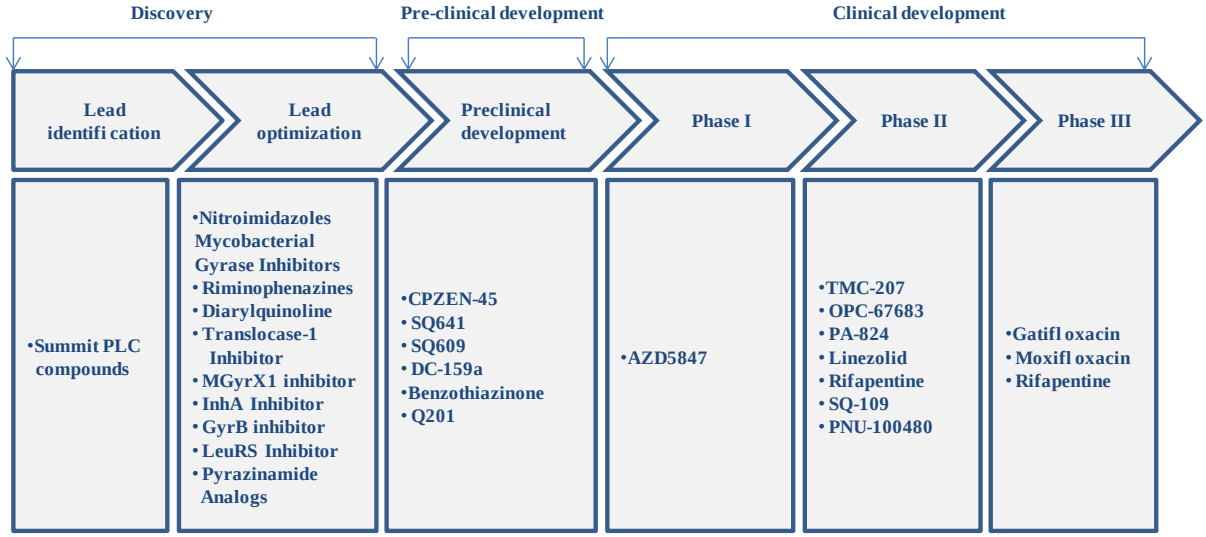

Figure 6.1. The development pipeline for new drugs (WHO, 2011).

Despite its association with a number of issues, rifampicin is still considered to be a powerful anti-tubercular agent. Rifampicin has poor and variable bioavailability because of its poor solubility, acid decomposition, variability in absorption and metabolism. It is associated with a number of side effects and known to cause severe liver damage when combined with isoniazid. It reduces the concentrations of anti-retroviral drugs used in AIDS by inducing the metabolising enzyme cytochrome P450. Another problem is attaining an effective concentration of rifampicin in the infected organ, the lungs. After oral administration of rifampicin, the concentration of rifampicin reaching the lungs is insufficient to provide anti-bacterial effects on the bacilli located in lung lesions and alveolar macrophages. This has been related the drug instability and its interaction with isoniazid after oral administration. Encapsulating rifampicin into a carrier delivery system that can release the drug in a controlled manner at therapeutic concentration over a period of time can solve most of the issues highlighted above (limited aqueous solubility, stability, poor

bioavailability, side effects and drug interactions) as well as improve patient compliance in terms of reducing dosing frequency. The ability of these carriers to deliver the drug directly to the lungs may allow therapeutic concentrations to penetrate effectively into lung lesions and eradicate the resident mycobacteria in alveolar macrophages.

In this context, nanotechnology appears be one of the promising approaches for the development of more effective drug delivery systems for the treatment of TB. Over the past 3 decades, the potential for replacing the administration of therapeutic agents in the free from with an approach of encapsulating them into nanoparticles has been extensively investigated. Many advantages of nanoparticle-based drug delivery have been recognized (Emerich *et al*., 2007; Groneberg *et al*., 2006). It improves the solubility of poorly water-soluble drugs, releases drugs at a sustained rate or in an environmentally responsive manner and thus lowers the frequency of administration, delivers drugs in a targeted manner to minimize systemic side effects, and can deliver two or more drugs simultaneously for combination therapy to generate a synergistic effect and suppress drug resistance. Currently, more than 20 nanoparticle therapeutics are in clinical use (Table 6.1), validating the ability of nanoparticles to improve the therapeutic index of drugs. In addition to the already approved nanoparticles, numerous other nanoparticle platforms are currently under various stages of preclinical and clinical development.

Composition	Trade name	Company	Indication	Administration	Status
Liposomal platforms					
Liposomal annamycin	L-Annamycin	Callisto	Acute lymphocytic leukemia, acute myeloid leukemia	i.v.	Phase I
Liposomal cisplatin	SLIT Cisplatin	Transave	Progressive osteogenic sarcoma metastatic to the lung	Aerosol	Phase II
Liposomal doxorubicin	Sarcodoxome	GP-Pharm	Soft tissue sarcoma	i.v.	Phase I/II
Liposomal fentanyl	AeroLEF	Delex Therapeutics	Postoperative analgesic	Aerosol	Phase II
Liposomal lurtotecan	OSI-211	OSI Pharmaceuticals	Ovarian cancer	i.v.	Phase II
Liposomal vincristine	Onco TCS	Inex, Enzon	Non-Hodgkin's lymphoma	i.v.	Phase II/III
Polymeric platforms					
HPMA copolymer-DACH platinate	ProLindac	Access Pharmaceuticals	Ovarian cancers	i.v.	Phase II
L-Leucine, L-glutamate copolymer, and insulin	Basulin	Flamel Technologies	Type I diabetes	s.c.	Phase II
PEG-anti TNF-α antibody fragment	Cimzia	Nektar	Rheumatoid arthritis and Crohn's disease	s.c.	Phase III
PEG-arginine deaminase	Hepacid	Phoenix	Hepatocellular carcinoma	i.v.	Phase I/II
PEG-camptothecin	Prothecan	Enzon	Various cancers	i.v.	Phase I/II
PEG-naloxol	NKTR-118	Nektar	Opioid-induced constipation	Oral	Phase I
PEG-uricase	Puricase	Phoenix	Hyperuricemia from gout	i.v.	Phase III
Pluronic block-copolymer doxorubicin	SP1049C	Supratek Pharma	Esophageal carcinoma	i.v.	Phase II
Polycyclodextrin camptothecin	IT-101	Insert Therapeutics	Metastatic solid tumors	i.v.	Phase I
Polyglutamate camptothecin	CT-2106	Cell Therapeutics	Colorectal and ovarian cancers	i.v.	Phase I/II
Polyglutamate paclitaxel	Xyotax	Cell Therapeutics	Non-small-cell lung cancer, ovarian cancer	i.v.	Phase III
Poly(iso-hexyl-cyanoacrylate) doxorubicin	Transdrug	BioAlliance Pharma	Hepatocellular carcinoma	i.a.	Phase I/II
Other platforms					
Calcium phosphate nanoparticle vaccine adjuvant	BioVant	BioSante	Vaccine adjuvant	s.c.	Phase I
Nanocrystalline paliperidone palmitate	Paliperidone palmitate	Elan, Johnson & Johnson	Schizophrenia	i.m.	Phase III
Nanocrystalline 2-methoxyestradiol	Panzem NCD	Elan, EntreMed	Various cancers	Oral	Phase II
Nanoemulsion-based therapy	NB-001	NanoBio	Herpes labialis	Topical	Phase II
Nanoemulsion-based therapy	NB-002	NanoBio	Onychomycosis	Topical	Phase I/II
Paclitaxel nanoparticles in porous, hydrophilic matrix	AI-850	Acusphere	Solid tumors	i.v.	Phase I
Poly-L-lysine dendrimer	VivaGel	Starpharma	Antimicrobial protection from genital herpes and HIV infection	Topical	Phase I
Propofol IDD-D	Propofol IDD-D	SkyePharma	Anesthetic	i.v.	Phase III

DACH, diaminocyclohexane; HIV, human immunodeficiency virus; i.a., intra-arterial; i.m., intramuscular; i.v., intravenous; PEG, polyethylene glycol; s.c., subcutaneous; TNF-α, tumor necrosis factor-α.

Table 6. 1. Clinically approved nanoparticle-based therapeutics (adapted from Zhang *et al*., 2008).

With regard to TB, some of the striking data have come from a number of *in vivo* studies using anti-TB drugs encapsulated into polymeric nanoparticles in animal models infected with M. Tuberulosis. Most of these studies used PLGA to encapsulate rifampicin, isoniazid or both into the nanocarriers (gelprina *et al*., 2005) Taking Sharma and colleagues study as an example, only three oral applications of the PLGA nanoparticle-loaded anti-TB drugs gave the same therapeutic protection against M. TB in guinea pigs as 45 daily doses of the free antibiotics (Sharma *et al*., 2004). Thus the nano-encapsulation of anti-TB drugs has the potential to substantialy reduce the dosing frequency for anti-TB drugs, leading to enhanced patient compliance, improved treatment success rate and reduced drug resistance incidence. Therefore, the aim of this project was to encapsulate rifampicin into new polymeric nanoparticles that can deliver and release the therapeutic agent in a controlled manner in the lungs, as well as have the potential to target the bacilli residing in alveolar macrophages and lung lesions.

Poly (vinyl alcohol) (PVA) is a synthetic crystalline polymer formed by the full or partial hydrolysis of poly (vinyl acetate) PVAc. Partially hydrolysed grades have both hydrophobic and hydrophilic character due to the presence of vinyl acetate and vinyl alcohol groups, respectively. The aqueous solubility of partially hydrolysed PVA is dependent on the degree of hydrolysis, which determines the ability of the PVA to form hydrogen bonds with water. The hydrophilic grades of PVA (70-95 % hydrolysed) have been used widely as coating and stabilising agents in pharmaceutical products, ranging from oral to topical formulations. However, the potential of using this amphiphilic polymer as drug carrier has never been investigated.

Using solvent displacement method, two types of nanoparticles were employed in this study: nanospheres (NS) and nanocapsules (NC). In NS, the therapeutic agent was shown to be entrapped in the hydrophobic polymer matrix and surrounded by hydrophilic stabilizing polymer. In NC, the drug is dissolved in the oily core (benzoyl benzoate) surrounded by thin hydrophobic PVA layer and stabilized by poloxamer 188 surfactant (Figure 6.2) (Fessi *et al*., 1989). The aqueous suspension of both NS and NC were physically stable. The absence of surface charge (neutral zeta potential value) indicated that both systems were stabilised by steric repulsion arising from the surfactants at the NP shell layer surface (Jumaa and Muller, 2002).

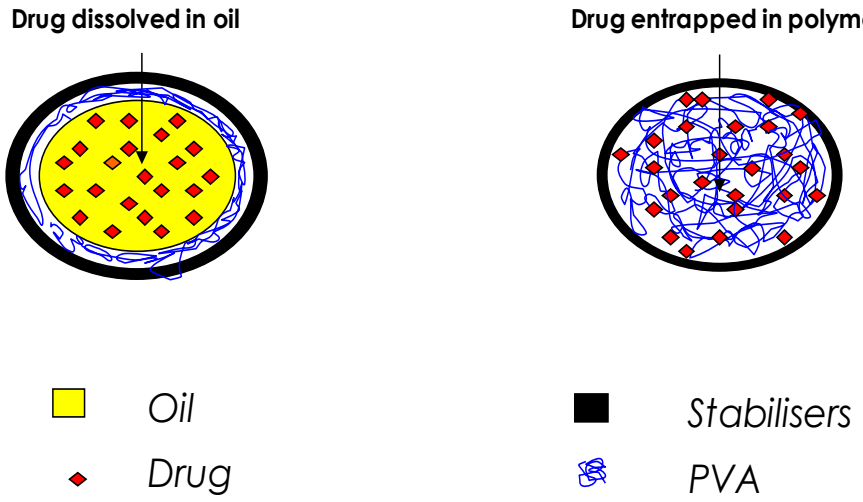

Figure 6.2. Schematic representation of nanospheres (right) and nanocapsules (left).

In this study, a hydrophobic grade (40 % hydrolysed) of PVA was used successfully for the encapsulation of rifampicin into nanocarriers. Despite, the hydrophobic nature of PVA, rifampicin had higher affinity to the aqueous phase than to the polymer. This was also observed by Esmaeili *et al*. (2005) when they attempted to encapsulate rifampicin into PLGA nanoparticles, although higher encapsulation efficiency was achieved in this work than the one reported by Esmaili et al., (2005). The diffusion to the continuous phase was decreased by employing pH 4.8 in this aqueous phase. In Chapter 2, it was demonstrated that rifampicin degrades rapidly in aqueous solutions and that encapsulating it into PVA nanocarriers would protect the drug after its administration, and increase its effectiveness.

A centrifugal filtration technique was employed to assess the drug release *in situ* from nanoparticles. The release characteristic was shown to be dependant on the pH of the dissolution medium. At pH 7.4 the release rate was slow for both nanoparticle systems. In contrast, higher release rates were observed in pH 4.2 and pH 10. This was due the accelerated erosion of the polymer in acidic and alkaline media. The mechanism of polymer erosion is postulated to involve the adsorption of the alkali or the acid catalyst onto the free hydroxyl groups resulting in the hydrolysis of the acetate groups of the polymer, also known as alcoholysis. This makes this polymer an interesting material for drug delivery purposes and it would be interesting to manufacture nanoparticles using different grades of the polymer to assess the effects on the encapsulation efficiency and release properties.

PVA nanocarriers interaction with J774A.1 cells was investigated in Chapter 4. It was shown that the nanoencapsulation of rifampicin not only reduced the toxicity of the drug to the cells but but also increased the association of the drug with these macrophages compared to free drug. This shows that the encapsulation delivers rifampicin into the cells using an additional cellular internalization process, presumably phagocytosis or endocytocis (Vauthier *et al.,* 2003). The *in vitro* particokinetics study provided us with some vital information on the system. It showed that delivered doses of PVA NSs and NCs to the cells during the experiment were significantly different. Therefore, nominal dose cannot be used to compare the two systems in terms of efficacy and toxicity.

Administration of anti-TB drugs by the pulmonary route for management of TB may lead to therapeutically effective drug concentrations in regions of the lungs containing large burdens of bacteria and reduce chances of infection reccurence and drug resistance. Nanoparticles have been previously delivered to the lungs by nebulisation of colloidal solutions (Kawashima *et al*., 1999; Vaughn *et al*., 2006; Yamamoto *et al*., 2005). However, nanoparticles prepared and stored in an aqueous medium will constantly release the drug to the outer phase prior administration, either by diffusion through the polymer barriers or by the erosion of the polymer over time. Suspension stability is another concern owing to particle-particle interaction, which could lead to poor functionality of the nebulizer. One way of solving the problem is the elimination of water from the nanoparticle formulation.

Spray drying has been reported to be a successful method for incorporating nanoparticles into dry powder. Drying nanoparticles and delivering as a dry powder is not easily achieved given that nanoparticles aggregate excessively in the dry state (Saez *et al*., 2000; Wendorf *et al*., 2006). Alternatively, nanoparticles delivered in unaggregated dry particle form do not deposit efficiently in the lungs and are generally exhaled from the lungs owing to their low inertia (Heyder *et al*., 1984). To overcome these issues, nanosuspensions were spray dried in the presence of a carbohydrate (lactose) to obtain microspheres that are physically stable in the powder form and have an appropriate size to deposit in the lungs.

The nanoparticle containing-microspheres produced were spherical in shape with diameters of 2 to 4 µm. The PVA NC-containing microspheres were shown to have a high tendency to agglomerate. The degradation of the nanocapsules coating the microsphere surface was responsible for the agglomeration of the primary NC and the adhesiveness of agglomerates (Tewa-Tagne *et al*., 2006). There was loss of the NCs during the spray drying procedure due to insufficient lactose concentration interacting with all NCs present in the feed. This resulted in low NC encapsulation efficiency in the microspheres compared to the NSs. Therefore more work needs to be carried out to optimise this formulation by investigating the effect of different NC: lactose ratios on the encapsulation of these NCs during the spray drying procedure.
Both PVA nanocarriers were instantly released from the microspheres after incubation in an aqueous medium. However, there was an enlargement in particle size. This was attributed to changes in conformation due to the thermal conditions of the spray-drying process (Sham *et al*., 2004). A twin-stage impinger was adapted to

accommodate a Transwell in the lower chamber where particles with an aerodynamic diameter of less than 6.4 µm deposit. The amount of powder depositing on the transwell and stage 2 was significantly higher for the PVA NS-containing microspheres than the PVA NC-containing microspheres ($p < 0.05$). The poor aerosolisation properties of the NC--containing powders is a result of particle agglomeration (French *et al*., 1996; Timsina *et al*., 1994). The introduction of a pH modifier (sodium hydroxide or succinic acid) to the powder successfully enhanced the release of the drug from the nanocarriers. The pattern correlated well with the data obtained when the nanoparticles were presented as suspensions. It was postulated the pH modifier, once dissolved, acts as a catalyst for PVA hydrolysis. The accelerated erosion of the polymer increased the amount of rifampicin released from PVA NS. Although the microencapsulated nanoparticle systems require further optimisation, the current study showed the potential of encapsulating PVA nanocarriers into a rapidly-dissolving carrier as a pulmonary delivery system. Encouraging results have been obtained with the PVA NS powders and PVA NS-sodium hydroxide powders in terms of drug release, flowability and aerolisation.

Administering rifampicin-loaded nanocarriers by the pulmonary route to the lungs may allow therapeutic concentrations of drug to penetrate effectively into lung lesions and alveolar macrophages harbouring mycobacteria. The approximate inhaled dose of rifampicin-loaded NS powder required for therapeutic use was calculated based on previous *in vivo* studies administering rifampicin-loaded nanoparticles by inhalation to animals (Pandey *et al*. 2003; Khuller *et al*., 2005; Sharma *et al.,* 2003; Zahoor *et al*., 2005). They demonstrated that the nebulisation

of rifampicin-loaded nanoparticles would result in a 13- to 19-fold increase in the bioavailability of the drug compared to the oral delivery of free drug. Taking that into account, a theoretical dose of rifampicin was calculated for use in this project. A reduced aerosol dose (by a factor of 13-19) would theoretically result in the same bioavailability as a 600mg delivered orally.

$$\text{Inhaled dose} = \frac{\text{Oral dose}}{\text{x}} = \frac{600\ \text{mg}}{\text{x}} = 40\ \text{mg}$$

where x was taken as 15

Considering the drug content capacity of the NS-containing powders produced in this project is approximately 200 µg of drug per 100 mg of powder. Thus 20 g of powder will be required to deliver 40 mg of active agent and would theoretically result in the same bioavailability as a dose of 600 mg orally every day. Delivering 20 g of powder is not practically possible. One way of improving dosimetry is by spray drying the nanoparticles in the absence of the carrier. This would produce large hollow or porous structures known as porous nanoparticle-aggregate paticles (PNAP) (Tsapsis *et al*., 2002). Considering that the produced powders would constistute rifampicin-loaded NSs only, the drug content capacity would be approximately 25 mg of drug per 100 mg of powder and the delivered dose required will be reduced from 20 g to approximately 160 mg of nanoparticle-loaded powders.

A different approach would be the local delivery of these nanoparticle-based systems as an adjunct to the oral conventional therapy (Figure 6.3C). Current clinical studies indicate that higher rifampicin doses might be desirable to avoid relapse of disease.

However, firmly established WHO protocols for treatment of TB worldwide by predefined dosage forms of oral drugs, and the large current market for fixed-dose combinations (FDC) means that realigning policies and the manufacturing industry towards altered dosage forms would be difficult and slow. Addition of a drug such as rifampicin in an inhaled formulation would make sense under such a scenario (Figure 6.3B). This has the potential to enhance local concentration in the lung, increase efficacy as well as allowing a reduction in the oral dose, dosing frequency and the duration of therapy. This may ultimately lead to less severe side effects, improved patient compliance and reduce the incidence of drug resistant strains of TB.

It is estimated that among the approximately 2 billion persons throughout the world with latent TB, between 100 and 200 million will develop active disease during their lifetimes. In North America and several other low-incidence countries, isoniazid has been used for the treatment of latent TB in persons at greatest risk of disease progression. Isoniazid has also been shown to be effective in persons with TB and HIV co-infection and has recently been recommended by WHO for such persons (WHO, 2011). The pulmonary delivery of a nanoparticle-based formulation as a prophylactic treatment in high risk patients would be benefitial. However, inhaled therapy will need to fit in with existing National TB programmes, and with initiatives such as the Directly Observed Treatment Short course (DOTS) programme. Increased costs, together with the need for strict control of infection precautions to prevent device-associated cross-infections and/or risk to health personnel, may limit the extent to which such technologies come to be widely available, particularly in developing countries. The large-scale production of a safe and effective nanoparticle-based drug formulation for pulmonary delivery of anti-TB drug at an

affordable cost will be the fundamental and decisive obstacle which will need to be overcome before contemplating human trials. However, the rationale behind inhaled anti-TB therapy is persuasive. Hopefully, current and future research efforts will eventually result in this concept from the bench to the bedside.

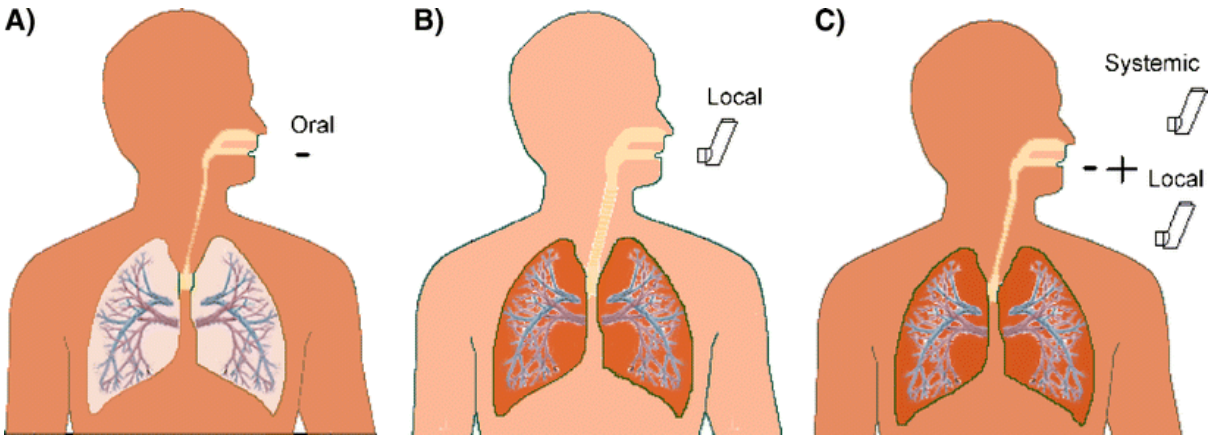

Figure 6.3. Schematic representation of drug distribution in the lungs and body when administered by (A) Orally, more drug in the systemic circulation compared to lungs, (B) Inhalation, more drug in the lung compared to systemic circulation, (C) Combined oral and inhalation, drug equilibrium in the lungs and the systemic circulation (color intensity qualitative indicator).

There are a number of areas in which further work is required in the future for the optimisation and the *in vitro* assessment of the developed nanoparticle-based delivery systems. The compatibility and the suitability of the PVA polymer as an excipient for pulmonary delivery have to be investigated further. It would also be interesting to employ different grades of this PVA for the encapsulation of the drug and assess the effect of degree of hydrolysis and molecular weight of the polymer on the encapsulation and the release kinetics of the drug.

For the uptake experiments, a thorough investigation of the effect of different parameters on the uptake of these nanocarriers by macrophages would provide us with more information on the mechanism of cell-particle interaction. Surface modification would also be an interesting aspect to explore. Particokinetics modelling can be used to adjust the nominal doses for accurate predicted doses in such studies so that any change in particle uptake would reflect the effect of the variable under investigation.

With regard to the nanoparticle-containing microspheres, the effect of incorporating a pH-modifier into NC-containing powders was not investigated fully to time constraints. More work is required to optimise both formulations in terms of spray drying parameters, nanoparticle:lactose ratios, nanoparticle:pH modifier ratio. It would also be necessary to carry out an aerodynamic assessment of the nanoparticle-containing powders using an andersson cascade impactor (ACI) or a new generation impactor (NGI) to determine fine particle fraction (FPF)

Despite the fact that so much future work is required to optimise the nanoparticle-based formulations, the results obtained in this project are very promising. The present study demonstrated the utility of PVA as a carrier for delivering therapeutic agents. The pH-dependant degradation of PVA makes it an interesting excipient for drug delivey purposes. The PVA nanocarriers were shown to target the drug to macrophages compared to the free form. Moreover, the successful incorporation of PVA nanoparticles into respirable carrier particles, with suitable size and shape for inhalation, enables the effective delivery of these nanocarriers to the lungs.

Figure 6.4. Schematic of the formulation concept for delivering rifampicin using inhaled PVA nanocarriers.

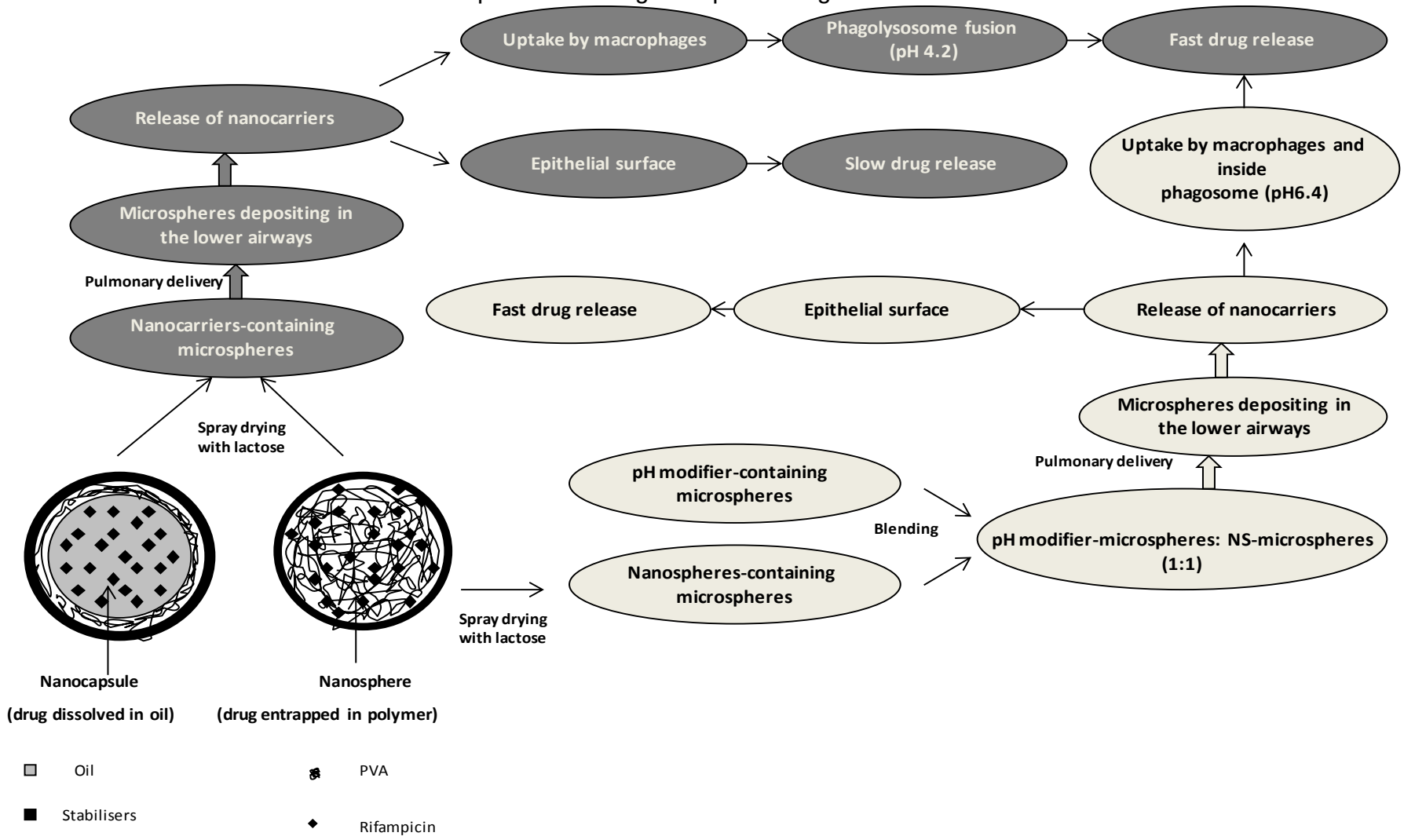

Despite the fact that the pathophysiology of TB is very complex, the work in this thesis demonstrated that the simplified hypothetical scenario in figure 6.4 is feasible. The manufactured PVA NS-containing microsheres can be delivered to the lungs. After reaching alveolar regions, the carrier is expected to dissolve instantly in the alveolar lining fluid releasing the nanoparticles, which can be taken up readily by the alveolar macrophages harbouring the bacteria. Once inside the acidic phagolysosome, the polymer is hydrolysed releasing the drug. Alternatively, the drug release at the epithelial surface can be induced by incorporating a pH modifier into these formulations to control the erosion of these nanocarriers. This delivery platform opens up a variety of treatment applications of pulmonary and possibly systemic diseases using targeted delivery strategies via nanoparticles.

References

- Agrawal, S., 2002. Assessment of bioequivalence of rifampicin, isoniazid and pyrazinamide in a four drug fixed dose combination with separate formulations at the same dose levels. Int. J. Pharm. 233: 169-177.
- Agrawal, S., Panchagnula, R., 2005. Implication of biopharmaceutics and pharmacokinetics of rifampicin in variable bioavailability from solid oral dosage forms. Biopharm. Drug. Dispos. 26: 321–334.
- Ahmad, Z., Pandey, R., Sharma, S., Khuller, G.K., 2008. Novel chemotherapy for tuberculosis: chemotherapeutic potential of econazole- and moxifloxacin-loaded PLG nanoparticles. Int. J. Antimicrob. Agents 31: 142-146.
- Anisimova et al., 2000. Nanoparticle as antituberculosis drug carriers: effect on activity against Mycobacterium tuberculosis in human monocyte-derived macrophages. J. Nanoparticle. Res. 2: 165-171.
- Azarmi, S., Roa, W.H., Löbenberg, R., 2008. Targeted delivery of nanoparticles for the treatment of lung diseases, Adv. Drug Deliv. Rev. 60: 863-875.
- Bain, D. F., Munday, D. L., Cox, P. J., 1998. Evaluation of biodegradable rifampicin-bearing microsphere formulations using a stability-indicating high-performance liquid chromatographic assay. Eur. J. Pharm. Sci. 7: 57-65.

- Barrow, E. L., Winchester, G. A., Staas, J. K., Quenelle, D. C., Barrow, W. W., 1998. Use of microsphere technology for targeted delivery of rifampin to Mycobacterium tuberculosis-infected macrophages. Antimicr. Agents. Chemother. 42: 2682-2689.
- Barry, P.W., O'Callaghan, C., 1999. An in vitro analysis of the output of budesonide from different nebulizers. J. Allergy. Clin. Immunol. 104:1168-1173.
- Bird, R. B et al., 1960. Transport phenomena. Wiley press, New York.
- Bloom, B.R., and Murray C.J.L., 1992. Tuberculosis: commentary on a reemergent killer. Science. 257:1055-1064.
- Bosquillon, C., Lombry, C., Pr´eat, V., Vanbever, R., 2001. Comparison of particle sizing techniques in the case of inhalation dry powders. J. Pharm. Sci. 90: 2032-2041.
- Brennan, P.J., 1997. Tuberculosis in the context of emerging and reemerging diseases. FEMS. Immunol. Med. Microbiol. 18: 263-269.
- British National Formulary 61, March 2011 (UK)
- Chan, E. D., and Iseman, M. D. 2008 .Multidrug-resistant and extensively drug-resistant tuberculosis: a review. Curr. Opin. Infect. Dis. 21: 587-595.
- Chana, J., Forbes, B., and Jones, S.A., 2008. The synthesis of high molecular weight partially hydrolysed Poly (vinyl alcohol) grades suitable for nanoparticle fabrication. J. Nanosci and Nanotech. 8: 5739-5747.
- Cheng, Y.H., Illum, L., Davis, S.S, 1998. A poly(D,L-lactide-co-glycolide) microsphere depot system for delivery of haloperidol. J. Control. Release. 55: 203-12.

- Chorny, M., Fishbein, I., Danenberg, H.D. and Golomb, G., 2002. Lipophilic drug loaded nanospheres prepared by nanoprecipitation: Effect of formulation variables on size, drug recovery and release kinetics. J. Control. Rel. 83: 389-400.
- Cohn, D.L., Bustreo, F. and Raviglione, M.C., 1997. Drug-resistant tuberculosis: review of the worldwide situation and the WHO/IUATLD global surveillance project. International union against tuberculosis and lung disease. Clin. Infect. Dis. 24: S121-S130.
- Cruz, T., Gaspar, R., Donato, A., Lopes, C., 1997. Interaction between polyalkylcyanoacrylate nanoparticles and peritoneal macrophages: MTT metabolism, NBT reduction, and NO production. Pharm. Res. 14: 73:79.
- Dannenberg, A. M., 1993. Delayed-type hypersensitivity and cell-mediated immunity in the pathogenesis of tuberculosis. Immunol. Today. 12: 228-233.
- Dannenberg, A.M., 1993. Immunopathogenesis of pulmonary tuberculosis. Hosp. Pract. 28: 51-58.
- DeMerlis, C.C. and Schoneker, D.R., 2003. Review of the oral toxicity of polyvinyl alcohol (PVA). Food. Chem. Toxico. 41: 319-326.
- Denkbas et al., 1995. Rifampicin carrying poly (lactide) microspheres: loading and release. J. Biomater. Sci. Polym. 6 (9): 815-825.
- Deol et al., 1997. Lung specific stealth liposomes: stability, biodistribution and toxicity of liposomal antitubercular drugs in mice. Biochem. Biophys. Acta. 1334 (2-3): 161-172.

- Dunne, M., Corrigan, O.I., and Ramtoola, Z., 1996. Influence of particle size and dissolution conditions on the degradation properties of polylactide-co-glycolide particles. Biomaterials. 21: 1659-1668.
- Duszyk, M., 2001. CFTR and lysozyme secretion in human airway epithelial cells. Eur. J. Physiol. 443: S45–S49.
- Du Toi. L. et al., 2006. Tuberculosis chemotherapy: current drug delivery approaches. Resp. Res. 7: 1-18.
- Emerich, D.F. & Thanos, C.G. 2007. Targeted nanoparticle-based drug delivery and diagnosis. J. Drug Target. 15: 163–183.
- Esmaeili, F et al., 2007, Preparation and antibacterial activity evalution of rifampicin-loaded poly lactide-co-glycolide nanoparticles. Nanomedicine. 3: 161-167.
- Evora, C., Soriano, I., Rogers, R.A., Shakesheff, K.N., Hanes, J., Langer, R., 1998. Relating the phagocytosis of microparticles by alveolar macrophages to surface chemistry: the effect of 1,2-dipalmitoylphosphatidylcholine. J. Control. Release. 51:143-152.
- Ferrari, G. et al., 1999. A coat protein on phagosomes involved in the intracellular survival of mycobacteria. Cell. 97: 435-447.
- Fessi, H., Puisieux, F., Devissaguet, J.P., Ammoury, N. and Benita, S., 1989. Nanocapsule formation by interfacial polymer deposition following solvent displacement. Int. J. Pharm. 55: R1-R4.
- Ficek, B., and Peppas, N.A., 1993. Novel preparation of poly (vinyl alcohol) microparticles without crosslinking agent for controlled drug delivery of proteins. J. Control. Rel. 27:259-264.

- Finlay, W.H., Stapleton, K.W., Zuberbuhler, P., 1997. Fine particle fraction as a measure of mass depositing in the lung during inhalation of nearly isotonic nebulized aerosols. J. Aerosol Sci. 28: 1301-1309.
- Finsy, R., 1994. Particle sizing by quasi-elastic light-scattering. Adv. Colloid Interface Sci. 52: 79-143.
- Forbes, B., Hashmi, N., Martin, G.P., & Lansley, A.B. 2000. Formulation of inhaled medicines: Effect of delivery vehicle on immortalized epithelial cells. J. Aerosol. Med. 13: 281-288.
- Fourie, B., Pillai, G., McIlleron, H., Smith, P., Panchagnula, R., 1999. Establishing the bioequivalence of rifampicin in fixed dose formulations containing isoniazid with or without pyrazinamide and/or ethambutol compared to single drug reference preparations administered in loose combination (Model Protocol) World Health Organization, WHO/CDS/ TB/99.27.
- Foye, W.O., Lemke, T.L., Williams, D.A. 1995. In: Principles of Medicinal Chemistry (Ed.), Williams and Wilkins, Baltimore. P. 896-900.
- French, D.L., Edwards, D.A., Niven, R.W., 1996. The influence of formulation on emission, deaggregation and deposition of dry powders for inhalation. J. Aerosol Sci. 27: 769–783.
- Galindo-Rodriguez, S., Allémann, E., Fessi, H., Doelker, E., 2004. Physicochemical parameters associated with nanoparticle formation in the salting-out, emulsification-diffusion, and nanoprecipitation methods. Pharm Res. 21(8):1428-39.
- Gallo, G.G., Radaelli, P., Rifampin. In: Florey, K. (Ed.), 1968. Analytical profiles of drug substances. Academic Press, New York, p. 467–513.

- Gelperina, S., Kisich, K., Iseman, M.D., Heifets, L. 2005. The potential advantages of nanoparticle drug delivery systems in chemotherapy of tuberculosis. Am. J. Resp. Crit. Care. Med. 172:1487-1490.
- Gelperina, S., Kisich, K., Iseman, M.D., Heifets, L., 2005. The potential advantages of nanoparticle drug delivery systems in chemotherapy of tuberculosis. Am. J. Respir. Crit. Care Med. 172 (12): 1487-1490.
- Gill, S., Lobenberg, R., Ku, T., Azarmi, S., Roa, W., Prenner, E.J., 2007. Nanoparticles: characteristics, mechanisms of action, and toxicity in pulmonary drug delivery-a review. J. Biomed. Nanotechnol. 3: 107–119.
- Gharbo, S.A., Cognion, M.M., Williamson, M.J., 1989. Modified dissolution method for rifampicin. Drug Dev. Ind. Pharm. 15: 331-335.
- Georgitis, J. W., 1999. The 1997 asthma management guidelines and therapeutic issues relating to the treatment of asthma. Chest. 115: 210-217
- Govender, T., Stolnik, S., Garnett, M.C., Illum, L. and Davis, S.S., 1999. PLGA nanoparticles prepared by nanoprecipitation: drug loading and release studies of a water soluble drug. J. Control. Rel. 57: 171-185.
- Grenha, A., Begona, S., and Remunan-Lopez, C., 2005. Microencapsulated chitosan nanoparticles for lung delivery. Eur. J. Pharm. Sci. 25: 427-437.
- Groneberg, D.A., Giersig, M., Welte, T. & Pison, U. 2006. Nanoparticle-based diagnosis and therapy. Curr. Drug Targets 7 **,** 643–648.
- Guo, Y., Laube, B., & Dalby, R., 2005. The effect of formulation variables and breathing patterns on the site of nasal deposition in an anatomically correct model. Pharm. Res. 22: 1871-1878.

- Gurny, R., Peppas, N.A., Harrington, D.D., and Banker, G.S., 1981. Development of biodegradable and injectable lattices for controlled release potent drugs. Drug. Dev. Inu. Pharm. 7: 1-25.
- Heyder, J., Gebhart, J., Rudolf, G., Schiller, C.F., Stahlhofen, W., 1986. Deposition of particles in the human respiratory-tract in the size range 0.005-15-Mu-M. J. Aerosol. Sci. 17: 811-825.
- Heyder, J., Rudolf, G., 1984. Mathematical-models of particle deposition in the human respiratory-tract. J. Aerosol. Sci. 15: 697-707.
- Heyder, J., and Svartengren, M.U. 2002. Basic principles of particle behavior in the human respiratory tract. In: Drug delivery to the lung, Bisgaard, H., O'Callaghan, C., and Smaldone, G. C., eds. (New York, Marcel Dekker, Inc.).
- Hickey, A.J., Mansour, H.M., 2008. Delivery of drugs by the pulmonary route. In: Florence AT, Siepmann J, editors. Modern Pharmaceutics. New York, NY: Taylor and Francis, Inc. p. 191–219.
- Hopewell, P.C., 1994. Overview of clinical tuberculosis, p. 25–46. In B. R. Bloom (ed.), Tuberculosis: pathogenesis, protection, and control. ASM Press, Washington, D.C.
- Howes, B.D., Guerrini, L., Sanchez-Cortes, S., Marzocchi, M.P., Garcia-Ramos, J.V., 2007. The influence of pH and anions on the adsorption mechanism of rifampicin on silver colloids. J. Raman. Spectrosc. 38: 859-86.
- Hyon, S.H., Cha, W.I., Ikada, Y., Kita, M., Ogura, Y., and Honda, Y., 1994. Poly (vinyl alcohol) hydrogels as soft contact lens material. J. Biomater. Sci. Polym. Ed. 5: 397-406.

- Jeffery, P. K., 1995. Microscopic structure of normal lung. In Respiratory Medicine, Brewis, R. A. L., Corrin, B., Geddes, D. M., and Gibson, G. J., eds. (London, W.B. Saunders Company Ltd).
- Johnson, C.M., Pandey, R., Sharma, S., Khuller, G.K., Basaraba, R.J., Orme, I.M., Lenaerts, A.J., 2005. Oral therapy using nanoparticle-encapsulated antituberculosis drugs in guinea pigs infected with Mycobacterium tuberculosis. Antimicrob. Agents Chemother. 49 (10): 4335-4338.
- Jumaa, M., Muller, B.W., 2002. Parenteral emulsions stabilized with a mixture of phospholipids and PEG-660-12-hydroxy-stearate: evaluation of accelerated and long-term stability. Eur. J. Pharm. Biopharm., 54: 207-212.
- Kahnert, A., Seiler, P., Stein, M., Bandermann, S., Hahnke, K., Mollenkopf, H., 2006. Alternative activation deprives macrophages of a coordinated defense program to Mycobacterium tuberculosis. Eur. J. Immunol. 36: 631-647.
- Kasim, N.A., Whitehouse, M., Ramachandran, C., Bermejo, M., Lennernas, H., Hussian, A.S., Junginger, H.E., Stavchansky, S.A., Midha, K.K., Shah, V.P. and Amidon, G.L. 2004. Molecular Properties of WHO Essential Drugs and Provisional Biopharmaceutical Classification. Mol. Pharm. 1: 85-96.
- Katsurya, K., Hatanaka, K., Matsuzaki, K., and Amiya, S., 2001. Assignement of finely resolved 13CNMR speactra of poly(vinyl alcohol). Polymer. 42: 9855-9858.
- Kawashima, Y., Yamamoto, H., Takeuchi, H., Fujioka, S., Hino, T. 1999. Pulmonary delivery of insulin with nebulized -lactide/glycolide copolymer (PLGA) nanospheres to prolong hypoglycemic effect. J Control Release; 62: 279–87.

- Kelly, C *et al*., 2011. Targeted Liposomal Drug Delivery to Monocytes and Macrophages. J Drug del; :10.1155/2011/727241.
- Khuller, G.K. and Pandey, R., 2005. Solid lipid particle-based inhalable sustained drug delivery system against experimental tuberculosis. Tuberculosis. 85: 227-234.
- Kumar, V., Robbins, S.L., 2007. Robbins Basic Pathology. Saunders/Elsevier, Philadelphia, PA
- Kumar, P.V., Asthana, A., Dutta, T. and Jain, N.K., 2006. Intracellular macrophage uptake of rifampicin loaded mannosylated dendrimers. J. Drug. Targeting. 14 (8): 546-556.
- Laura, J.V.P., Kerstin, J.W., 2000. Vito, R. Accumulation of rifampicin by Mycobacterium aurum, Mycobacterium smegmatis and Mycobacterium tuberculosis. J. Antimicrob. Chemother. 45: 159-165.
- Lansley, A.B., 1993. Mucociliary clearance and drug delivery via the respiratory tract.Ad. Drug. Del. Rev. 11(3) 299-327.
- Limbach, L., Grass, R.N; Brunner, T.J., Hintermann, M.A., Muller, M., Gunther, D. and Stark, W.J., 2005. Oxide nanoparticle uptake in human lung fibroblasts: effect of particle size, agglomeration, and diffusion at low concentrations. Environ. Sci. Technol. 39: 9370-9376
- Lombry, C., Edwards, D.A., Preat, V., Vanbever, R., 2004. Alveolar macrophages are a primary barrier to pulmonary absorption of macromolecules. Am. J. Physiol. Lung. Cell. Mol. Physiol. 286: 1002-1008.
- Maeakin, P., 1988. Fractal aggregates. Adv. Colloid. Interface. Sci. 28: 249-331.

- Makino, K., Terada, H., Nakajima, T., Tomoda, K., 2006. Preparation and properties of inhalable nanocomposite particles: Effects of the temperature at a spray-dryer inlet upon the properties of particles. Colloids & Surfaces B: Biointerfaces. 61: 138-144
- Maggi, N., Pallanza, R., Sensi, P., 1965. New derivatives of Rifamycin SV. Antimicrob. Agents Chemother.97: 765-769.
- Maggi, N., Pasqualucci, C.R., Ballotta, R., Sensi, P., 1966. Rifampicin: A new orally active rifamycin. Chemotherapy. 11: 285-292.
- Mariappan, T.T., Singh, S., 2003. Regional gastrointestinal permeability of rifampicin and isoniazid (alone and their combination) in the rat. Int. J. Tuberc. Lung. Dis. 7: 797-803.
- Mandell, G.L., Sande, M.A., 1985. Antimicrobial agents. In: Gilmans A, Goodman LS, Rall TW., (eds). The pharmacological basis of therapeutics. New York: Macmillan. 1199-218.
- Mathias, N.R., Hussain, M,A., 2010. Non-invasive systemic drug delivery: developability considerations for alternate routes of administration. J. Pharm. Sci. 99:1-20.
- McConville, J.T., Overhoff, K.A., Sinswat, P., Vaughn, J.M., Frei, B.L., Burgess, D.S., Talbert, R.L., Peters, J.I., Johnston, K.P., Williams, R.O., 2006. Targeted high lung concentrations of itraconazole using nebulized dispersions in a murine model, Pharm. Res. 23 (5): 901–911.
- Mercer, R.R., Russell, M.L., Crapo, J.D. 1992. Mucous lining layers in human and rat airways. Am Rev Respir Dis . 145: A355.

- Mo, L., Lim, L., 2004. Mechanistic study of the uptake of wheat germ agglutinin-conjugated PLGA nanoparticles by A549 cells. J. Pharm. Sciences. 93: 20-28.
- Moinard-Chécot, D., Chevalier, Y., Briançon, S., Fessi, H. , and Guinebretière, S. 2006. Nanoparticles for drug delivery: review of theformulation and process difficulties illustrated by the emulsiondiffusion process. J. Nanoscience. & Nanotech. 6 (9–10): 2664-2681.
- Moller, W., Barth, W., Kohlhaufl, M., Haussinger, K., Stahlhofen, W., Heyder, J., 2001. Human alveolar long-term clearance of ferromagnetic iron oxide microparticles in healthy and diseased subjects. Exp. Lung. Res. 27: 547-568.
- Morehead, R.S., 2000. Delayed death from pulmonary tuberculosis: unsuspected subtherapeutic drug levels. South. Med. J. 93: 507-510.
- Moritani, T., Fujiwara, Y. 1977. 13C and 1H-NMR investigation of sequence distribution in vinyl alcohol-vinyl acetate co-polymers. Macromolecules. 10 (3): 532-535.
- Myers, M.A., Thomas, D.A., Straub, L., Soucy, D.W., Niven, R.W., Kaltenbach, M., 1993. Pulmonary effects of chronic exposure to liposome aerosols in mice. Exp. Lung. Res. 19: 1-19.
- Mygind., N & Dahl, R. 1998. Anatomy, physiology and function of the nasal cavities in health and disease. Ad. Drug. Del. Rev. 29: 3-12.
- Nardell, E., 1993. Pathogenesis of tuberculosis, Lung biology in health and disease. Marcel Dekker, Inc., New York.
- Nahata, M.C., Morosco, R.S., Hipple, T.F., 1994. Effect of preparation method and storage on rifampicin concentration in suspensions. J. Clin. Pharm. Ther. 28: 182-184.

- Onyebujoh, P., Rodriguez, W., Mwaba, P., 2006. Priorities in tuberculosis research. Lancet. 367, 940-942.
- Oppolzer, W., Prelog, V., 1973. The constitution and configuration of rifamycins B, O, S. and SV. Helv. Chim. Acta. 56: 2287-2314.
- Pandey, R., Khuller, G.K., 2007. Nanoparticle-based oral drug delivery system for injectable-antibiotics streptomycin. Chemotherapy. 53: 437-441.
- Pandey, R., Sharma, A., Zahoor, A., Sharma, S., Khuller, G.K., Prasad, B., 2003. Poly (DLlactide-co-glycolide) nanoparticle-based inhalable sustained drug delivery system for experimental tuberculosis, J. Antimicrob. Chemother. 52: 981-986.
- Pandey, R.., Khuller, G.K., 2004. Subcutaneous nanoparticle-based antitubercular chemotherapy in an experimental model, J. Antimicrob. Chemother. 54 (1): 266–268.
- Pandey, R., Khuller, G.K., 2005. Antitubercular inhaled therapy: opportunities, progress and challenges, J. Antimicrob. Chemother. 55: 430-435.
- Parrish, N.M., Dick, J.D., Bishai, W.R,. 1998. Mechanisms of latency in Mycobacterium tuberculosis. Trends. Microbiol. 6:107-112.
- Patton, J.S., and Byron, P.R., 2007. Inhaling medicines: delivering drugs to the body through the lungs. Nature. Rev. Drug. Disc. 6: 67-74.
- Pelizza, G., Nebuloni, M., Ferrari, P., Gallo, G.G., 1977. Polymorphism of rifampicin. Farmaco. 32: 471-481.
- Petrini, B., Hoffner, S., 1999. Drug-resistant and multidrug-resistant tubercle bacilli. Int. J. Antimicrob. Agents. 13: 93-97.

- Plopper, C.G., 1996. Structure and function of the lung. In: Respiratory system, Jones, T. C., Dungworth, D. L., and Mohr, U., eds. (Berlin, Sprinter Verlag), pp. 135-150.
- Rohde, K., Yates, R.M., Purdy, G.E., Russell, D.G., 2007. Mycobacterium tuberculosis and the environment within the phagosome. Immunol. Rev. 219: 37-54.
- Russel, D.G., 2009 Foamy macrophages and the progression of the human TB granuloma. Nat. Immunol. 10(9): 943-948.
- Saez, A., Guzman, M et al., 2000. Freeze-drying of polycaprolactone and poly(-lactic-glycolic) nanoparticles induce minor particle size changes affecting the oral pharmacokinetics of loaded drugs. Eur J Pharm Biopharma 50: 379–87.
- Samet, J,M. & Cheng, P.W., 1994. The Role of Airway Mucus in Pulmonary Toxicology. Env. Health Perspectives. 102: 89-103.
- Sanjeeb, K. et al., 2003. Nanotech approaches to drug delivery and imaging. Drug. Disc. Today. 8 (24): 1112-1120.
- Schlesinger, L.S., 1996. Role of mononuclear phagocytes in M tuberculosis pathogenesis. J. Investig. Med. 44(6): 312-323.
- Schulz, H., Brand, P., and Heyder, J., 2000. Particle deposition in the respiratory tract. In: Particle-lung interactions, Gehr, P., and Heyder, J., eds. (New York, Marcel Dekker, Inc.), pp. 229-290.
- Schurch, S., Gehr, P., Hof, V. I., Geiser, M. and Green, F. 1990. Surfactant displaces particles towards the epithelium in airways ans alveoli. Respir. Physiol. 80: 17-32.

- Selwyn, P.A., Hartel, D., Lewis, V.A., Schoenbaum, E.E., Vermund, S.H., Klein, R.S., Walker, A.T., Friedland, G.H., 1989. A prospective study of the risk of tuberculosis among intravenous drug users with human immunodeficiency virus infection. N. Engl. J. Med. 320, 545-550.
- Seydel, J.K., 1970. Physicochemical studies of rifampicin. Antibiot. Chemotherapia. 16: 380-391.
- Sham, J.O., Zhang, Y., Finlay, W.H., Roa, Lobenberg, R., 2004. Formulation and characterization of spray-dried powders containing nanoparticles for aerosol delivery to the lung, Int. J. Pharm. 269: 457-467.
- Sharma, A., Sharma, S. and Khuller, G. K., 2004. Lectin-functionalized poly (lactide-co-glycolide) nanoparticles as oral/aerosolised antitubercular drug carriers for treatment of tuberculosis. J. Antimicrob. Chemother. 54: 761-766.
- Sharma, R., Muttil, P., Yadav, A.B., Rath, S.K., Bajpai, V.K., Mani, U.,2007. Uptake of inhalable microparticles affects defence responses of macrophages infected with Mycobacterium tuberculosis H37Ra. J. Antimicrob. Chemother. 59: 499-506.
- Shephard, E.G., Joubert, J.R., Finkelstein, M.C., Kuhn, S.H., 1981. Phagocytosis of liposomes by human alveolar macrophages. Life. Sci. 29: 2691-2698.
- Sibille, Y., Reynolds, H.Y., 1990. Macrophages and polymorphonuclear neutrophils in lung defense and injury. Am. Rev. Respir. Dis. 141: 471-501.
- Singh, S., 2004. Tuberculosis. Curr. Anae. & Crit. Care. 15 (3)**:** 165-171.
- Smith, I., 2003. Mycobacterium tuberculosis pathogenesis and molecular determinants of virulence, Clin. Microbiol. Rev. 16: 463–496.

- Soppimath, K.S., Aminabhavi, T.M., Kulkarni, A.R., Rudzinski, W.E., 2001. Biodegradable polymeric nanoparticles as drug delivery devices. J. Control. Release. 70: 1-20.
- Spencer, H. 1985. Pathology of the lung, 4th ed., vol. 1. Pergamon Press, Oxford.
- Sreenivasa et al., 2002. Studies on rifampicin release from ethylcellulose coated nonpareil beads. Int J. Pharm. 231: 97-106.
- Suarez et al., 2001. Respirable PLGA microspheres containing rifampicin for the treatment of tuberculosis: screening in an infectious disease model. Pharm. Res. 18: 1315-1319.
- Sturgill-Koszycki, S. et al., 1994. Lack of acidification in Mycobacterium phagosomes produced by exclusion of the vesicular proton-ATPase. Science. 263: 678-81.
- Tabata, Y., Ikada, Y., 1988. Effect of the size and surface charge of polymer microspheres on their phagocytosis by macrophage. Biomaterials. 9: 356–362.
- Telenti, A. & Iseman, M., 2000. Drug-resistant tuberculosis: what do we do now? Drugs. 59: 171-179.
- Tewa-Tagne, P., Briancon, S., Fessi, H., 2007. Preparation of redispersable dry nanocapsule by means of spray drying: development and characterization. Eur. J. Pharma. Sci. 30(2): 124-35.
- Thanoo, B.C., and Sunny, M.C., 1993. A Controlled release of oral drugs from cross-linked polyvinyl alcohol microspheres. J. Pharm. Pharmacol. 45: 16-20.

- Thioune, O., Fessi, H., Devissaguet, J.P. and Puisieux, F.,1997. Preparation of pseudolatex by nanoprecipitation: influence of the solvent nature on intrinsic viscosity anfd interaction constant. Int. J. Pharm. 146: 233-238.
- Timsina, M.P., Martin, G.P., Marriott, C., Ganderton, D., Yianneskis, M., 1994. Drug delivery to the respiratory tract using dry powder inhalers. Int. J. Pharm. 101: 1–13.
- Tomoda, K et al. 2008. Preparation and properties of inhalable nanocomposite particles: effects of the temperature at a spray-dryer inlet upon the properties of particles. Colloids & Surfaces. 61:138-144.
- Touw, D.J., Brimicombe, R.W., Hodson, M.E., Heijerman, H.G.M. and Bakker, W. 1995. Inhalation of antibiotics in cystic fibrosis. Eur. Respir. J. 8: 1594-1604.
- Tsapis, N., Bennett, D., Jackson, Weitz, D.A., Edwards, D.A., 2002. Trojan particles: large porous carriers of nanoparticles for drug delivery. Proc. Natl. Acad. Sci. 99: 12001-12005.
- Ulrichs, T., Kaufmann, S.H., 2006. New insights into the function of granulomas in human tuberculosis. J. Pathol. 208 (2): 261-269.
- USP DI, Drug Information for the Health-care Practitioners, 1996. US Pharmacopoeial Convention, Rockville, MD, vol. 1, 16th edn, p. 2567–2572
- Vauthier, C., Dubernet, C., Fattal, E., Pinto-Alphandary, H., Couvreur, P., 2003. Poly(alkylcyanoacrylate) as biodegradable materials for biomedical applications. Adv. Drug. Del. Rev. 55: 519-48.
- Vaughn, J. M, et al. 2006. Single dose and multiple dose studies of itraconazole nanoparticles. Eur J Pharm Biopharma 63:95–102.

- Venkatesan, K. 1989. Clinical pharmacokinetic considerations in the treatment of patients with leprosy. Clin. Pharmacokinet. 16: 365-386.
- Vyas et al., 2004. Design of liposomal aerosols for improved delivery of rifampicin to alveolar macrophages. Int. J. Pharm. 269: 37-49.
- Walters, D.V., 2002. Lung lining liquid – The hidden depths. Biol. Neonate. 81: S2–S5.
- Weibel, E.R., 1991. Design of airways and blood vessels considered as branching trees. In: The Lung: Scientific Foundations, Crystal, R. G., and West, J. B., eds. (New York, Raven Press Ltd.), pp. 711-720.
- Wendorf, J., Singh, M., et al. 2006 A practical approach to the use of nanoparticles for vaccine delivery. J Pharm Sci. 95:2738–50.
- World Health Organization (WHO). 2003. Revision approved June 2004. Treatment of Tuberculosis: Guidelines for national programmes.
- World Health Organization. 2001. Global Tuberculosis Control 2011.
- Wong, D., and Parasrampuria, J., 1996. Polyvinyl alcohol. In: Brittain, H. H. (Ed.). Analytical profiles of drug substances. Academic Press, New York. pp. 397-441.
- Yadav, A.B., Sharma, R., Muttil, P., Singh, A.K., Verma, R.K., Mohan, M., 2009. Inhalable microparticles containing isoniazid and rifabutin target macrophages and ’stimulate the phagocyte’ to achieve high efficacy. Indian. J. Exp. Biol. 47: 469-474.
- Yamamoto, H., Kuno, Y., Sugimoto, S., Takeuchi, H., Kawashima, Y., 2005. Surface-modified PLGA nanosphere with chitosan improved pulmonary

delivery of calcitonin by mucoadhesion and opening of the intercellular tight junctions, J. Control. Release 102 (2): 373-381

- Yajko, D.M., Nassos, P.S., Sanders, C.A. and Hadley, W.K. 1989. Effects of antimicrobial agents on survival of Mycobacterium avium complex inside alveolar macrophages obtained from patients with human immunodeficiency virus infection. Am. Rev. Respir. Dis. 140:1198-1203,
- Zahoor, A., Khuller, G.K., and Sharma, S., 2005. Inhalable alginate nanoparticles as antitubercular drug carriers against experimental tuberculosis. Int. J. Antimicrob. agents. 26: 298-303.
- Zhang *et al*., 2008. Nanoparticles in Medicine: Therapeutic Applications and Developments. Clinical Pharmacology & Therapeutics**.** 83: 761–769.
- Zhao, Y., Brown, M.B, Jones, S.A., 2010. The effects of particle properties on nanoparticle drug retention and release in dynamic minoxidil foams. Int. J. Pharm. 383: 277-284.
- Zhao, Y., Brown, M.B., Jones, S.A., 2010b. The topical delivery of benzoyl peroxide using elegant dynamic hydrofluoroalkane foams. J. Pharm. Sci. 99:1384-1398.
- Zahoor, R., Pandey, S., Sharma, G.K., Khuller, 2006. Pharmacokinetic and pharmacodynamic behavior of antitubercular drugs encapsulated in alginate nanoparticles at two doses. Int. J. Antimicrob. 27:409–416.